Chromospheric Activity Induced by Short-Period Planets

A Search for Modulation of Ca II H & K Emission

by

Evgenya Shkolnik

B.Sc. (Physics and Mathematics), Dalhousie University, 1998
M.Sc. (Astronomy), The University of British Columbia, 2000

A THESIS SUBMITTED IN PARTIAL FULFILMENT OF
THE REQUIREMENTS FOR THE DEGREE OF

DOCTOR OF PHILOSOPHY

in

The Faculty of Graduate Studies

(Department of Physics and Astronomy)

We accept this thesis as conforming
to the required standard

THE UNIVERSITY OF BRITISH COLUMBIA

December 4, 2003

Abstract

I have detected the first evidence of magnetic interaction between an extrasolar planet and its parent star.

Of the > 100 extrasolar planets discovered to date, approximated 20% of them are '51 Peg'-type with a Jupiter-mass planet orbiting within 0.1 Astronomical Units. The systems with the tightest orbits ($P_{orb} < 5$ days) offer the best opportunity to observe a tidal or magnetic interaction between the planet and its parent star. Stellar chromospheric activity could be modulated in two ways. For magnetic interaction, the modulation is predicted to be at the orbital period with enhancement near the sub-planetary point ($\phi = 0$). Tidal interaction would stimulate activity with a period of $P_{orb}/2$ with enhancements near both $\phi = 0$ and 0.5.

The Ca II H & K line reversals at 3968 and 3933 Å are the best chromospheric activity indicators visible from the ground. I observed the H & K emission cores of five sun-like stars with short period planets: τ Boo, HD179949, HD 209458, 51 Peg and υ And. I acquired 10 nights of high resolution ($\approx$ 110,000), high S/N ($\sim$ 500) data at the Canada-France-Hawaii Telescope over three semesters: 2001 August, 2002 July and 2002 August. The superb quality of the data yielded differential radial velocities to better than 20 m s^{-1}. Fitting known orbital parameters such as period and velocity amplitude to the radial velocities, I determined updated ephemerides and accurate orbital phases.

Night-to-night modulation of the H & K emission was observed in 4 of the 5 stars. Our two standards, τ Ceti and the sun, showed no such variability. Three of the 4 'active' stars did not appear to show a correlation between activity and orbital phase. However, HD 179949, the star with the tightest planetary orbit ($P_{orb} = 3.093$ days), repeatedly showed a 2.5% enhancement in the Ca II K emission leading the sub-planetary point by 0.17 in phase. A decrease was observed when the planet was behind the star. The activity persisted for 108 orbits (or 37 stellar rotations). This is the first detection of magnetic interaction between a star and its giant planet, as well as a first

glimpse of an extrasolar planetary magnetosphere.

As an exaggerated example of enhanced chromospheric activity induced by a companion, we observed ER Vul, an RS CVn binary system with P_{orb} = 17 hours. Using the same setup at the CFHT, we obtained Ca II H & K spectra with nearly complete phase coverage. This system shows increased activity near the sub-binary longitudes of both components. There is also evidence of Ca II emission from between the two stars.

Observations of κ^1 Ceti, an active single dwarf star, show periodic H & K activity modulated by the stellar rotation (P_{rot} = 9.4 d.) with an enhancement level of $\approx$ 7%. The stimulating mechanism for its activity is unknown and may be evidence of a yet unseen, nearby companion.

Contents

List of Tables

List of Figures

Preface

Refereed Papers published from this research:

Cuntz, M., Shkolnik, E., 2002, *Chromospheres, Flares and Exoplanets*, AN, 323, 387.

Walker, G.A.H., Shkolnik, E., Bohlender, D.A., Yang, S., 2003, *The Radial Velocity Precision of Fiber-fed Spectrographs*, PASP, 115, 700.

Shkolnik E., Walker, G.A.H., Bohlender, D.A., 2003, *Evidence for Planet-Induced Chromospheric Activity on HD 179949*, ApJ, 597, 1092.

Acknowledgements

There were many people who assisted me in the research and writing of this PhD thesis. Firstly, this work would never have begun nor have been completed if it were not for the ideas, enthusiasm and collaboration of my supervisor, Gordon Walker. His guidance, support and wisdom exceed all expectations for a mentor. Secondly, David Bohlender, a tireless collaborator, taught me fundamental astronomical techniques and, along with Stephenson Yang and Slavek Rucinski, answered my many questions. These three astronomers generously shared their time and knowledge with me whenever needed.

I also received many forms of support from many people: a place to work, a place to stay, words of wisdom, editing skills and overall friendship. I would particularly like to express my appreciation to the astronomers at the University of British Columbia, the Herzberg Institute of Astrophysics, and the University of Victoria. Also, to Tony Berger, Colin Borys, James Di Francesco, Aaron Dragushan, Carol Harris, Julienne Hills, Janet Johnson, Karen Levitt, Janis McKenna, Siân Messinger, Mette Gam Pederson, Anna Shkolnik, Leon Shkolnik, Kristy Skaret, Derick Snell, Jeff Stoesz and Sigrid Walker.

I thank all of you.

Chapter 1

Introduction

1.1 Contemplating New Worlds

The ancient Greeks developed the earliest recorded view regarding multiple worlds in the cosmos approximately 2500 years ago. This first viewpoint on the "the plurality of worlds" was introduced by early atomists such as Democritus (c. 470 - 400 B.C.E.) and Epicurus (341 - 270 B.C.E.). They taught that the universe was composed of nothing but identical, indestructible particles (atoms) moving at random in a vacuum. If the earth was randomly formed of such universal particles then it was likely that other worlds and forms of life were created in the same way elsewhere in the universe. The atomists, however, considered these other worlds to be so far away that they would be inaccessible to us.

At that time, the existence of multiple worlds was purely conceptual. The lack of empirical evidence allowed the teachings of the atomists to be eclipsed by the those of Aristotle (384 - 322 B.C.E.). According to Aristotle, the earth was the only world containing life, while all other bodies were unchanging and fixed on the celestial sphere. The geocentric model which reigned over much of western thought for the next 2000 years consisted of seven concentric transparent spheres gliding together to include the sun, the moon, and the five naked-eye planets, surrounded by an eighth sphere retaining the fixed stars.

During the early days of the Renaissance, discussion regarding the existence of other worlds was left to Christian religious leaders. They accepted that God could create other inhabited earths but questioned whether He would choose to. Because there was no way to prove the existence of other worlds with the Christian scriptures alone, it was not until Copernicus' theory of the heliocentric universe in 1543 that the discussion of other worlds was revisited in both a scientific and philosophical sense.

Equipped with this new model of the universe, Giordano Bruno (1548 - 1600), asked why the sun should be the center of the universe. This Italian-

born Dominican monk and nomadic philosopher also wondered why the sun would remain stationary if the earth moved around the sun. While Copernicus and even Galileo considered the solar system to be at the centre of a great sphere of stationary stars, Bruno conceived of an infinitely extending universe where the seemingly fixed stars were actually huge suns at vast and varying distances. If all of those stars were suns, then it became plausible that they housed other earths and other life. For his radical cosmic model and other "heretical" opinions, he was tried by the Inquisition and burned at the stake (Darling 2003).

1.2 Discovering Extrasolar Planets

Bruno explained that planets around other stars are not visible due to their small size and great distances. In order to ascertain the existence of extrasolar planets, direct astronomical observations are required. It was not until the mid-20^{th} century that sufficiently precise astronomical techniques were developed, allowing the search for these planets to begin. These first methods consisted of astrometry, pulsar timings and precise radial velocity measurements (Dorminey 2002).

Edmund Halley conceived of astrometry in 1718 when he noticed that several stars had shifted in position relative to measurements recorded 2000 years earlier by Hipparchus. Measuring a star's motion across the line-of-sight (proper motion) can be used to determine stellar masses of binaries, characterise galaxy dynamics, and advance the cosmic distance scale. Also, tiny cyclic perturbations in a star's proper motion indicate the gravitational pull from an orbiting companion. With enough precision, such shifts can lead to discoveries of sub-stellar companions such as brown dwarfs, Jupiter-mass planets and even Earth-like planets. The precision required, however, makes planet-hunting with astrometry a difficult task. As an example, the pull on the sun due to the orbital motion of Jupiter as seen from 10 parsecs away would shift the sun's position by only 0.3 *milli*arcseconds. Such displacements on images that are several arcseconds in diameter are challenging.

However, the precision required did not stop several such searches for astrometric "wobbles" to lead to claims of extrasolar planets. For example, Strand (1943) reported the first detection of a sub-stellar companion (16 M_J) to 61 Cygni, based on observations taken at the Sproul Observatory. At the same observatory, van de Kamp (1963) observed a perturbation

in the proper motion of Barnard's Star, with a period of about 24 years, using photographic plates taken between 1938 and 1962. He attributed the motion to two orbiting Jupiter-mass planets. Both Strand's and van de Kamp's results were considered controversial for many years and were never confirmed. The slight shifts they observed in the stars' positions are now believed to have been effects of the lens adjustment schedule of the telescope.

Despite the history of false claims due to astrometric mis-measurements, the method still holds promise for detecting extrasolar planets and characterising their orbits. The precision required is very difficult to achieve from the ground, meaning that the best results will come from space-based telescopes such as NASA's Space Interferometry Mission (SIM), due for launch in 2009.[1]

More sophisticated techniques have been developed during the past two decades, leading to the unambiguous discovery of planets around other stars. Unexpectedly, the first extrasolar planet was discovered by Wolszczan and Frail in 1991 around a pulsar, the fast-spinning neutron star remnant of a 15 - 30 solar-mass star. Pulsar radio emissions have periods on the order of 0.002 - 2 seconds. Due to the extreme regularity of the pulses, small perturbations in their timing have led to discoveries of planets smaller than Earth. The radial velocity (RV) precision of this method can be as good as 1 m s^{-1}, unachievable by any other current method (as discussed below). To date, four planets around the pulsar PSR 1257+12 have been found, with masses ranging from 0.02 - 100 earth-masses and periods from 25 days to 170 years (Wolszczan 1994). These findings form the initial proof of the existence of planets outside of our solar system (Schnieder 2003).

Although pulsar planets are interesting, their formation scenarios and habitability potential differ greatly from planets around sun-like stars. Detecting and characterising planets around other 'suns' contributes direct information on the formation and evolution of our own solar system. The most successful method to date for detecting such planets was pioneered by Bruce Campbell, Gordon Walker and Stephenson Yang (1988). The method measures the Doppler shift in a star's spectral lines as it orbits the common center-of-mass due to the gravitational pull of any unseen companions. The shifts measure movements toward and away from the observer along the line-of-sight (i.e. perpendicular to the directions sampled by astrometry).

Motions in the stellar photosphere can limit the precision of absolute ra-

[1] http://sim.jpl.nasa.gov/mission/index.html

dial velocities by as much as 1 km s^{-1} (Campbell & Walker 1979). Differential radial velocities can be 2 - 3 orders of magnitude more precise. Campbell and Walker (1979) carried out the first high-precision radial velocity search for extrasolar planets around solar-type stars at the Canada-France-Hawaii Telescope (CFHT) with an unprecedented precision of 13 m s^{-1}. They used a hydrogen-fluoride (HF) gas cell to impose absorption features as zero-velocity standards directly onto the stellar spectrum against which to measure the Doppler shifts (Walker et al. 1995). Of the 21 bright stars they surveyed, γ Cephei, a K1 IV binary system, showed a clear 2.7-year period, which they initially attributed to an extrasolar planet (Campbell et al. 1988). Further RV measurements showed a low-amplitude variation with a 2.52-year period. This was coincident with Ca II λ8662Å (a chromospheric activity indicator) variations with a period of 2.5 years (Walker et al. 1992). This led the team to retract their planetary hypothesis and attribute the RVs to activity on the stellar surface. It was not until 2002 that Hatzes et al. (2003) combined data from the McDonald Observatory with those from the CFHT and reported that the primary star of γ Cephei showed steady RV periodicity spanning over 20 years, while the Ca II variations had ceased. The longevity of the RV variations revived the planet interpretation. The minimum mass of the putative planet is 1.25 M_J, with an orbital period of 2.47 years.

The revival of the planet around γ Cephei came seven years after the first discovery of an extrasolar planet around a sun-like star. Mayor and Queloz (1995) discovered a Jupiter-mass planet around 51 Pegasi (G2 IV). They used iodine (I_2) absorption features as zero-velocity fiducials to obtain RVs with a precision of 3 m s^{-1}. This precision neared the intrinsic noise limit produced by granular motions on the stellar surface. The orbital period, semi-major axis and the minimum mass of the planet ($M_p \sin i$, where i is the unknown inclination angle of the orbit) were determined from the sinusoidal shape of 51 Peg's RV curve. Accompanying the exciting discovery of the extrasolar planet, 51 Peg b, came the surprise of finding it orbiting the star with a period of only 4.23 days at a distance of 0.05 AU, about 1/8 the distance between Mercury and the sun. The tight orbit of 51 Peg b came as a shock to planet hunters, since most were seeking planets at distances of 5 - 10 AU with periods on the order of 10 years. As the number of new planets grew, it became clear that short-period giant planets are not rare at all. Approximately 20% of the more than 100 known planets are of the '51 Peg'-type.

Seventeen research groups are currently monitoring the radial velocities

of solar-type stars. In total, 119 planets in 104 extrasolar planetary systems have been found thus far, 13 of which possess more than one planet (Schneider 2003). The California & Carnegie Planet Search[2] and the Elodie & Coralie Planet Searches[3] are the most fruitful to date.

The discovery of the short-period systems was a challenge to the current planet formation theories as they were based exclusively on our solar system. The gravitational collapse of a giant molecular cloud of hydrogen and helium into a protoplanetary disk began the formation process. Approximately 100,000 years after the proto-sun began its thermonuclear fusion, icy cores formed from the dust in the outer parts of the disk. These later formed into gas giants while the terrestrial planets formed in the warmer inner region. Since there seems to be no way for giant planets to form at 0.05 AU, current theories require the planets to form at distances > 1 AU and then migrate inward and halt at the short-period orbits due to dynamical friction (Yeşilyurt et al. 2003).

Follow-up observations, such as astrometric measurements and transit searches, can constrain the orbital inclination, resolving the $M_p \sin i$ ambiguity. In the case of a transit, the planet's radius and hence its density can also be determined. Benedict et al. (2002) reported the first astrometrically determined mass of an extrasolar planet around Gliese 876 using Hubble Space Telescope (HST) observations. They determined that the planet Gliese 876 b has an orbital inclination of $84° \pm 6°$ and a mass of 1.89 ± 0.34 M_J. In addition, the astrometric measurements further constrain the period, velocity amplitude, longitude of periastron and the eccentricity, first extracted from the RV curve.

Charbonneau et al. (1999) reported the first planetary transit of HD 209458, another '51 Peg'-type system, for which a 2% dip in the stellar lightcurve was observed every 3.3 days. The transit observations yielded three values unattainable with the RV measurements alone: an orbital inclination of 86°, a planetary mass of 0.69 M_J and a radius of 1.4 R_J. The high scientific return of planetary transits has fueled 14 transit search teams, who have collectively found only one transit to date in addition to HD 209458 (Schneider 2003).

Clearly, planet hunting is a pursuit with a long future. As of now, there are 15 planned space-based missions whose primary science goals are devoted to extrasolar planet research. Seven of these missions hope to find planets

[2]http://exoplanets.org

[3]http://obswww.unige.ch/~udry/planet/elodie.html

through transits or astrometry while the others aim to observe the planets directly through imaging and spectroscopy. It seems inevitable that as technology advances, so will our understanding of the formation and evolution of extrasolar planetary systems.

1.3 Follow-up Probes of Extrasolar Planets

Other than astrometric observations and transit searches, several follow-up investigations of the known planetary systems have been carried out. For instance, time-critical spectroscopic observations of the star (and potentially of the planet) may yield information beyond the Keplerian orbital parameters. In the case of the transiting system HD 209458, the STIS[4] spectrograph has been used by two groups to detect planetary atmospheric absorption during transit. Charbonneau et al. (2002) reported a detection of excess absorption of the sodium resonance doublet at 5893 Å at the 2×10^{-4} level. This is less than cloudless planetary atmospheric models predicted by Seager & Sasselov (2000). They offer several possible explanations including photoionization of sodium by stellar flux or the presence of clouds high in the planet's atmosphere. Vidal-Madjar et al. (2003) observed excess Lyman α (λ1216Å) absorption during transit. They attribute the 15% absorption to a tidally extended planetary atmosphere plus evaporation of atomic hydrogen out to 200,000 km. If confirmed, these two exciting results will provide much needed constraints for planetary atmospheric models. So far, near-infrared searches for CO (Brown et al. 2002) and He I (Moutou et al. 2003) absorption in the transmission spectrum of HD 209458 have not been successful, but useful upper limits have been set.

The atmosphere of an extrasolar planet could also be probed via its own spectrum, providing yet another highly desirable detection. One of the best candidates for this is the 3.87 M_J planet orbiting τ Boo at 0.05 AU. Collier-Cameron et al. (1999) used high-resolution optical spectroscopy to look for the Doppler-shifted signature of starlight reflected by the planet. Wiedemann et al. (2001) searched for methane produced by the planet in τ Boo's infrared spectrum. Neither group has managed to detect a planetary spectrum, but further investigations are in progress.

[4]The Space Telescope Imaging Spectrograph (STIS) aboard the HST provides data in the UV and optical wavelengths.

If these planets are magnetized similarly to Jupiter and have a source of energetic (keV) electrons in their magnetospheres, or have an Io-like satellite, they may be strong emitters in the decimetre and metre wavelengths. In yet another follow-up experiment, Bastian et al. (2000) used the Very Large Array (VLA) to look for this type of *cyclotron maser radiation* from seven extrasolar planets. No detections were reported, presumably due to the low sensitivity of the VLA to this emission.

Even with these various efforts to investigate the newly discovered planets, the lack of constraints on extrasolar planetary atmospheres and structure motivates astronomers to explore alternate probes. Cuntz et al. (2000) suggested that there may be an observable interaction between a parent star and its close-in giant planet in the form of an enhanced heating of the star's outer atmosphere. Due to the strong tidal forces between a star and such a planet, the chromosphere and corona would undergo tidal heating. A large planetary magnetic field would enhance the heating of these layers through magnetic effects as well. With this suggestion in mind, we designed a research programme to search for periodic chromospheric heating by monitoring the Ca II H & K emission in stars with giant planets within a few stellar radii. These tightest orbits offer the best opportunity to observe planet-induced chromospheric activity.

1.4 Stellar Chromospheres

For sun-like stars, the chromosphere is the 2000 km thick layer of low-density gas immediately above the photosphere that can reach temperatures of up to 20,000 K (Carroll & Ostlie 1996). Beyond the chromosphere, the diffuse plasma of the corona can extend out to a few stellar radii and reach several millions of degrees. In sun-like stars, the chromosphere and corona are responsible for the majority of their UV and X-ray emission. Figure 1.1 shows outer atmospheric temperature as a function of height for a sun-like star. The part with the steepest temperature gradient is referred to as the 'transition region'. The increasing temperature with decreasing pressure seems to violate the Second Law of Thermodynamics since there can be no purely thermal process whose net effect is energy flow from a cooler to a hotter gas. This provokes the question: how is the chromosphere heated? Even though efficient cooling through continuum radiation ceases above the stellar photosphere (causing a temperature inversion such that $dT/dh > 0$), photospheric

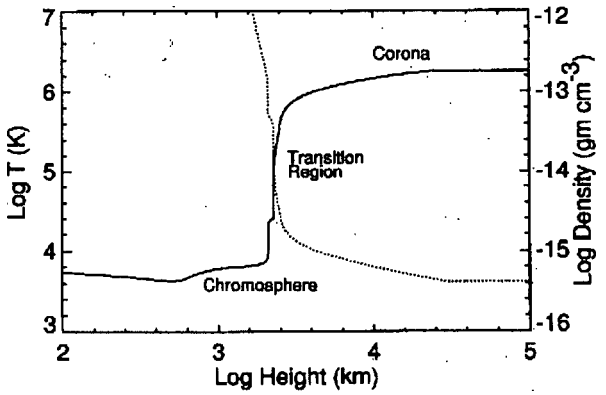

Figure 1.1 The temperature inversion (solid line) and density (dashed line) as a function of atmospheric height above the convection zone for the sun (Mariska 1992, reproduced by Carroll & Ostlie 1996).

radiation does not contain enough energy to heat the chromosphere to those temperatures (Böhm-Vitense 1989). Nonradiative sources of heat are required. Acoustic and magnetic energy are most likely the principal sources of this heating (Fawzy et al. 2002). Mechanical energy that originates from pressure fluctuations in the stellar convection zone[5] generates acoustic waves that dissipate through shocks as they hit the sharply decreasing density gradient at the base of the chromosphere. Since the depth of the convection zone is largely independent of stellar rotation, the acoustic energy produced depends mainly on the effective temperature and local gravity (Cuntz et al. 1999).

The generation of magnetic fields in a star, on the other hand, is best described by dynamo theory. As Cowling (1957) explains, the dynamo theory "ascribes the maintenance of the magnetic field to electric currents induced in the material as a result of its motion across the lines of force, so that there is a general resemblance to the behaviour of a self-exciting dynamo." Dynamos require a complex velocity-field structure in order to regenerate the magnetic field. A simple motion with finite conductivity would allow the field strength to decay. It is the complicated pattern of velocity fields within

[5]the turbulent outer layer which occupies $\sim$ 30% of the stellar radius in solar-mass stars

a star, mainly stellar convection and differential rotation, that maintain the dynamo action. A more rapidly rotating star generates stronger dynamos in its convection zone, therefore its stellar surface is more densely populated with magnetic fields.

Two mechanisms for heating the chromosphere and corona by magnetic fields have been identified, though it is not yet clear which of these two dominates. The first is heating by continuous energy dissipation of the changing magnetic field. The second is an intermittent contribution with the energy guided and then dissipated by magnetohydrodynamic waves (MHD or Alfvén waves). The energy propagates from the convection zone to reach the upper stellar atmosphere. Current theories suggest that the direct energy dissipation mechanism heats the closed-looped regions while MHD waves heat regions of open magnetic field lines (see reviews by Narain & Ulmschneider 1996 and Ulmschneider et al. 1991).

Despite the close proximity of the earth to the Sun, there is still not enough spatial resolution to clearly distinguish between acoustic and magnetic heating sources. Studying chromospheric activity of other stars has been more informative. Cuntz et al. (1999) simulated longitudinal and transverse MHD waves for a K2 V star to get the resulting total emission flux of the Ca II resonance lines (chromospheric activity indicators discussed further in Section 1.6) as a function of rotation period, P_{rot}. Figure 1.2 shows there is a clear correlation between Ca II emission and P_{rot} which agrees with observations. The dashed line is the theoretical 'Basal' flux level attributed solely to heating by acoustic waves. This figure suggests that the MHD-waves may be the dominant magnetic heating mechanism of chromospheres in dwarf stars.

1.5 Planet-Induced Stellar Activity

Cuntz et al. (2000) suggested that an increase in stellar activity induced by a nearby giant planet could take the form of enhanced tidal and/or magnetic heating of a star's outer atmosphere. The acoustic wave energy that contributes to the heating depends on the local turbulent velocity as v_t^8 (e.g. Musielak et al. 1994). The steepening of the density gradient in the two tidal bulges caused by the planet's presence would increase v_t, producing excess shocks, waves, and flows in the upper atmosphere. Secondly, if the planet has a sufficiently extensive magnetosphere, it could interact through

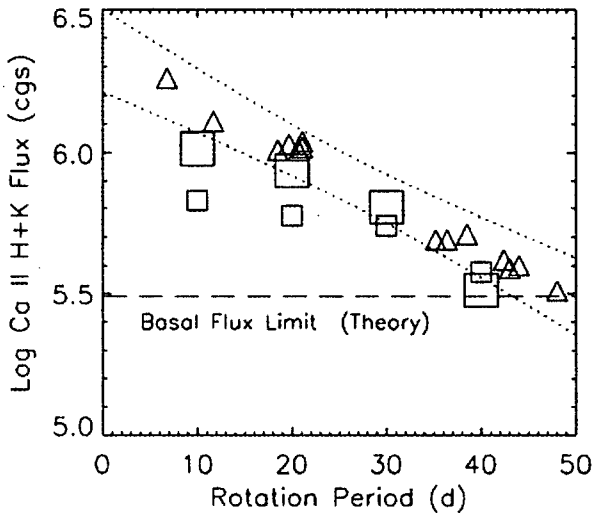

Figure 1.2 Ca II H + K emission flux as function of stellar rotation period. The triangles are observations for a set of stars with spectral type between K0V and K3V. The squares indicate the results from theoretical chromosphere models with both magnetic and acoustic heating for K2V stars. Large squares give the theoretical simulations for uniformly distributed magnetic flux tubes over the star. Small squares are models of tubes arranged in network regions. The dotted lines indicate the 3-σ flux limit errors of the observations. The dashed line is the theoretical Ca II H + K basal flux limit from pure acoustic heating (Cuntz et al. 1999).

reconnection with the stellar magnetic fields, also increasing v_t. Magnetic wave energy has a v_t^6 dependence (Ulmschneider & Musielak 1998), so even a modest increase in v_t would dramatically enhance local dynamo generation, magnetic energy and nonradiative heating.

If planet-induced heating is confined to a narrow range in stellar longitude, the heated regions will track the planet throughout its orbit. This implies that the period of any observed activity will depend on the planet's orbital period, P_{orb}. Tidally-induced activity, appearing in both tidal bulges, will have a period of $P_{orb}/2$ while localized magnetic activity will have a period of P_{orb}. It is also possible that the increased dynamo action is confined to the tachocline, the thin, rotationally sheared layer below the convection

zone. In this case, any dynamo-induced activity will extend over a wide range of longitudes, and the excess heating will not show strong periodic variation (Saar & Cuntz 2001). Magnetic interaction must also be a function of the magnetic field strengths of both the star and the planet ($\propto B_* B_p$ (Saar, Shkolnik & Cuntz, 2003), where B_p and B_* are the magnetic fields of the planet and star, respectively). It is expected that these planets have magnetic fields similar to Jupiter's (4.3 Gauss). However, if the planet is tidally locked its field might be substantially smaller due to its slower rotation. More sophisticated future models of planet-induced stellar activity can be combined with observations to make the first estimates of an extrasolar planet's magnetic field strength.

Since tidal and magnetic interactions depend on the distance from the planet to the star as $1/d^3$ and $1/d^2$ respectively, it is best to look at the closest (i.e. shortest period) systems. Also, magnetic interaction is likely greatest in the outermost layers of the star. This is so because these layers are physically much closer to the planet and their temperatures are dominated by magnetic heat sources. These imply that the magnitude of the heating should be greatest in the stellar corona. However, coronal activity indicators emit at far ultra-violet and X-ray wavelengths, so they are nearly impossible to observe from the ground. They require space-based observatories such the Far-Ultraviolet Spectral Explorer and the Chandra X-ray Observatory. We therefore chose to concentrate on the optical chromospheric activity indicators Ca II H & K of five of the short-period planetary systems.

Prior to this thesis, there was only brief mention of such planet-star interactions in the literature. Rubenstein and Schaefer (2000) observed "superflares" on nine single dwarf stars, suggesting that this increased activity could be attributed to interaction with unseen, giant, close-in planets. More recently, Santos et al. (2003) offered planet-induced activity (as first demonstrated by Shkolnik et al. 2002) as an explanation for photometric variations with a very similar period to the RV variations of the K dwarf HD 192263. The stability of the 24.4-day periodic radial velocity (Henry et al. 2002, Santos et al. 2003) through almost 4 years of data (Santos et al. 2000) rules out the interpretation that stellar activity alone is the cause of the RV curve and supports the existence of a planetary-sized companion around the star.

Even though the interpretation of Rubenstein & Schaefer (2000) and Santos et al. (2003) are uncertain, there exists ample observational evidence of such tidal and magnetic interactions in the exaggerated case of the RS Canum Venaticorum (RS CVn) stars, which are tightly-orbiting binary sys-

tems consisting of two chromospherically active late-type stars. For example, Catalano et al. (1996) found as many starspots and plages within the 45° around the sub-binary point[6] as on the rest of the stellar surface for several RS CVn systems. λ And, a relatively long-period system (P_{orb} = 20.1 d; Walker 1944), shows modulation of the Mg II UV chromospheric emission lines with a period of 10 days, half the orbital period. Glebocki et al. (1986) interpreted this as a tidal heating of the primary by its companion, possibly a brown dwarf (Donati et al. 1995). Furthermore, Lanza et al. (2001, 2002) reported on the long-term starspot evolution and correlation with orbital period for SZ Piscium and RT Lacertae. Both systems exhibit increased starspot activity at their sub-binary longitudes. This phenomenon is plausible since the common circularization and tidal locking (where $P_{orb} = P_{rot}$) in the RS CVn stars lead to increased stellar rotation and dynamo field generation (Catalano et al. 1996). In addition, ER Vul, composed of two almost identical solar-type stars with a 17-hour orbit, exhibits excess activity along the sub-binary longitudes on both stars (Piskunov 1996). This is seen in activity indicators Hα, the Ca II IR triplet, Mg I b lines as well as excess absorption in the He I D_3 line. (See Gunn & Doyle 1997, and references within.) Gunn & Doyle find that the activity arises in plage-like formation, possibly covering nearly half of the secondary's surface. We observed ER Vul as part of this thesis work in Ca II H & K and present the results in Chapter 5.

1.6 Ca II H & K as Chromospheric Activity Indicators

Light absorbed by the large opacity of resonance lines such as H I, Ca II, Mg II and the Lyman continuum of late-type stars re-radiates to cool the chromosphere such that temperatures in the chromosphere reach 20,000 K gradually over many scale heights. Most chromospheric indicators are UV emission lines which are not easily accessible from ground-based telescopes. However, the optical resonance lines of Ca II H & K at 3968 and 3933 Å ($4^2P_{1/2} \rightarrow 4^2S$ and $4^2P_{3/2} \rightarrow 4^2S$, respectively) exhibit chromospheric emission in late-type stars (i.e., later than F0). Because the strength of the lines

[6]The 'sub-binary' point refer to the longitude on the star that faces the binary system's centre-of-mass.

is dominated by collisional broadening, they are sensitive probes of temperature and electron density.

Figure 1.3 shows the sun's (a relatively inactive star) Ca II K reversal. The K1 feature stems from absorption at the top of the photosphere where the photon scattering outside the Doppler core is balanced between coherent and noncoherent scattering. The K2 feature is the double-peaked emission that is formed in the chromosphere at $\sim$ 8000 K where the source function is essentially monochromatic. The asymmetry of the emission is thought to be a consequence of up-flows in the chromosphere's plage-like regions. The central emission, K3, is produced at a temperature of $\sim$ 20,000 K (Montes et al. 1994), and appears as a self-reversal due to the large optical depth of the line. (See Linsky 1980 for a comprehensive review.)

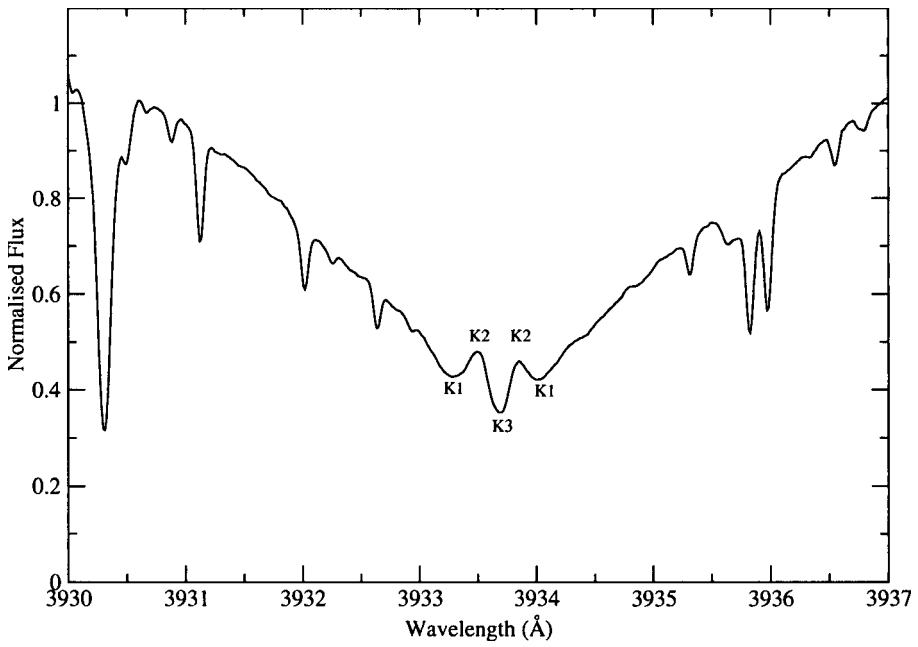

Figure 1.3 The solar Ca II K core normalised near 3930 and 3937 Å. The K1, K2 and K3 features are discussed in the text. The observation was made at the CFHT during our July 2002 run.

Ca II H & K emission is an optimal choice with which to monitor chromospheric activity and has become a classical activity diagnostic. The broad, deep photospheric absorption allows the H and K reversals to be seen at higher contrast. Furthermore, these lines are easily accessible from the ground. Since 1966, a group of astronomers at Mount Wilson Observatory has been dedicated to monitoring the flux of the cores of the Ca II H & K lines toward thousands of stars (e.g. Duncan et al. 1991). They have used two triangular bandpass filters, with a 1-Å full-width-half-maximum (FWHM) centered on the H and K cores and two rectangular filters, 20 Å wide, outside of the lines. A measurement index, S_{HK}, obtained from the ratio of the emission and the pseudo-continuum fluxes has been adopted as a standard measure for chromospheric activity.

Saar & Cuntz (2001) first attempted to search for planet-induced chromospheric heating by looking at seven stars with close-in giant planets (including τ Boo, υ And, and 51 Peg). They derived the infrared equivalent to the Mount Wilson S_{HK} index from spectra of resolution R = 50,000 and S/N typically of 200. They used the Ca II IR line at 8662 Å which shares an upper level with the Ca II H & K lines. They saw no clear $\geq 2\ \sigma$ detection of increased S_{IR} flux and set an upper limit at the 3 to 5% level.

1.7 Goals of this Thesis

The goal of this thesis was to search for night-to-night modulation in the Ca II H & K emission of stars that have known short-period (i.e., $P_{orb} < 5$ d) giant planets. As classic diagnostics of chromospheric activity, night-to-night modulation of the H and K reversals would imply that activity was stimulated on timescales shorter than stellar rotation periods or intrinsic activity cycles. If the modulation has a period comparable to that of the planet's orbit, then it is likely the planet is stimulating the activity through some tidal and/or magnetic mechanism.

The correlation of enhanced stellar activity with the orbital phase will provide information on the source and form of the interaction. Increased activity may be about the sub-planetary point (at $\phi = 0$, where the planet is between us and the star) or may exhibit a lag or lead about this phase. If so, this would reveal tidal friction effects and/or a delay in the reaction of the stellar chromosphere. Furthermore, such a detection will aid in setting the first estimates of the magnetospheric strengths of the extrasolar planets,

producing important constraints on planetary structural models. Finally, this method may provide the groundwork needed to use periodic chromospheric activity as a planet-searching method in chromospherically active stars for which the Doppler method does not work (Saar & Donahue 1997).

With the collaboration of Gordon Walker and David Bohlender, I undertook an observing program at the CFHT, to explore planet-star interaction. Our target stars have planets with orbital periods between 3.1 and 4.6 days, eccentricities $\simeq 0$ and semi-major axes < 0.06 AU. Stars with the closest-in planets offer the best chance of observing upper atmospheric heating. The five stars observed were τ Boo, HD 179949, HD 209458, 51 Peg and υ And. These stars were chosen because they are bright, are accessible by the CFHT throughout a night, and have orbital periods that can be covered during a single observing run. Stellar and orbital parameters for these five stars are listed in Table 2.1. The observations, data reduction and radial velocity measurements are described in Chapter 2. With the high resolution of the data, we achieved measurements of differential radial velocities (ΔRV) to better than 20 m s^{-1}, from which updated ephemerides, revised orbital periods and accurate orbital phases were derived.

After our first observing run at the CFHT, we attempted the experiment using the 1.2-m telescope at the Dominion Astrophysical Observatory (DAO) where longer observing runs were more easily attainable. Unfortunately, the 60 nights allocated for this project did not yield useful data even for our brightest target due to poor weather, lower resolution and low S/N.

We continued on with the CFHT. The results from three observing runs are presented in Chapter 3. Four of the 5 target stars monitored show night-to-night H & K modulation while our two standards, τ Ceti and the sun, which are known to lack close-in giant planets, show no such modulation within a 5-night observing run. HD 179949 exhibits the most convincing case for planet-induced activity and is further discussed in Chapter 4. In Chapter 5, the H & K observations and the phase-dependent chromospheric activity of ER Vul are presented. This system acts as an amplified example of planet-induced stellar activity. The results of our observations of another over-active dwarf star, κ^1 Ceti are discussed in Chapter 6. In Chapter 7, I summarize the conclusions and describe current and potential follow-up research programmes.

Chapter 2

Observations and Radial Velocity Measurements

2.1 The Spectra

No one has thus far predicted with any certainty the strength or character of tidal or magnetic interaction between a star and its close-in giant planet, largely for two reasons: first, the physics of chromospheric heating is not completely understood and secondly, no estimate for the strength or size of an extrasolar planetary magnetosphere exists.

Unsure of what level or form of activity to expect, we designed an experiment to search for modulation in the stellar Ca II H & K emission with the highest signal-to-noise (S/N) and spectral resolution available to us. These two criteria allowed for variations of both narrow and broad features to be detected to a fraction of a percent.

We first proposed to observe bright stars with short-period planets with the Canada-France-Hawaii 3.6-m telescope (CFHT) using Gecko, its high-resolution coudé spectrograph.[1] After the tantalizing results of this first observing run in 2001 August, it was apparent that the long-term monitoring of these systems would be very valuable. We then attempted the experiment using the medium-resolution McKellar spectrograph at the Dominion Astrophysical Observatory's (DAO) 1.2-m telescope where longer observing runs were more easily accessible. While poor weather reduced our allotted 60 nights to 15, observations of the brightest of our targets (51 Peg, υ And, and τ Ceti) proved not to be fruitful due to the poor S/N and lower resolution. We continued the program exclusively at the CFHT.

We were allocated 15 nights over three semesters at the CFHT, of which approximately 30% was lost to poor weather and instrument difficulties. The observations were made on 3.5, 4, and 2 nights in 2001 August, 2002 July and

[1] http://www.cfht.hawaii.edu/Instruments/Spectroscopy/Gecko/GeckoWebMan.html

2002 August, respectively. We used the Gecko échellette spectrograph fiber fed by CAFE (CAssegrain Fiber Environment) from the Cassegrain to Coudé focus (Baudrand & Vitry 2000). Spectra were centered at 3947 Å which was isolated by a UV grism (300 lines mm^{-1}) with $\simeq$60 Å intercepted by the CCD. The dispersion was 0.0136 Å $pixel^{-1}$ and the 2.64-pixel FWHM of the thorium-argon (Th/Ar) lines corresponded to a spectral resolution of R = 110,000. The detector was a back-illuminated EEV2 CCD (13.5 μm^2 pixels, 200 × 4500 pixels) with spectral dispersion along the rows of the device.

Because a number of pixels in the CCD suffer from non-linear dark signal, we took a large number of dark exposures with integration times matching those of the various stellar, Th/Ar and flat-field exposures. After three major reduction attempts, we decided on the following procedure which maintains the highest level of consistency and precision. Rather than using biases to remove the baseline from each observation, the appropriate mean darks were subtracted from all the exposures. Flat-fields were then normalised to a mean value of unity along each row. All the stellar exposures observed on a given night were combined into a mean spectrum to define a single aperture for the extraction of all stellar and comparison exposures, including subtraction of residual background between spectral orders (prior to flat-fielding). This aperture was ultimately used to extract one-dimensional spectra of the individual stellar and comparison exposures and of the mean, normalised flat-field. The extracted stellar and comparison exposures were then divided by the one-dimensional flat-field to obtain flat-fielded spectra. All the data were processed with standard IRAF (Image Reduction and Analysis Facility) routines[1]. The preliminary data reduction was done by David Bohlender. I calibrated the wavelength of the specta using the Th/Ar arcs and applied heliocentric and differential radial velocity corrections to each stellar spectrum using IRAF's *rvcorrect* routine. A specimen, flat-fielded spectrum of τ Ceti is shown in Figure 2.1. The Ca II H & K reversals are weak yet visible at 3968 and 3933 Å. The $\sim$ 20 Å of the spectrum used to measure the radial velocities is indicated in the figure.

Table 2.1 lists the five programme stars and the standard, τ Ceti, with their spectral types and U magnitudes plus details of the 2002 July observations such as average S/N and exposure time (used in the discussions of

[1]IRAF is distributed by the National Optical Astronomy Observatories, which is operated by the Association of Universities for Research in Astronomy, Inc. (AURA) under cooperative agreement with the National Science Foundation.

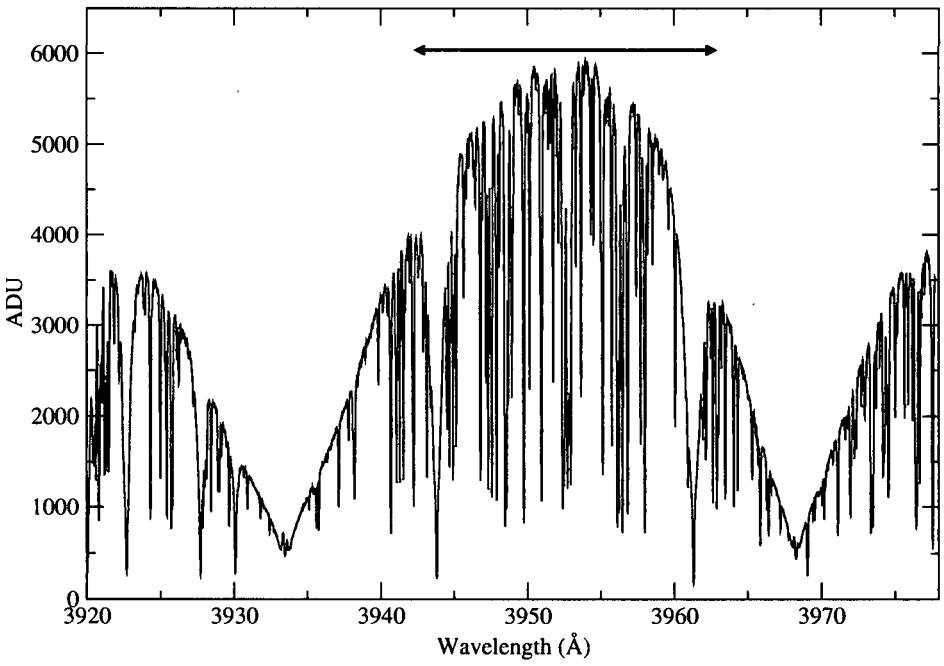

Figure 2.1 A single spectrum of τ Ceti flat-fielded as described in the text. The arrows define the 3942 – 3963 Å region bounded by two strong Al I lines which was used to measure the differential radial velocities (ΔRV).

Sec 2.2). Before each night, we obtained sky spectra of comparable S/N in order to use the sun as a second standard star. The orbital parameters of each system are also presented in Table 2.1.

Table 2.1. The Program Stars: 2002 July Observations

Star	Spectrum	U	Exp. time s	S/N[a]	n[b]	K_{max}[c] m s^{-1}	σ_{RV} m s^{-1}	$M_p \sin i$[c] M_J	P_{orb}[c] days	Semi-major axis[c] AU
τ Boo	F7 IV	5.02	1200	470	12	467	31 (18)[d]	3.87	3.3128	0.046
HD 179949	F8 V	6.83	2400	250	13	102	18	0.84	3.093	0.045
HD 209458	G0 V	8.38	2400	150	12	87	32 (18)[e]	0.69[f]	3.524738	0.045
51 Peg	G2 IV	6.36	1200	270	17	56	26 (18)[d]	0.47	4.2293	0.05
υ And	F7 V	4.69	1200	490	8	70	11	0.71[g]	4.617	0.059
τ Cet	G8 V	4.43	1200	620	10	–	9	–	–	–

[a]Nightly average per 0.0136 Å pixel in the continuum

[b]Number of spectra

[c]Published orbital solutions: τ Boo & υ And (Butler et al. 1997), HD 179949 (Tinney et al. 2000), 51 Peg (Marcy et al. 1996), HD 209458 (Charbonneau et al. 1999); K_{max} is the radial velocity amplitude.

[d]Value in brackets omits a single outlying point – see Figure 2.2 and discussion in Walker et al. (2003).

[e]Value in brackets omits two outlying points – see Figure 2.2 and discussion in Walker et al. (2003).

[f]Transiting system; $i = 86.1° \pm 0.1°$ (Mazeh et al. 2000)

[g]Closest of three known planets in the system

2.2 Differential Radial Velocities and Updated Ephemerides

Radial velocity measurements are of fundamental importance in astronomy. For stars, absolute radial velocities can be uncertain by as much as 1 km s^{-1} because of motion in the stellar photosphere. Differential radial velocities (ΔRV) can be much more precise, yielding important information about pulsation in single stars and masses for those in double or multiple systems. The most spectacular return from high precision radial velocities in the last decade has been the discovery of more than 100 planets.

As discussed in Section 1.2, imposing zero-velocity fiducials directly onto the stellar spectrum can lead to an RV precision of 3 m s^{-1}. For many programs it is not always possible or appropriate to include either suitable telluric lines (generally water vapor) or captive-gas lines. This is certainly true for the blue/ultra-violet region at high spectral resolution. In Walker et al. (2003) we demonstrated that, with minimal precautions, a precision of $\leq$ 20 m s^{-1} is possible for R > 100,000 with a fiber-fed spectrograph over runs lasting at least several nights and probably for much longer.

We became aware of that high precision is obtainable following our first observing run at CFHT in 2001 August when comparison arcs of thorium-argon gas were taken before and after each target. We realised that the radial velocity measurements would be vastly improved by taking more frequent arcs in order to track the CCD drift or any creaking in the system throughout the night. For the subsequent observing runs, a single Th/Ar arc was taken immediately before and after each stellar spectrum and, like the flat fields, was fed through the same fiber as the starlight. More comparison spectra should have been taken but time was extremely limited for this programme.

Radial velocities were estimated with the *fxcor* routine in IRAF which performs a Fourier cross-correlation on the dispersion-corrected spectra. We took the first spectrum in the series for each star as the template, hence, all ΔRV's are relative to the first spectrum on the first night of a the run. Both the template and the input spectrum were normalised with a low order polynomial and the correlation was taken over that part of the spectrum bounded by (and including) the two strong Al I lines (3942 – 3963 Å) as shown in Figure 2.1.

In Figure 2.2 the ΔRVs for the five '51 Peg' stars, as measured during the 2002 July run, are plotted as a function of relative orbital phase, and for

τ Ceti, as a function of time. The sine curves have the published planetary orbital period and velocity amplitude, K_{max}, and were shifted in phase and ΔRV to give the least-squares best fit. A pure sinusoid is sufficient since all five systems have eccentricity $e \leq 0.05$ (Schneider 2003). The sine-function yielded current orbital ephemerides and hence accurate phases (± 0.03) for each observation. Table 2.3 contains the 2002 July times of sub-planetary position along with the revised periods. For τ Ceti the best fit is to a line of constant velocity. Below each velocity curve are shown the ΔRV residuals from the curves. Note that, because the amplitude of the stellar reflex velocity is very different in each case, the individual ΔRV scales in Figure 2.2 (y-axis) vary widely. The RMS values (labeled σ_{RV}) corresponding to the residuals are listed in Table 2.1. The measurement error of the individual points is < 5 m s^{-1}. If four out of the 72 data points with $\sigma_{RV} > 100$ m s^{-1} are omitted, all of the σ_{RV}s are < 20 m s^{-1} and the two stars observed at the highest S/N have $\sigma_{RV} \sim 10$ m s^{-1}. This precision was unexpected and may be the best achievable for a single spectrum with this spectrograph.[2]

[2]A more detailed discussion of the RV measurements can be found in Walker et al. 2003.

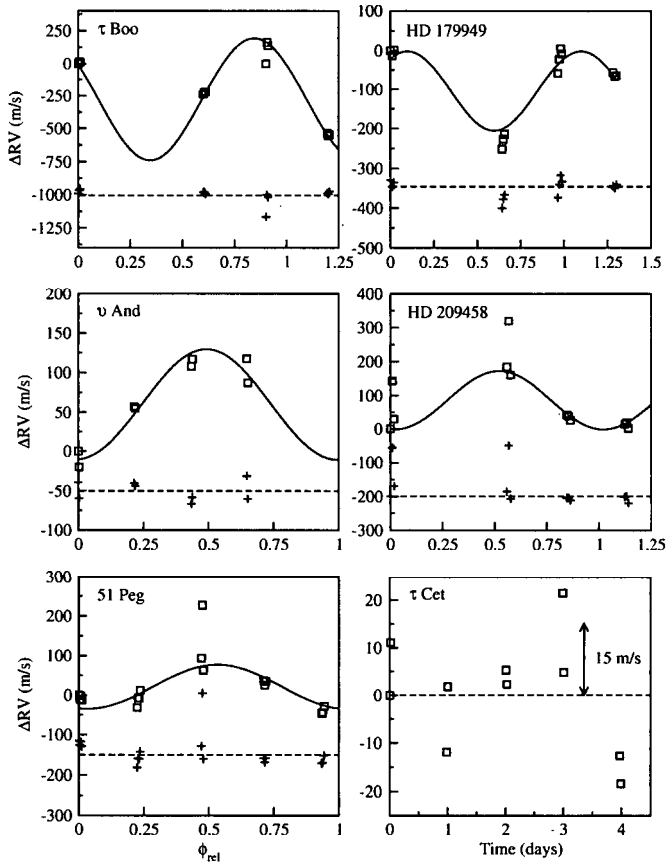

Figure 2.2 The differential radial velocities for the five '51 Peg' stars are plotted as a function of relative orbital phase, and the unvarying star, τ Ceti, as a function of time. The sine curves have the published planetary orbital period and K_{max} for each star (see Table 2.1) and have been shifted in phase to give the best fit to the ΔRVs. The measurement error of the individual points is < 5 m s^{-1}. The residuals of the ΔRV from the curves are shown below each one. A line of constant velocity is shown for τ Ceti which is plotted on a much smaller scale.

Table 2.2. Differential Radial Velocities for 2002 July Data

Star	HJD[a]	ϕ_{rel}[b]	ΔRV[c] m s^{-1}	|data − fit| [d] m s^{-1}
τ Boo	2452481.768	0.000	0	9
	2452481.785	0.005	13	35
	2452481.800	0.010	11	44
	2452483.758	0.601	−239	19
	2452483.774	0.605	−223	21
	2452483.790	0.610	−223	8
	2452484.755	0.902	−1	166
	2452484.771	0.906	162	2
	2452484.787	0.911	137	17
	2452485.733	1.197	−538	13
	2452485.749	1.202	−554	7
	2452485.765	1.206	−547	26
HD 179949	2452481.833	0.000	0	20
	2452481.863	0.010	−13	4
	2452481.896	0.020	1	15
	2452483.821	0.643	−251	50
	2452483.844	0.650	−227	27
	2452483.867	0.658	−215	16
	2452484.818	0.965	−58	23
	2452484.842	0.973	−21	10
	2452484.865	0.980	5	33
	2452484.887	0.988	−8	17
	2452485.797	1.282	−57	6
	2452485.827	1.291	−67	1
	2452485.856	1.301	−64	10
HD209458	2452481.922	0.000	0	1
	2452481.953	0.009	143	144
	2452481.983	0.017	29	31
	2452483.892	0.559	185	14
	2452483.923	0.568	320	151
	2452483.954	0.577	161	7
	2452484.906	0.847	42	4
	2452484.936	0.855	39	3

Table 2.2 (cont'd)

Star	HJD[a]	ϕ_{rel}[b]	ΔRV[c] m s^{-1}	|data − fit| [d] m s^{-1}
	2452484.966	0.863	27	12
	2452485.882	1.124	15	1
	2452485.913	1.132	19	1
	2452485.943	1.141	2	20
51 Peg	2452482.018	0.000	0	34
	2452482.034	0.004	−11	24
	2452482.050	0.008	−2	33
	2452482.068	0.012	−14	21
	2452482.967	0.224	−32	32
	2452482.983	0.228	−8	9
	2452482.998	0.232	−8	11
	2452483.016	0.236	12	8
	2452484.013	0.472	93	21
	2452484.029	0.475	227	155
	2452484.045	0.479	62	11
	2452485.026	0.711	37	8
	2452485.043	0.715	25	18
	2452485.059	0.719	34	8
	2452485.971	0.934	−46	21
	2452485.987	0.938	−45	19
	2452486.009	0.943	−29	2
υ And	2452483.067	0.000	0	11
	2452483.082	0.003	−20	9
	2452484.059	0.215	57	10
	2452484.075	0.218	55	6
	2452485.073	0.435	108	17
	2452485.089	0.438	117	8
	2452486.055	0.647	118	19
	2452486.071	0.651	87	10
τ Ceti	2452482.115	–	0	0
	2452482.131	–	11	11

Table 2.2 (cont'd)

Star	HJD[a]	ϕ_{rel}[b]	ΔRV[c] m s^{-1}	|data − fit| [d] m s^{-1}
	2452483.101	–	−12	12
	2452483.117	–	2	2
	2452484.125	–	5	5
	2452484.141	–	2	2
	2452485.107	–	22	22
	2452485.123	–	5	5
	2452486.089	–	−13	13
	2452486.106	–	−18	18

[a]Heliocentric Julian Date for mid-exposure time

[b]Orbital phase relative to the first spectrum using revised ephemerides listed in Table 2.3

[c]Differential radial velocities measured relative to the first spectrum of the series

[d]Residuals to the best-fit sine curve

Table 2.3. 2002 July Ephemerides

Star	HJD at $\phi = 0$ days	δ(HJD)[a] days	Revised P_{orb} days	$\delta(P_{orb})$[a] days
τ Boo	2452478.770	0.099	3.31245	0.00033
HD 179949	2452479.823	0.093	3.09285	0.00056
HD 209458	2452481.129	0.106	3.52443	0.00045
51 Peg	2452481.108	0.127	4.23067	0.00024
υ And	2452481.889	0.139	4.61794	0.00064

[a]Uncertainties in the respective measurements

Chapter 3

Modulation of Ca II Emission

3.1 Timescales of Stellar Activity

Stellar activity timescales vary greatly depending on the source of the activity. On the sun, phenomena develop on timescales of hours to decades, ranging from short-lived flares to the well-known 11-year activity cycle. Sunspots typically last just one 27-day rotation or less, but it is possible that large sunspot groups can last a couple of months. Aside from the actual lifespan of the surface features, changes can also be observed due to the sun's rotation as a feature simply rotates in and out of sight.

The stars in this observing programme are generally sun-like and therefore solar-type of activity is expected. When monitoring their Ca II emission, intrinsic stellar activity will also appear along with any potential activity stimulated by the planet. It is key to discern the two potential contributors to modulated chromospheric emission.

The star with the shortest rotation period in our sample is τ Boo. It has the largest $v\sin i$ and is believed to be in synchronous rotation with its tightly-orbiting planet ($P_{rot} = 3.2 \pm 0.5$ d, Henry et al. 2000; $P_{orb} = 3.3128 \pm 0.0002$ d, Butler et al. 1997). In this case, observed nightly activity is for the most part a consequence of the star's rotation of 112° per day. For the other targets that have longer rotation periods ($P_{rot} \geq 3P_{orb}$), changes in activity seen over just one night are probably not due solely to the star's rotation. The nightly variations may indicate planet-induced activity such as flaring or hotspots. If coupled to the planet, the localized activity may not be short-lived, but may be travelling on the stellar surface faster than the star is rotating as it tracks the planet in its orbit.

Nightly modulation of the Ca II H & K emission over one observing run is a glimpse into a star's short-term chromospheric variability. Increasing the baseline to over a year between observations allows characterisation of the star's longer-term activity cycle. Both are important. Until now, planet-star interaction has never been observed and is still very much not understood.

A clearer picture will emerge by monitoring these systems long enough for the stellar long- and short-term activity cycles to become better determined.

3.2 A Comparison of Ca II Emission

3.2.1 Extracting the H, K and Al I Lines

The spectral region near the very strong Ca II H & K lines has a suppressed stellar continuum making it difficult to normalise each 60-Å spectrum consistently. For this reason, a specific analysis by which to isolate any nightly modulated Ca II emission was devised. For each star, portions of the spectra centered on Ca II H and K, each 7 Å wide, were extracted. Figure 3.1 shows the spectral ranges used on a flat-fielded spectrum of HD 179949. The 7-Å width was chosen such that we could isolate the H and K reversals while minimizing any continuum differences from varying illumination of the CCD. This window is also wide enough such that a few photospheric absorption features are included, which can be tested for variability as well.

Also, 7-Å and 2-Å cuts, centered on the strong photospheric Al I line at 3944 Å, were used as internal standards. The first includes a range of photospheric absorption lines while the second looks at just the Al I line which has a comparable depth to the Ca II H & K lines. To normalise each sub-spectrum, the end points were normalised with a straight line. The spectra were grouped by date and a nightly mean was computed for each of the three lines. The spectrum centered on the Al I line of HD 179949 is shown in Figure 3.2 (top). Below it are the residuals relative to the normalised mean of the 2002 July data set. The RMS of the Al I residuals for each star is less than 0.0005 of the normalised mean. These are representative of the Al I residuals for all stars in all three runs, demonstrating both the level of stellar photospheric stability as well as the reliability of the data reduction and analysis. Within each night, the spectra in the H and K lines was stable to the 0.001 level on average. Figure 3.3 shows intra-night residuals (relative to the nomalised mean of that night) for the K core of HD 179949 for spectra taken on a night in 2001 August and a night in 2002 August. The K emission intra-night noise (which on average is twice that of the variations in the Al line) is due to minor, short-term intrinsic stellar activity changes and ranges from 0.0001 to 0.0014.

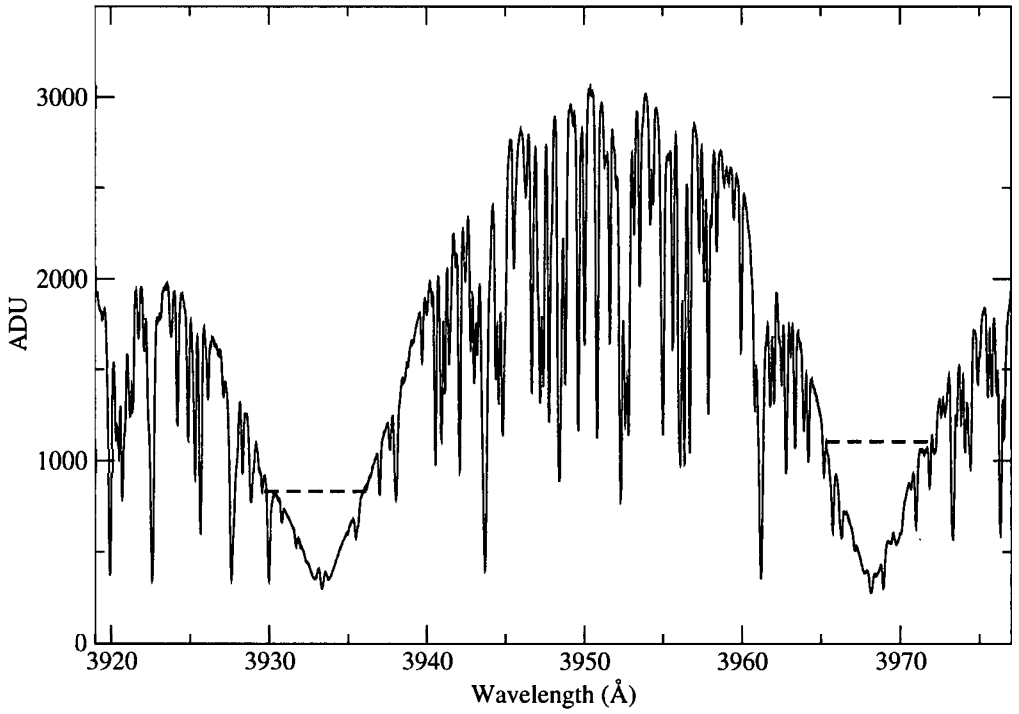

Figure 3.1 A single 40-minute flat-fielded spectrum of HD 179949. The dashed lines represent the 7-Å range used for normalisation of the H and K cores.

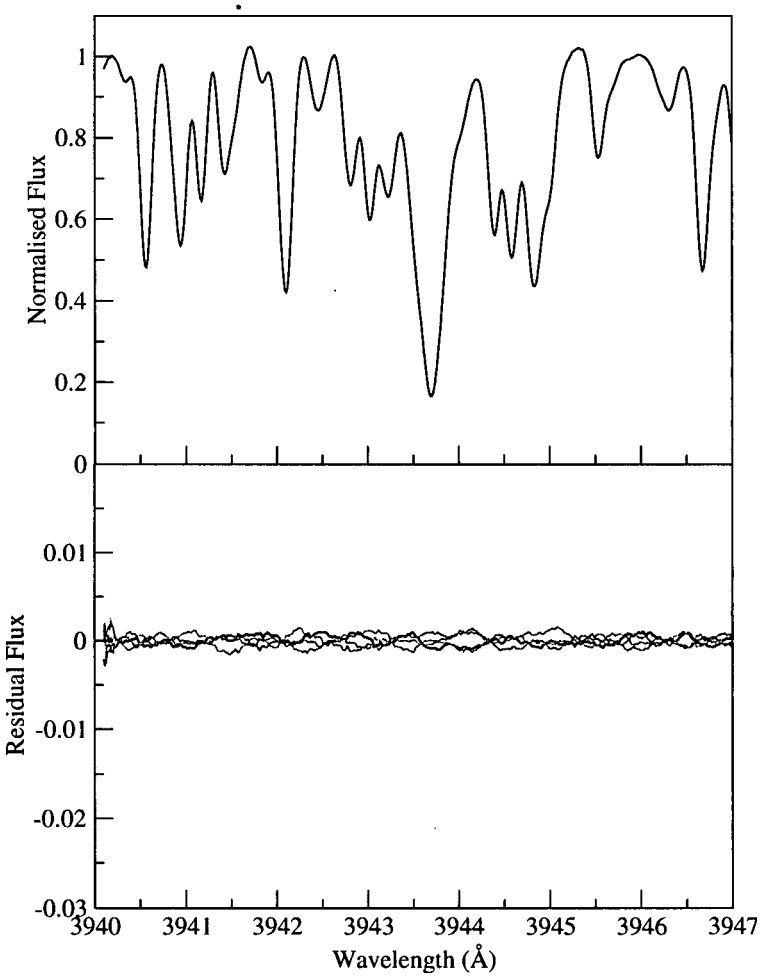

Figure 3.2 Top: the mean normalised 7-Å cut centered on the Al I line of HD 179949. Bottom: the residuals (smoothed by 21 pixels) relative to the normalised mean from the 5 nights of the 2002 July data set.

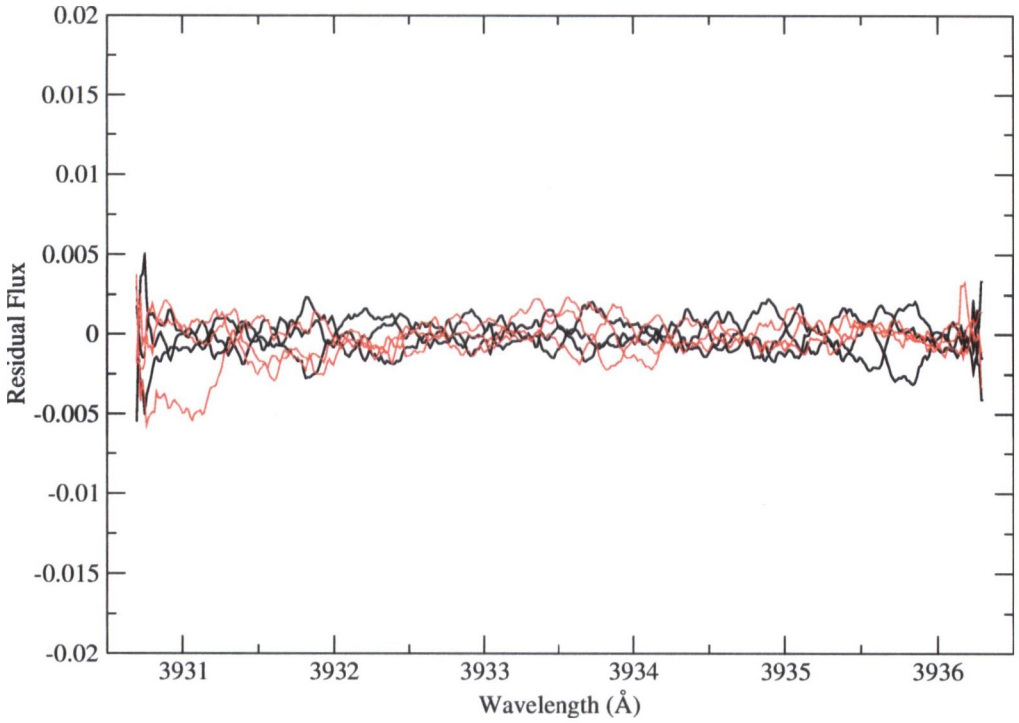

Figure 3.3 HD 179949 intra-night residuals for spectra taken during a night in 2001 August (black) and a night in 2002 August (red).

3.2.2 Dependence on Stellar Global Parameters

The program stars were originally chosen for Doppler planet searches in part because of their weak chromospheric emission as indicated by the modest Mt. Wilson S_{HK} index (Baliunas et al. 1995). Still, there are marked differences in the reversal structure of each of these stars. The mean Ca II K cores for target stars are shown in Figure 3.4. (The sun's spectrum was shown in Figure 1.3.)

Approximately 70% of the integrated H & K flux is photospheric emission and depends mainly on the effective temperature (T_{eff}) and local gravity ($log(g)$). These two parameters (listed in Table 3.1) do not vary widely from one programme star to another implying that the photospheric flux contribution remains relatively constant throughout the sample. Therefore, it is the different stellar rotation rates that affect the chromospheric contribution, producing the range of emission strengths.

I measured the integrated flux of the average, normalised Ca II K core bounded by the K1 features (see Figure 1.3). This measurement is essentially and equivalent width which includes both the photospheric and chromospheric emission. The integrated flux is listed in Table 3.1 and plotted against its projected rotational velocity, $v\sin i$, in Figure 3.5. Even with the small number of programme stars, there is a reasonable linear relationship between stellar activity and $v\sin i$ (Pasquini et al. 2000). The non-zero intersection of the line indicates the base photospheric flux level. HD 179949's K flux is about twice that expected by the trend. The differences in the photospheric contribution due to varying T_{eff} are not large enough to account for this as there is no correlation between the stars' T_{eff} and Ca II K emission. This implies that HD 179949's K emission is anomalously high for its $v\sin i$. The sun lies above the trend line as well, but this is an effect of increased activity seen during the 2002 observing runs.[1]

[1] We observed the naked-eye sunspot grouping of 2002 July and August in transit during our CFHT run with the Sunspotter® Solar Telescope supplied by the Visitor Information Center at the Onizuka Center for International Astronomy.

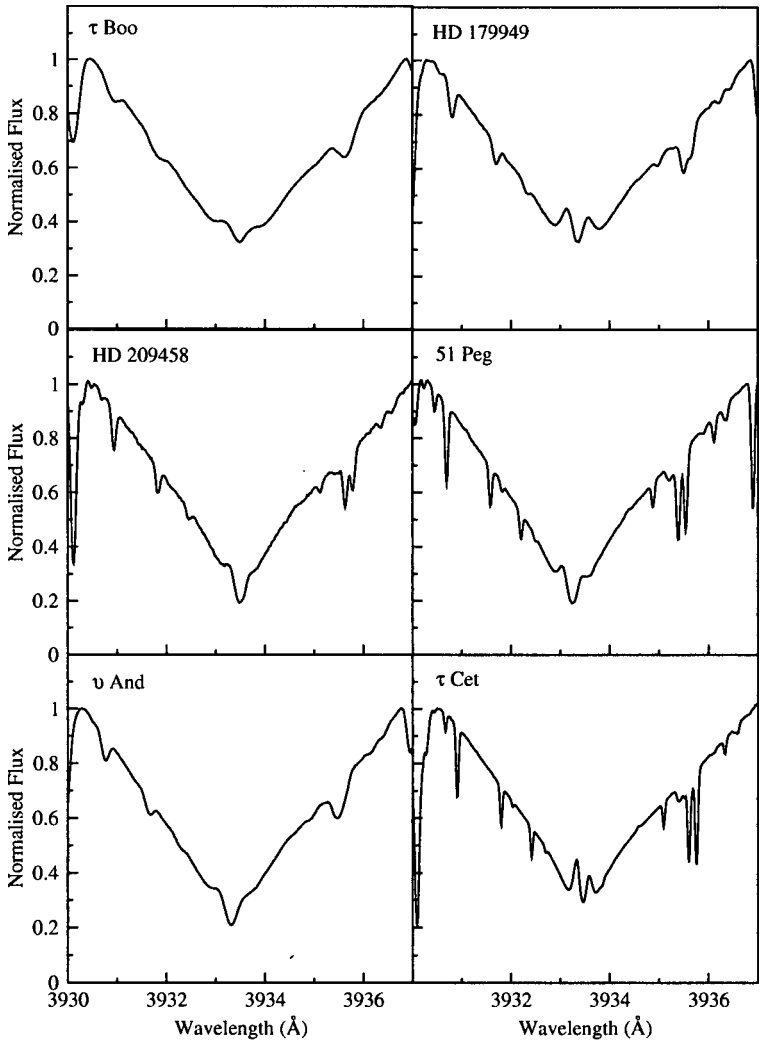

Figure 3.4 The mean normalised Ca II K cores for the programme stars.

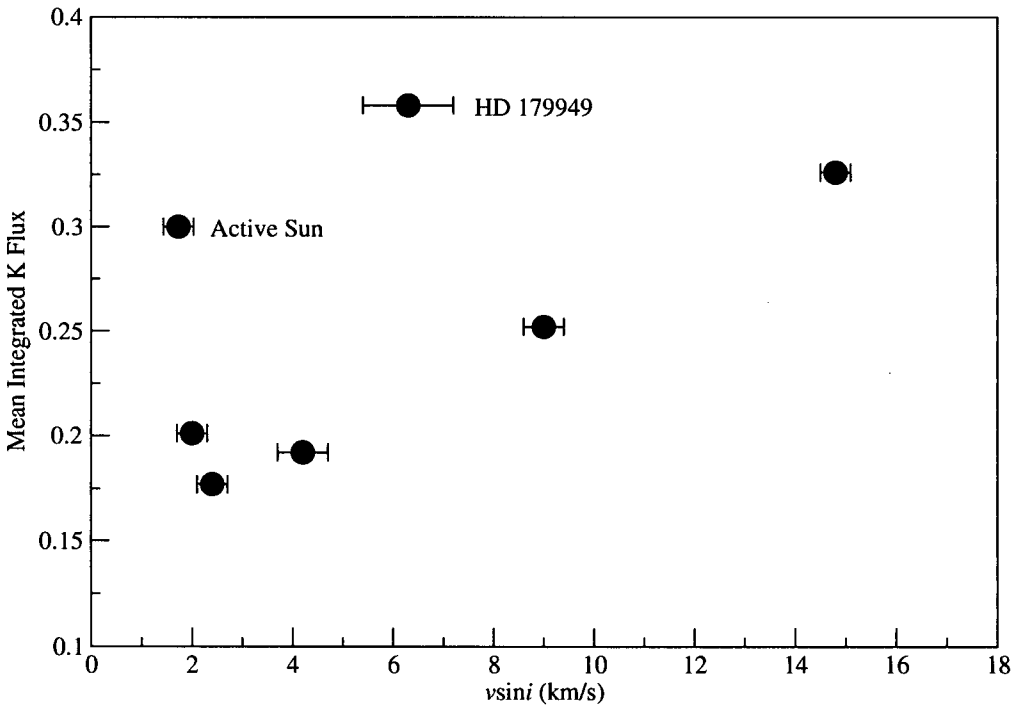

Figure 3.5 Published $v\sin i$ values for the program stars plotted against the integrated flux of the mean normalised Ca II K cores in units of normalised flux Angstroms. The measurement errors in flux are $\pm$ 0.006 and are within the size of the points. (Values are listed in Table 3.1.)

Table 3.1. Basic Stellar Parameters and Ca II K Emission

Star	T_{eff} K	$log(g)$ cgs	P_{rot} day	$vsini$ km s^{-1}	K Flux [a] Å	σ_K [b] Å	MAD K[c] Å	δ(MAD K)[d]	MAD H[c] Å	Sources [e]
τ Boo	6380	4.30	3.2	14.8 ± 0.3	0.326	0.0055	0.0046	0.0005	0.0029	1,2,3,4
HD 179949	6235	4.41	<9[f]	6.3 ± 0.9	0.358	0.0093	0.0054	0.0007	0.0036	5,6,7,6
HD 209458	6082	4.33	15.7	4.2 ± 0.5	0.192	0.0025	0.0024	0.0007	0.0020	8,2,9,8
51 Peg	5760	4.18	21.9	2.4 ± 0.3	0.177	0.0011	0.0010	0.0004	0.0004	3,2,3,10
υ And	6170	4.10	14[g]	9.0 ± 0.4	0.252	0.0050	0.0044	0.0004	0.0024	1,2,3,4
τ Cet	5250	4.50	>28[e]	< 2	0.201	0.0003	0.0005	0.0006	0.0003	2,2,11,11
Sun	5777	4.44	27	1.73 ± 0.3	0.300	0.0039	0.0035	0.0003	0.0021	2,2,10,10

[a]Total integrated flux bounded by the K1 features of mean normalised Ca II K core (as shown in Figure 1.3).

[b]The standard deviation is a measure of night-to-night K flux variation for each star.

[c]Integrated "intensity" of the mean absolute deviation (MAD) of the K and H residuals.

[d]The mean absolution deviation outside of the emission cores, which scales inversely with S/N.

[e]The sources of the values given for T_{eff}, $log(g)$, P_{rot}, and $vsini$, respectively. References: (1) Gimenez 2000; (2) Cayrel de Strobel 1996; (3) Henry et al. 2000; (4) Gray 1986; (5) Vogt et al. 2000; (6) Groot et al. 1996; (7) Tinney et al. 2001; (8) Mazeh et al. 2000; (9) Gonzalez et al. 2001; (10) François et al. 1996; (11) Fekel 1997.

[f]P_{rot} is calculated from the $vsini$ and stellar radius (see Section 4.2.1). The other rotation periods were measured photometrically or spectroscopically.

[g]Value considered uncertain.

3.2.3 Mean Absolution Deviation of Night-to-Night Residuals

To isolate the chromospheric activity of the reversals, nightly residuals were calculated from the average spectrum of all the data. The 9 spectra of the K-core of HD 179949 are overlaid in Figure 3.6. Each residual spectrum had a broad, low-order curvature removed which was an order of magnitude less than the variations in the H and K lines discussed below. The residuals of the normalised spectra (smoothed by 21 pixels) were used to calculate the Mean Absolute Deviation (MAD = $N^{-1}\Sigma|data_i - mean|$ for N spectra). Figure 3.7 (top) shows the MAD plot for HD 179949 with the corresponding K-core superimposed. The nightly residuals used to generate the MAD plot are displayed just below. The identical analysis described above was performed on the Ca II H line. As the two lines share the same upper level and connect to the ground state, stellar activity must be seen in both. The MAD plot and residuals of HD 179949's H-core are shown in Figure 3.8. where activity is also apparent in the Balmer line Hϵ at $\approx$ 3970 Å. This line is also known to be a chromospheric activity indicator and correlates well with Ca II K emission for active stars as shown by Montes et al. (1996).

The MAD plots for the other stars are displayed in Figure 3.9. The activity seen in four of the five stars with planets, HD 179949, τ Boo, υ And and HD 209458, shows significant deviations in the H & K reversals. The residuals for the latter three are plotted in Figures 3.10 – 3.12. The widths of their MAD peaks are the same as those of the reversals themselves, as illustrated in Figure 3.7 for HD 179949. This is yet another indication (as is the stability of the Al I lines) that the variability is confined to the stellar chromosphere.

In the sun's case, images from the Michelson Doppler Imager (MDI) aboard the Solar Heliospheric Observatory[2] (SOHO) confirm the increase in activity in 2002. The magnetograms taken during our 2001 August, 2002 July and 2002 August runs are reproduced in Figure 3.13. The Doppler-shifted light from the receding active regions is apparent in the asymmetry of the solar MAD plot. Most importantly, the sun did not show any daily variation within a single observing run to the same level of stability as τ Ceti.

The strong coherence between the H and K activity is apparent in Figure 3.14 where the integrated "intensity" of the mean absolute deviation for

[2]http://sohowww.nascom.nasa.gov/ and http://soi.stanford.edu/

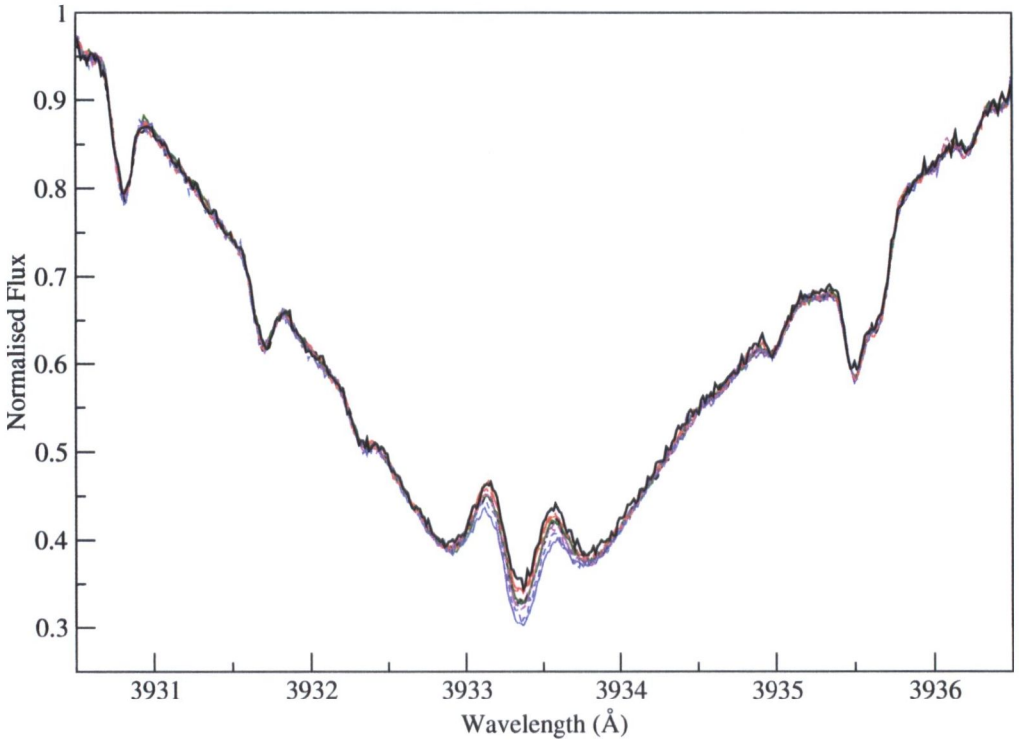

Figure 3.6 The Ca II K cores (unsmoothed) of HD 179949 for 9 nights of data from 2001 August, 2002 July and 2002 August. The phase of each curve is labeled in Figure 4.5.

the H and K cores, also bound by the K1 features, is plotted for each star. The slope of the best-fit line is 0.665. This agrees with the ratio of the total absorption of the two lines, H/K = 0.64 (Sanford & Wilson 1939).

Figure 3.15 shows a clear correlation between the intrinsic mean Ca II K emission and the integrated MAD intensity. This indicates that for our sample of stars, the more intrinsically active the star, the larger is its nightly modulation. The diagram also offers an explanation for the apparent inactivity of 51 Peg, a slow rotator with the lowest mean Ca II K emission.

3.3 Nightly Modulation with Orbital Phase

As seen in the MAD plots of Figures 3.7 (top) and 3.9, four of the five program stars show significant chromospheric activity over the three observing runs while the standard, τ Ceti, shows no such modulation. Of the four 'active' stars, HD 179949 has the strongest level of activity, which (as will be discussed in the next chapter) correlates with orbital phase during all three observing runs. The case is not as clear for the other stars, τ Boo, υ And and HD 209458. In Figures 3.16 – 3.18, their integrated flux of the normalised K residuals is plotted against orbital phase. As the phase dependence of the activity is not consistent from run to run, it is difficult to ascribe it to a particular source. Individually, each epoch may offer some insight, but the overall picture is far from clear. One thing that is clear from the various stability tests is that these variations are intrinsic to the stellar chromosphere and are not systematic effects.

τ Boo is the only star believed to be tidally synchronised with its planet ($P_{rot} \simeq P_{orb}$). This would make any periodic chromospheric activity of 3.3 days difficult to attribute to the planet, as it is possible that intrinsic stellar activity is modulated exclusively by stellar rotation. In this case, the longevity and orbital phasing of any enhanced emission would be the discerning factors. Looking at the individual observing runs in Figure 3.16, both the 2001 August and 2002 July data show an increase in activity near the sub-planetary point relative to the other observations in their respective runs. However, this is not the case for the 2002 August observations when the relative enhancement occurs at $\phi \approx 0.4$. This inconsistency does not allow us to make any conclusions about planet-induced heating. However, the night-to-night variations are still large, which indicates an excess of activity for such a dwarf star.

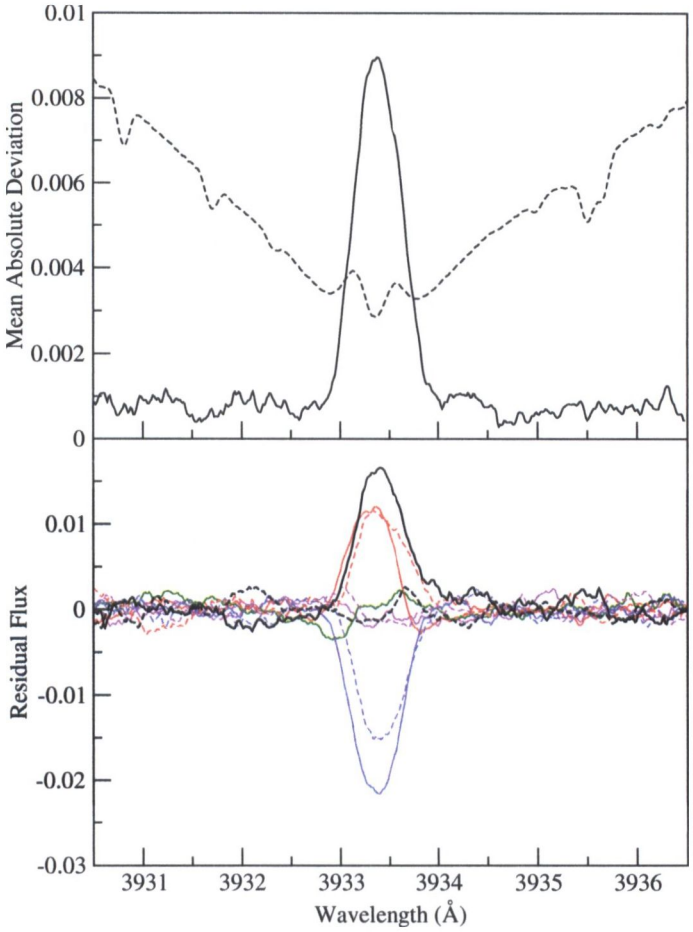

Figure 3.7 Top: the mean absolute deviation (MAD) of the Ca II K core (solid line) of HD 179949. The units are intensity as a fraction of the normalisation level. Overlayed (dashed line) is the mean spectrum (scaled down) indicating that the activity in HD 179949 is confined to the K emission. Bottom: residuals (smoothed by 21 pixels) from the normalised mean spectrum of the Ca II K core of HD 179949. The phase of each curve is labeled in Figure 4.5.

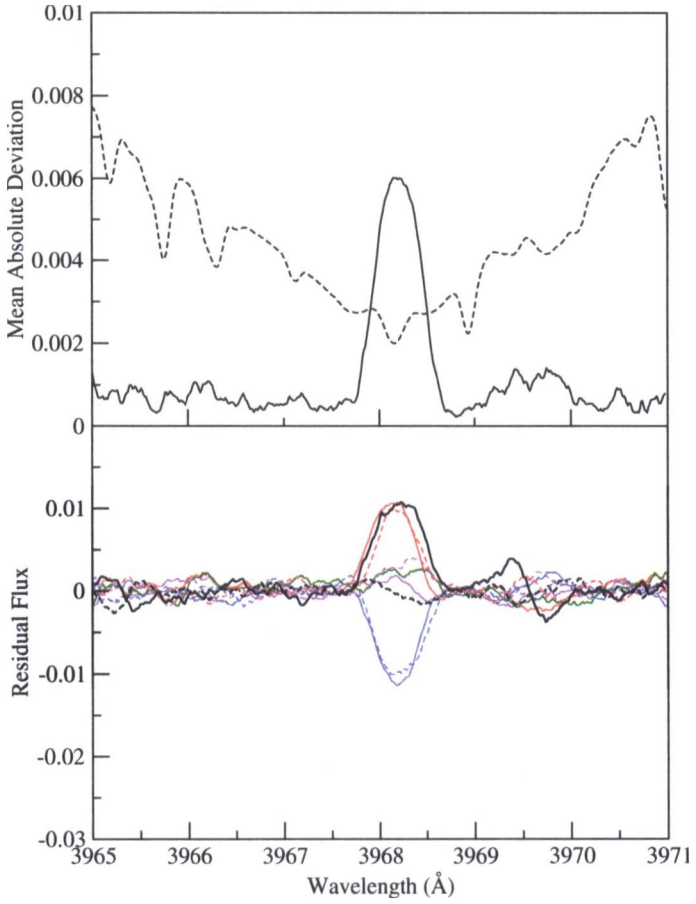

Figure 3.8 Top: the mean absolute deviation (MAD) of the Ca II H core (solid line) of HD 179949. The units are intensity as a fraction of the normalisation level. Overlayed (dashed line) is the mean spectrum (scaled down) indicating that the activity in HD 179949 is confined to the H emission. Bottom: residuals (smoothed by 21 pixels) from the normalised mean spectrum of the Ca II K core of HD 179949. Some variation is also seen in Hϵ at $\approx$ 3970 Å. The phase of each curve is labeled in Figure 4.5.

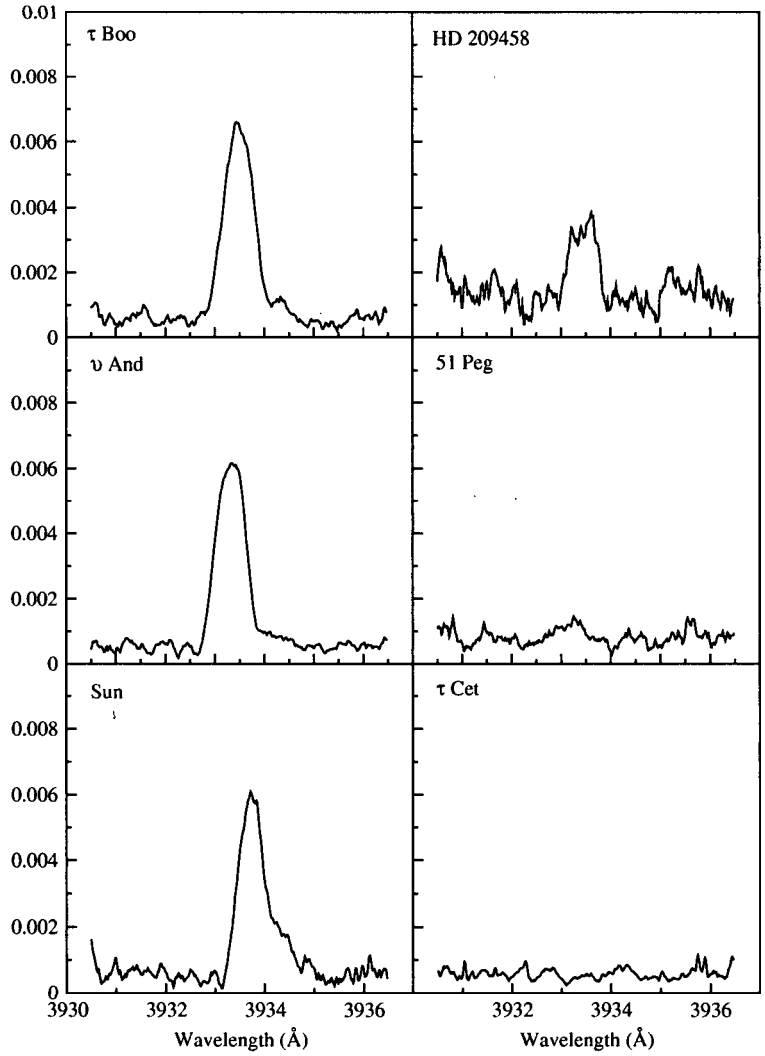

Figure 3.9 MAD plots for the other six programme stars. Units are intensity as a fraction of the normalisation level.

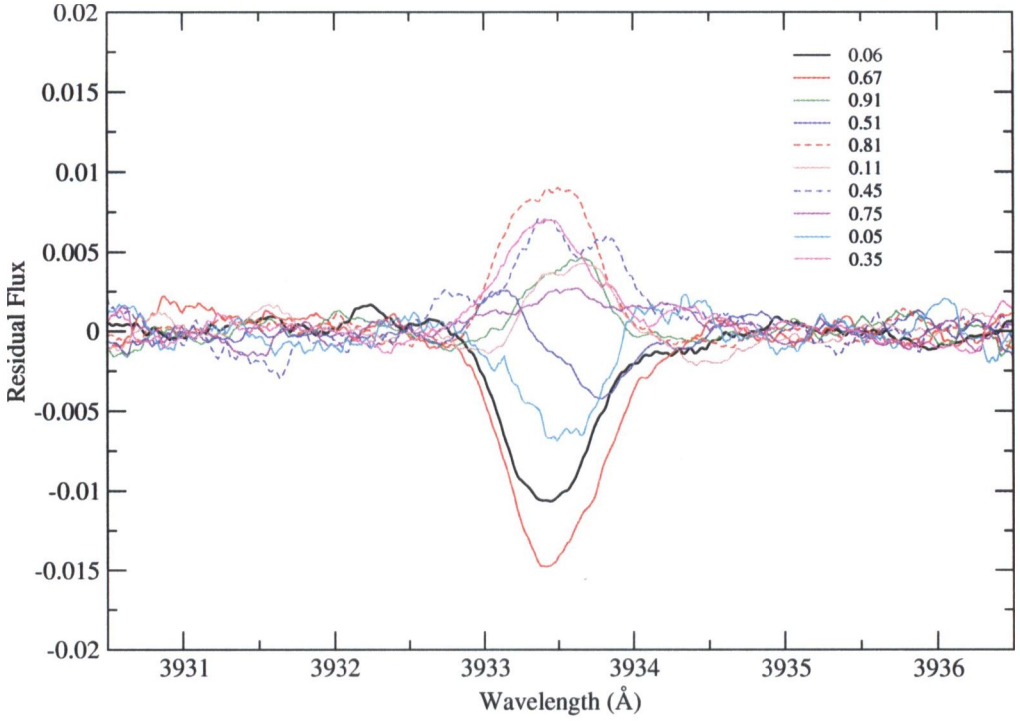

Figure 3.10 Residuals (smoothed by 21 pixels) from the normalised mean spectrum of the Ca II K core of τ Boo. The orbital phases are listed for each curve.

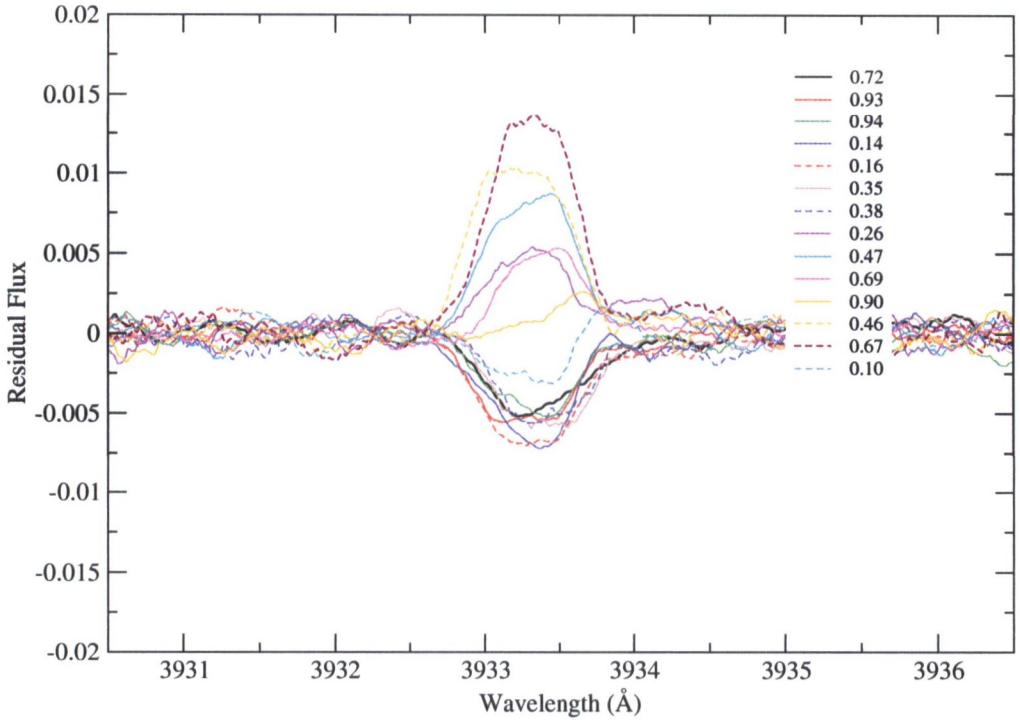

Figure 3.11 Residuals (smoothed by 21 pixels) from the normalised mean spectrum of the Ca II K core of υ And. The orbital phases are listed for each curve.

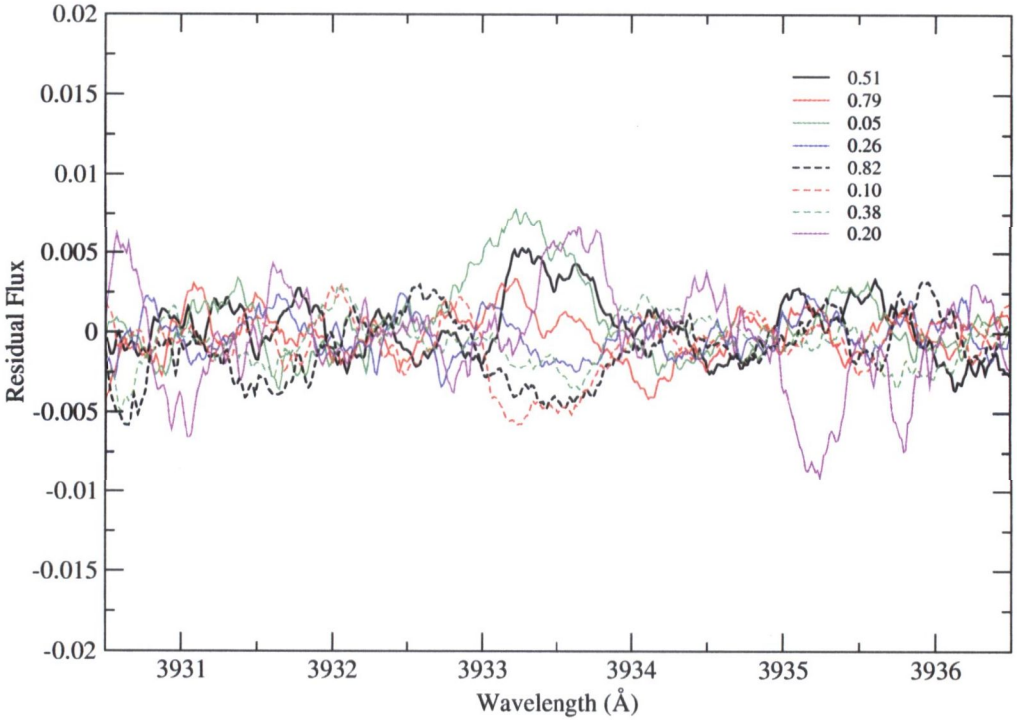

Figure 3.12 Residuals (smoothed by 21 pixels) from the normalised mean spectrum of the Ca II K core of HD 209458. The orbital phases are listed for each curve.

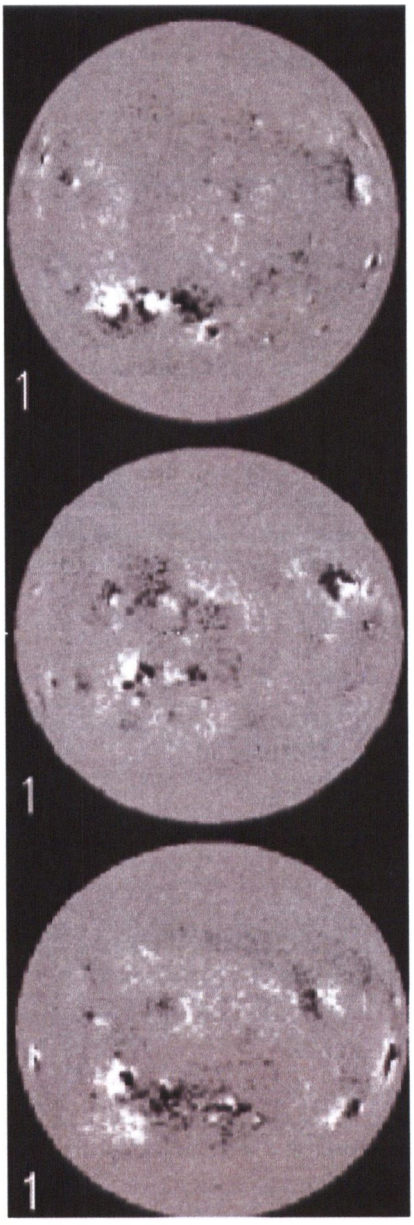

Figure 3.13 SOHO-MDI magnetograms of the sun taken during our 2001 August (top), 2002 July (middle) and 2002 August (bottom) observing runs (http://sohowww.nascom.nasa.gov/). The bottom two images show more solar activity than the top one from the year before.

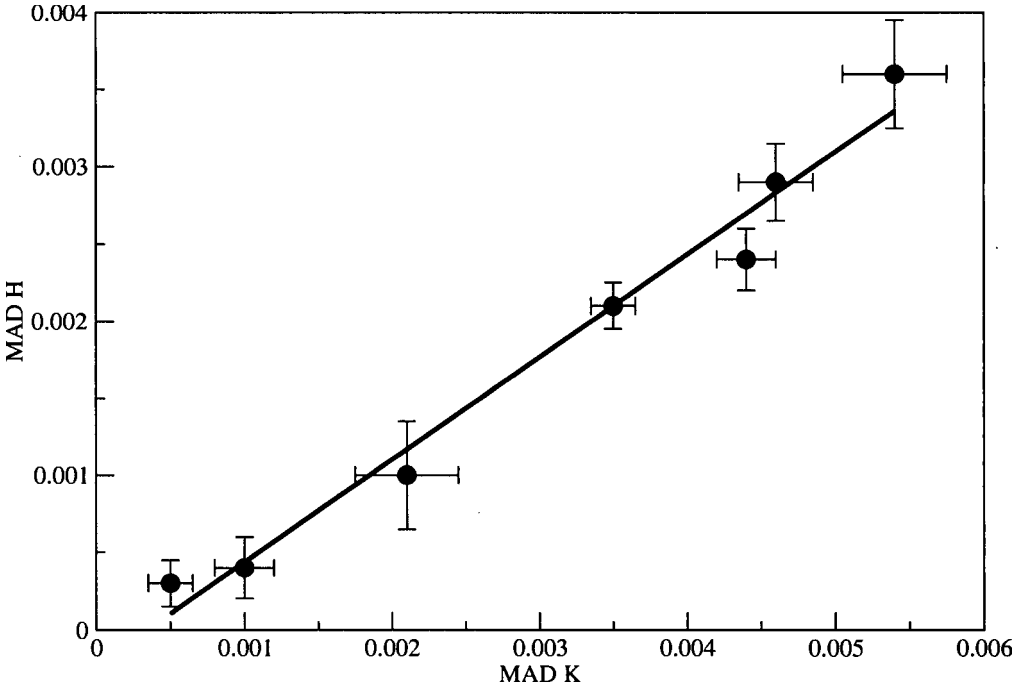

Figure 3.14 Integrated "intensity" of the MAD of the H and K residuals for the program stars. The slope of the best-fit line is 0.665 as expected since the ratio of the line strengths of H to K is close to 2/3.

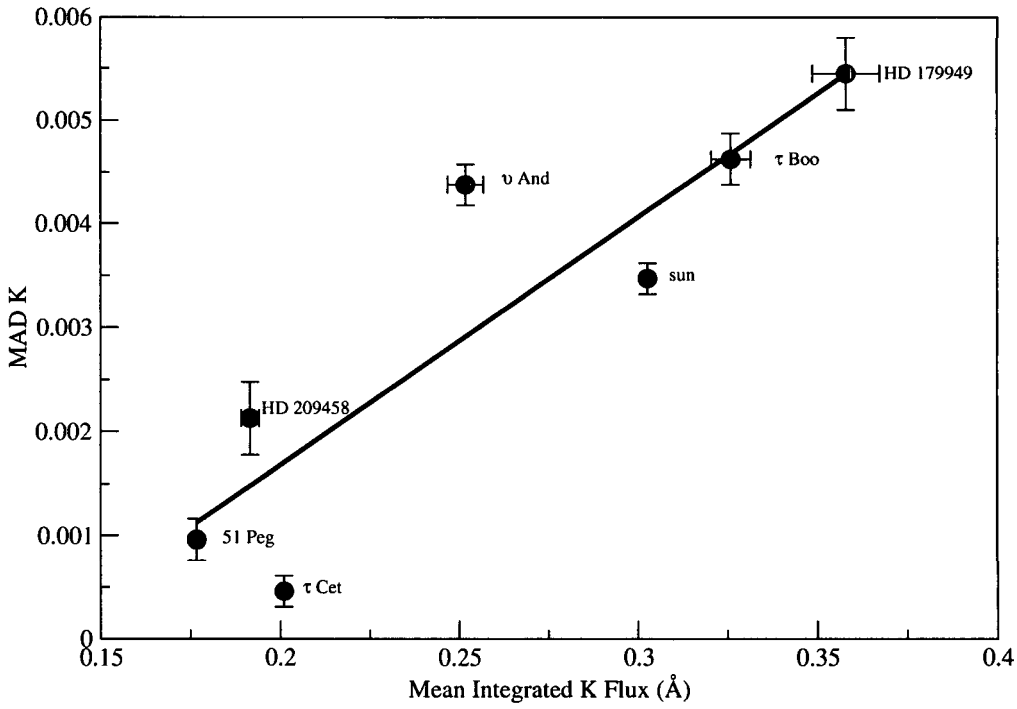

Figure 3.15 The integrated "intensity" of the MAD of the K residuals plotted against the integrated mean K flux for the programme stars. The error bars in the K flux are $\pm 1\sigma$ and are a measure of the level of night-to-night variation. Values are listed in Table 3.1.

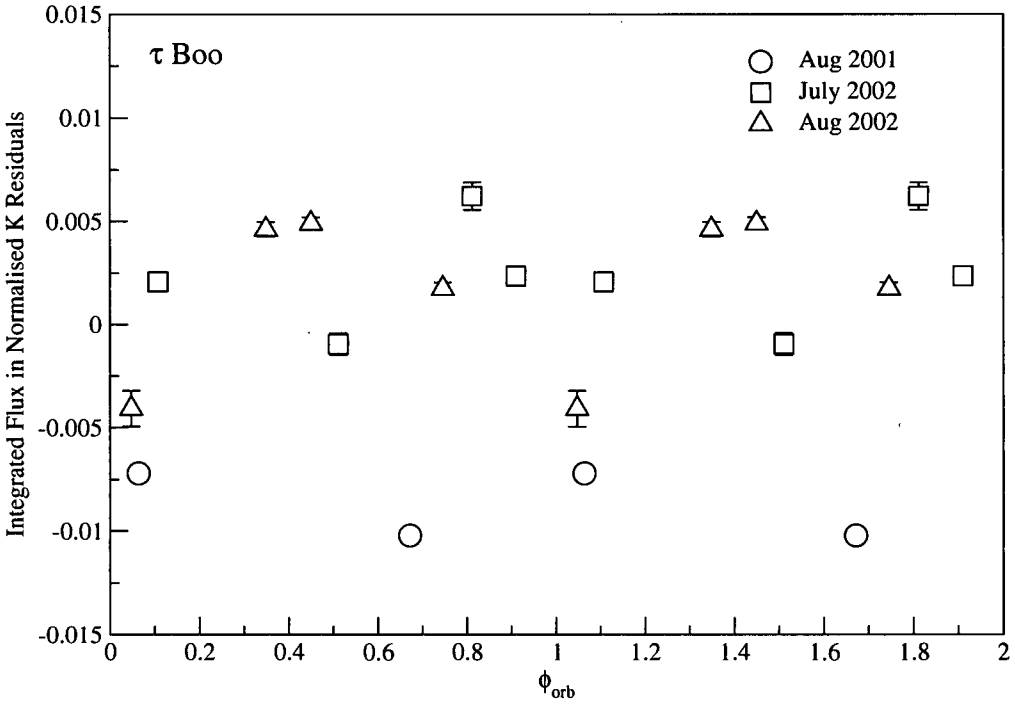

Figure 3.16 Integrated flux of the K-line residuals from a normalised mean spectrum of τ Boo as a function of orbital phase. Units of the integrated flux are in equivalent Angstroms relative to the normalisation level which is approxiamtely 1/3 of the stellar continuum. The error bars in residual flux are $\pm$ 1 σ as measured from the intra-night variations. The size of the phase error is within the size of the points. The data are listed in Table 3.2.

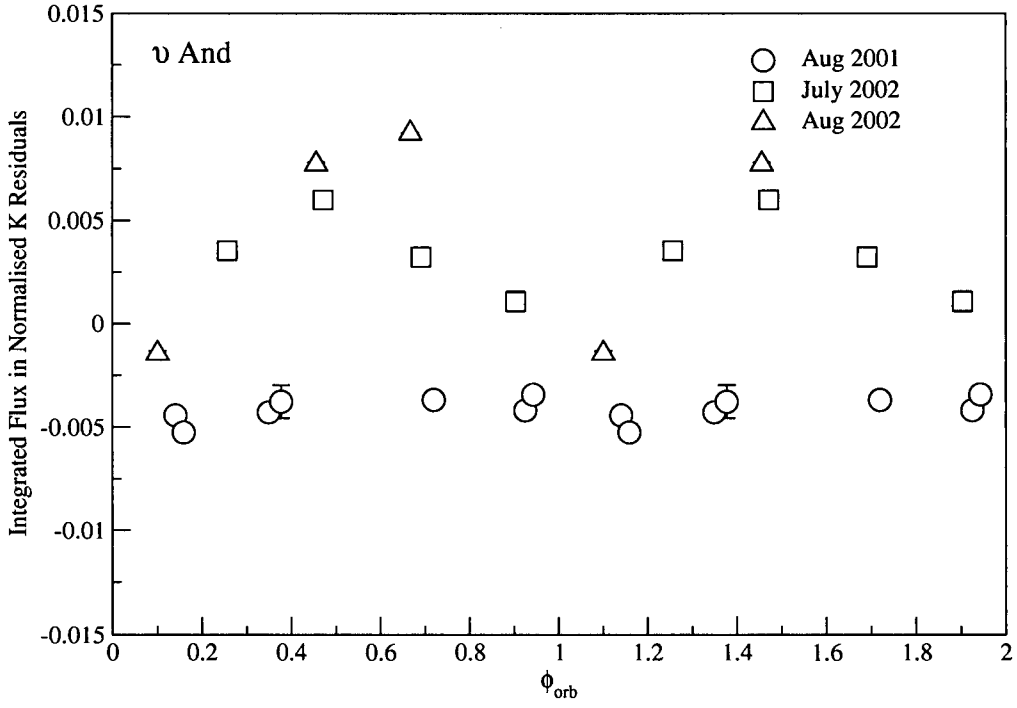

Figure 3.17 Integrated flux of the K-line residuals from a normalised mean spectrum of υ And as a function of orbital phase.

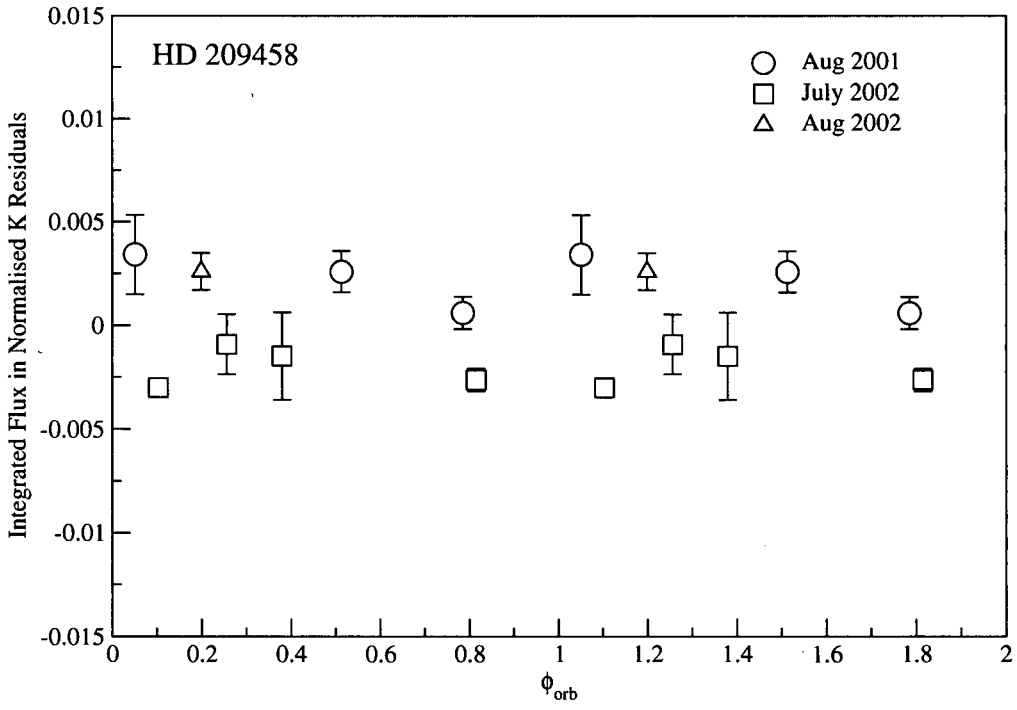

Figure 3.18 Integrated flux of the K-line residuals from a normalised mean spectrum of HD 209458 as a function of orbital phase.

In the case of υ And (3.17), the 2002 July and 2002 August runs show reasonable agreement in the phase-dependent activity with an enhancement at $\phi \sim 0.5$. If well determined, such a phase shift relative to the sub-planetary point may shed light onto the nature of the activity. It may imply some physical process in the chromosphere that would induce a phase lag such as tidal and/or magnetic friction. The 2001 August modulation is low yet significant ($> 2\sigma$) and the observation at $\phi = 0.5$ was unfortunately missed. These 2001 fluxes are lower than the mean of all three observing runs, which indicates a lower level of intrinsic stellar activity at that time, offering some insight into the star's long-term activity cycle.

Similar to τ Boo, HD 209458 shows night-to-night modulation, but with less scatter, during all runs but without any phase continuity (3.18). In 2001 August, we caught the system during transit at which time we observed a slight enhancement in the Ca II emission relative to all other observations. However, due to the relatively low S/N of these data and the intra-night scatter, this error bars are too large to form any conclusions. In the 2002 July run, an increase in emission occured at $\phi \sim 0.25$ with no apparent rise toward $\phi = 0$.

One consistent result for these 'active' stars is their night-to-night modulation of H & K emission. Other than for τ Boo, this timescale of activity is short compared to the stellar rotation period. Unfortunately, due to the large uncertainties in the rotation periods of the other stars, phasing with rotational phases is uninformative at this stage. Better photometric monitoring of these stars will solve this problem. However, we do know that υ And and HD 209458 both have $P_{rot} > 3P_{orb}$ and rotate only $\approx 20°$ per day, respectively. The high level of significance of the variation proves that the variations are truly intrinsic to the each star but cannot be explained with starspots rotating in and out of view. There must be a yet unidentified mechanism of short-term chromospheric activity, possibly connected with the close-in giant planet.

Table 3.2. Residual K Flux and Orbital Phases

Star	UT Date	Number [a] of spectra	HJD[b]	ϕ_{orb}[c]	Residual[d] K flux (Å)
τ Boo	8/26/2001	4	2452147.736	0.06	−0.00720
	8/28/2001	2	2452149.751	0.67	−0.01021
	7/26/2002	3	2452481.786	0.91	0.00236
	7/28/2002	3	2452483.775	0.51	−0.00096
	7/29/2002	3	2452484.773	0.81	0.00623
	7/30/2002	3	2452485.751	0.11	0.00208
	8/20/2002	2	2452506.762	0.45	0.00490
	8/21/2002	3	2452507.741	0.75	0.00175
	8/22/2002	3	2452508.739	0.05	−0.00408
	8/23/2002	3	2452509.740	0.35	0.00461
HD 179949	8/26/2001	3	2452147.837	0.66	−0.00066
	8/27/2001	3	2452148.849	0.99	0.00600
	8/29/2001	3	2452150.803	0.62	−0.00014
	7/26/2002	3	2452481.864	0.66	−0.00010
	7/28/2002	3	2452483.844	0.30	−0.01230
	7/29/2002	4	2452484.853	0.63	−0.00021
	7/30/2002	3	2452485.827	0.94	0.00638
	8/21/2002	3	2452507.847	0.06	−0.00822
	8/23/2002	3	2452509.858	0.71	0.00907
HD209458	8/26/2001	3	2452147.977	0.51	0.00259
	8/27/2001	3	2452148.937	0.79	0.00060
	8/28/2001	8[e]	2452149.874	0.05	0.00341
	7/26/2002	3	2452481.922	0.26	−0.00091
	7/28/2002	3	2452483.892	0.82	−0.00263
	7/29/2002	3	2452484.906	0.10	−0.00302
	7/30/2002	3	2452485.882	0.38	−0.00148
	8/23/2002	2	2452509.918	0.20	0.00260
51 Peg	8/26/2001	3	2452147.905	0.76	0.00007
	8/27/2001	3	2452149.005	0.50	−0.00084
	8/28/2001	4	2452149.992	0.27	−0.00100
	8/29/2001	3	2452151.095	0.00	0.00267

Table 3.2 (cont'd)

Star	UT Date	Number [a] of spectra	HJD[b]	ϕ_{orb}[c]	Residual[d] K flux (Å)
	7/26/2002	4	2452482.039	0.22	0.00015
	7/27/2002	4	2452482.987	0.44	−0.00010
	7/28/2002	3	2452484.025	0.69	−0.00016
	7/29/2002	3	2452485.039	0.93	−0.00110
	7/30/2002	3	2452485.985	0.15	0.00016
	8/23/2002	3	2452509.987	0.83	0.00033
υ And	8/26/2001	3	2452148.103	0.72	−0.00370
	8/27/2001	3	2452149.053	0.93	−0.00420
	8/27/2001	3	2452149.135	0.94	−0.00344
	8/28/2001	3	2452150.048	0.14	−0.00443
	8/28/2001	3	2452150.133	0.16	−0.00526
	8/29/2001	3	2452151.012	0.35	−0.00429
	8/29/2001	3	2452151.14	0.38	−0.00378
	7/27/2002	2	2452483.075	0.26	0.00352
	7/28/2002	2	2452484.068	0.47	0.00599
	7/29/2002	2	2452485.081	0.69	0.00321
	7/30/2002	2	2452486.063	0.90	0.00108
	8/20/2002	2	2452507.085	0.46	0.00772
	8/21/2002	2	2452508.061	0.67	0.00921
	8/23/2002	2	2452510.062	0.10	−0.00144
τ Ceti	8/26/2001	2	2452148.061	–	−0.00002
	8/27/2001	2	2452149.094	–	−0.00008
	8/28/2001	2	2452150.097	–	−0.00033
	8/29/2001	2	2452151.053	–	0.00023
	7/26/2002	2	2452482.121	–	0.00015
	7/27/2002	2	2452483.107	–	0.00027
	7/28/2002	2	2452484.131	–	−0.00033
	7/29/2002	2	2452485.113	–	−0.00064
	7/30/2002	2	2452486.096	–	0.00006
	8/20/2002	2	2452507.12	–	0.00021
	8/21/2002	2	2452508.095	–	0.00062
	8/22/2002	2	2452509.121	–	−0.00013
	8/23/2002	2	2452510.097	–	0.00008

Table 3.2 (cont'd)

Star	UT Date	Number [a] of spectra	HJD[b]	ϕ_{orb}[c]	Residual[d] K flux (Å)
	8/24/2002	1	2452511.106	–	−0.00020
Sun	8/26/2001	6	2452147.672	–	−0.00400
	8/29/2001	2	2452150.685	–	−0.00357
	7/28/2002	4	2452483.685	–	0.00305
	7/29/2002	3	2452484.684	–	0.00358
	7/30/2002	3	2452485.678	–	0.00349
	8/23/2002	5	2452509.674	–	0.00072

[a]Number of spectra was determined by the S/N required but mediated by the observations lost due to poor weather and instrument difficulties. The spectra of each night were averaged to increase S/N. Exposure times of individual spectra are listed for each star in Table 2.1. The exposure times for the solar spectra were 300 s of varying S/N since they were taken during sunset.

[b]Heliocentric Julian Date at mid-exposure time

[c]Orbital phase calculated using revised ephemerides in Table 2.3

[d]Residual K flux from the normalised mean integrated over the wavelength range bounded by the K1 features (as shown in Figure 1.3).

[e]We took 8 1200 s exposures of HD 209458 in order to get better time resolution during a transit. All other exposures were 2400 s.

Chapter 4

HD 179949: A Convincing Case of Planet-induced Activity

4.1 Introduction

Night-to-night activity on a sun-like star does not alone imply an interaction with a close-in giant planet. If the activity is stimulated by a nearby planet, the following three conditions should be met to make such a claim:
1) the activity has a period of $P_{orb}/2$ if the interaction is tidal and P_{orb} if magnetic;
2) according the the original prediction by Cuntz et al. (2000), the phasing of the activity is such that it peaks near the sub-planetary point;
3) the activity persists for longer than the usual lifespan of a starspot.

In our sample of 5 sun-like stars with short-period planets, four show significant night-to-night chromospheric variations that do not appear in τ Ceti or the sun. Of these four, HD 179949, having the tightest planetary orbit ($a = 0.045$ AU), exhibits the most convincing case for planet-induced stellar activity. It also distinguishes itself from the group by displaying the greatest night-to-night modulation and the strongest mean Ca II emission.

4.2 Phase-Dependent Activity

The integrated flux of the Ca II K residuals of HD 179949 shown in Figure 3.7 (bottom) are plotted against orbital phase in Figure 4.1. To demonstate that the H activity is coherent with the K emission, both values are plotted in Figure 4.2 where the slope of the best-fit line is 0.61. The slope is slightly lower than the expected ratio of 0.67 in part due to the intensity of the H and K cores relative to their respective normalisation levels (see Figure 3.1). The K emission clearly increases by $\sim 2.5\%$ when the planet is in front of the star, near the sub-planetary point and decreases when the planet is behind

the star.

Even though a periodogram is unreliable for less than 20 points, IRAF's *pdm* routine (Phase Dispersion Minimization; Stellingwerf 1978) returns the most significant period of 2.96 d with a significance level of 1 (see Figure 4.3. The routine calculates a period's signficance using Fisher's Randomization Method with 100 iterations. The significance of a 3.093-d period is 0.87. As a test of this, I randomized the data 100 times and found also that the significance of the 3.093-d period is 0.87. This is most likely due to the poor phase sampling of our data. With an orbital period of nearly an integer number of days, it is impossible to get good phase coverage in one or two observing seasons.

The solid line in Figure 4.1 is a truncated, best-fit sine curve with $P = P_{orb}$ = 3.093 d corresponding to the change in projected area of a bright spot on the stellar surface before being occulted by the stellar limb. The equation of the model was taken from Vogt (1981) where, for a purely geometric effect, the peak intensity drops off as

$$cos(\gamma) = cos(\theta)cos(i) + sin(\theta)sin(i)cos(\phi) \tag{4.1}$$

where γ is the angle between the local surface normal and the line of sight, θ is the stellar colatitude (with 0 radians at the pole), ϕ is the longitude or phase angle, and i is the stellar inclination. While visible, the hot spot varies as $\cos(\phi)$ however when the spot is on the far side of the star, the intensity is constant. If the spot is small and near the stellar equator, the model should be zero at these phases. However, the model does account for the possibility of a large spot that due to the non-90° inclination, would still be slightly visible. The solid line is a least-squares best-fit bright-spot model with the spot at a latitude of 30° and stellar inclination angle $i = 87°$. The dashed line is a model with $i = 83°$.

Even though Ca II emission is optically thin outside the self-absorption core, limb brightening is not included. According to solar observations discussed by Engvold (1966), limb brightening in the emission is negligible and would essentially not alter the geometric model.

The peak of the model leads the sub-planetary point by 0.174 ± 0.004 in phase. Potentially, any phase lead or lag may help identify the nature of the interaction. For example, the phase offset of a starspot or group of starspots can be a characteristic effect of tidal friction (Santos et al. 2003) or due to other physical processes such as magnetic drag or reconnection with off-centre stellar fields.

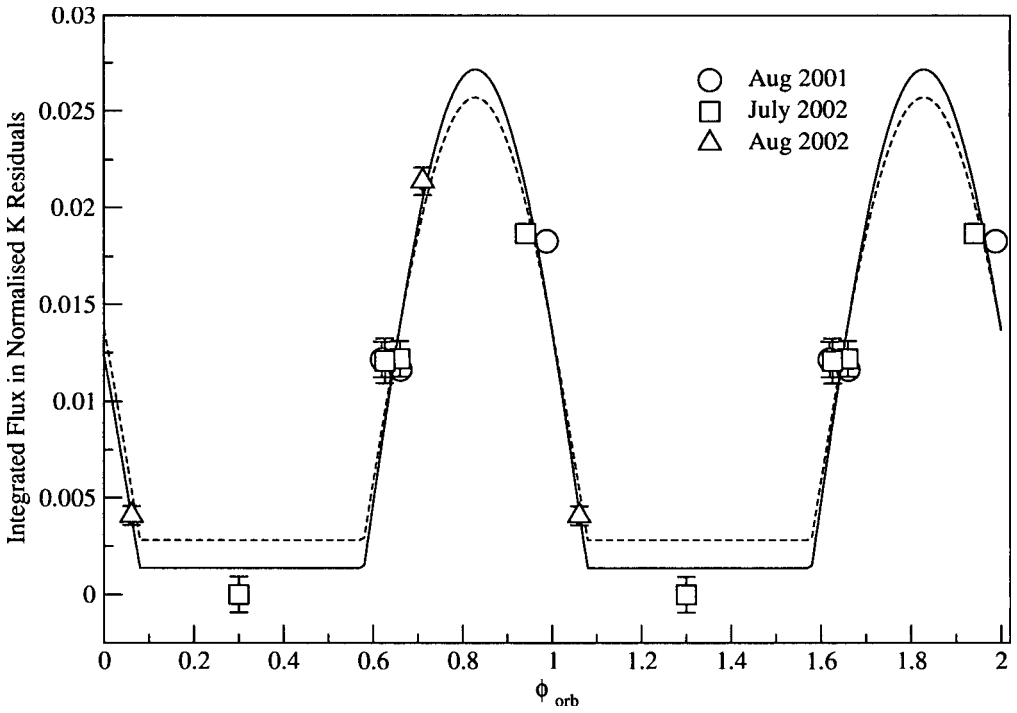

Figure 4.1 Integrated flux of the K-line residuals taken from a normalised mean spectrum as a function of orbital phase. Units of the integrated flux are in equivalent Angstroms relative to the normalisation level which is approximately 1/3 of the stellar continuum. The minimum flux was set to zero and all others scaled accordingly. The flux error bars are $\pm 1\sigma$ taken from the intra-night residuals, while the phases are known to $\pm$ 0.005, making the error bars well within the size of the points. The points are repeated for $\phi > 1$. The solid line is the best-fit (least-squares) bright-spot model discussed in the text with the spot at a latitude of 30° and stellar inclination angle $i = 87°$. The dashed line is a model with $i = 83°$.

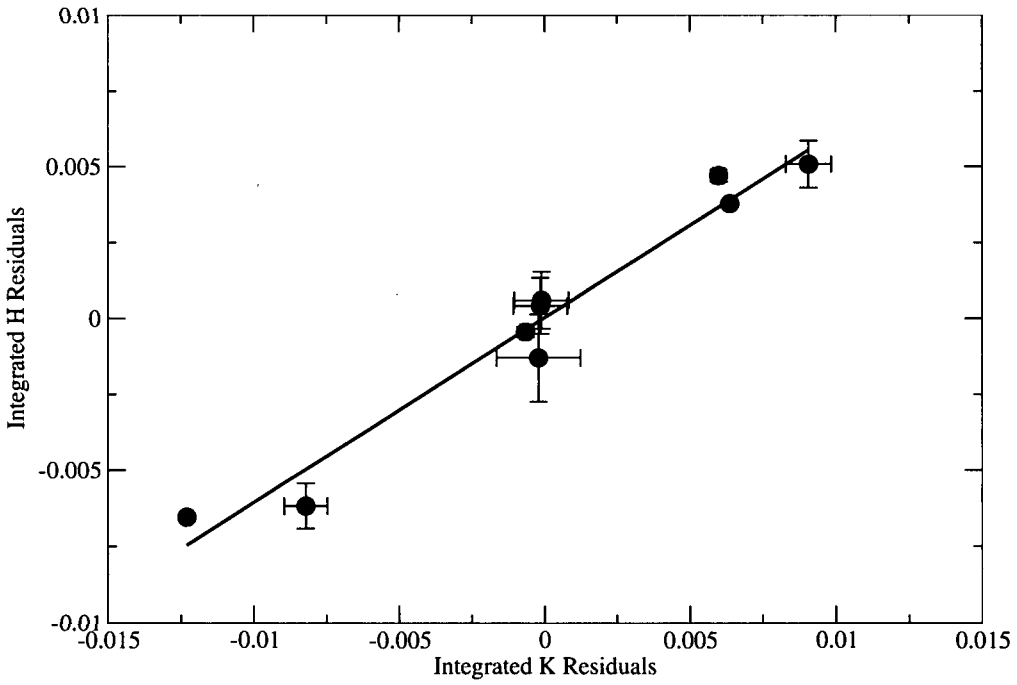

Figure 4.2 The integrated residual H and K emission for HD 179949. The slope of the best-fit line is 0.61.

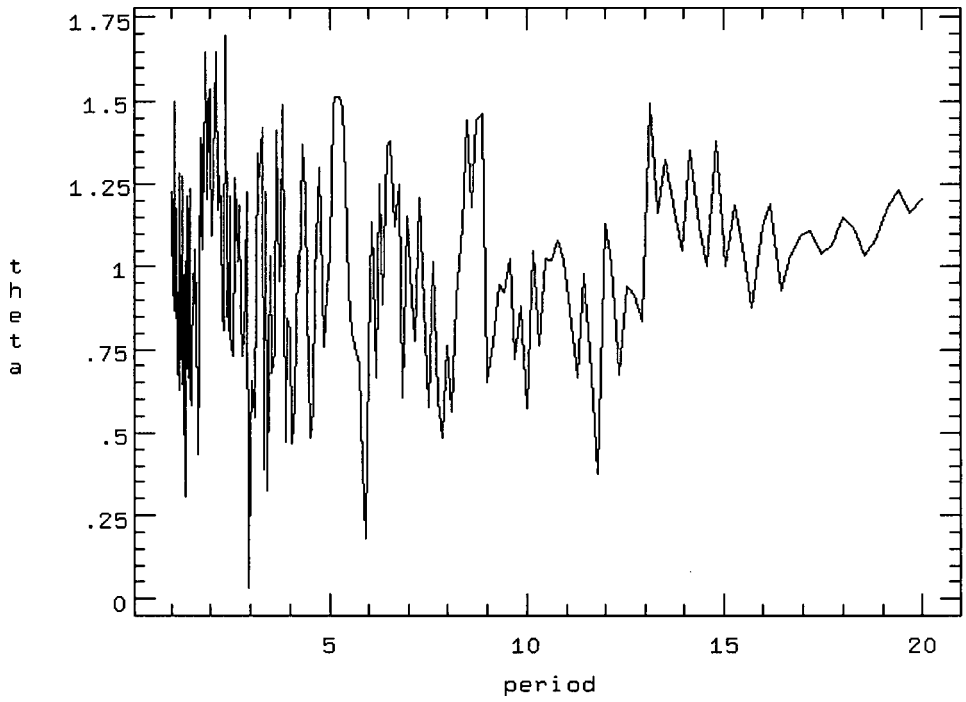

Figure 4.3 A periodogram for the nine data points of the integrated residual K flux of HD 179949. The period is in days and the theta statistic is defined in Stellingwerf (1981). The most significant period determined is $P = 2.96$ d.

All three conditions outlined in Section 4.1 are largely met by the activity observed on HD 179949:
1) The period of the activity is equal to the orbital period. A periodogram (Stellingwerf 1978) of even these few data points produces the most significant peak at a period of 3 days.
2) The activity enhancement is phased with the planet leading the sub-planetary point by 0.17 in phase. A similar lead in phase is also observed on ER Vul, an RS CVn binary system discussed in Chapter 5. In this case, the companion-induced chromospheric activity is seen on both components. Such a phase lead on HD 179949 and on ER Vul will offer further physical constraints on the physics of the interaction. Because of this, the original constraint of the enhancement appearing at the sub-planetary point is no longer valid.
3) The amplitude and period of this activity have persisted during the year between observations (equal to 108 orbits or at least 37 stellar rotations). The observations are consistent with a planet-induced magnetic heating scenario and may be a first glimpse at the magnetosphere of an extrasolar planet!

A similar phenomenon to the third condition has been described by Toner & Gray (1985, 1988). Over four years of optical spectroscopic monitoring, they observed evidence for a persistent, large active region modulated with rotation on ξ Boo A, a magnetically active G8 dwarf star. The period of the activity did not change over this time and is quoted as 6.43 ± 0.01 d. Even though they offer no explanation for the physical origins of this region, they fit a geometric and temperature model to the data. This region, which they have dubbed a 'starpatch' covers $\sim$ 10% of the stellar disk, is 85% of the brightness of the rest of the disk with a temperature drop of 3.7%. The starpatch is quite unusual when compared with regular sunspots. Ca II H & K emission also appears to be rotationally phased with a period of 6.2 d (Noyes et al. 1984, Baliunas et al. 1985) and is enhanced above the starpatch. However, Toner & Gray (1985) measure the temperature drop using the coherent phase-dependent variations observed in the ratio of the Fe to V absorption lines. This indicates that the starpatch originated at the photosphere, contrary to our observation of HD 179949, for which the strong photospheric Al I lines are very stable.

Since then, no other discussion of starpatches on this star or any other have been published. Gray et al. (1996) discuss long-term activity cycles on ξ Boo A using data from 1984 to 1993 but make no mention of the starpatch again.

Cummings et al. (1999) searched for radial velocity variations in ξ Boo A as part of The Lick Planet Search. They found an RV variation with a period of 3.78 d with a false-alarm-probablility of 0.0007 but exclude it from their list of stars with planet candidates due to its relatively high level of intrinsic magnetic activity. Perhaps there is a yet-unconfirmed planet around ξ Boo A that stimulated the starpatch of the late 1980s.

Similar to ξ Boo A, κ^1 Ceti, also a late-type, active dwarf, shows Ca II H & K emission clearly modulated with its rotation period. However, the variations have persisted for over 20 years and the photospheric Al I lines are quite stable. This star is discussed in further detail in Chapter 6. It appears as if what we observed on HD 179949 is different from both these cases.

4.2.1 Rotation of HD 179949

HD 179949 has no directly measured rotation period, though it is estimated to be $\leq$ 9 d from the star's $v\sin i$ and a Hipparcos astrometric radius of 1.24 $R_\odot$ (Groot et al. 1996).

Since there were no transits detected for this system, an upper limit for the orbital inclination is 83° (Tinney et al. 2001). Assuming that the orbital axis of the planet and stellar rotation axis are aligned, this value places a limit on the stellar inclination as well. The best-fit spot model (solid line in Figure 4.1) requires the hotspot to be at a latitude of 30° and a stellar inclination angle i of 87°. (Figure 4.4 is a schematic of this model drawn to scale.) The dashed model in Figure 4.1 has $i = 83°$ as it is generally assumed that the orbital and stellar inclination angles are comparable.

These models are inconsistent with the possibility that the star may be tidally synchronized with the planet's orbit. Non-synchronicity is also supported by the long tidal synchronization timescale, which for this system is $\approx$ 700 Gyr using an $M_p \sin i = 0.84$ M_J (Equation 1 of Drake et al. 1998). Even if $i = 21°$, as would be the case for $P_{rot} = 3$ d, $v = 17.5$ km s^{-1} and $M_p = 2.34$ M_J, then the sychronization timescale is still too long at 80 Gyr. However, from Figure 3.5, the Ca II K emission in HD 179949 is unusually strong compared to the other targets. This implies that either the inclination of the star is low, $i \sim 21°$ such that $v \simeq 17.5$ km s^{-1} and $P_{rot} \approx P_{orb} \approx 3$ d., or that P_{rot} is closer to 9 days and the Ca II emission is anomalously enhanced in HD 179949. The latter case is consistent with HD 179949's X-ray luminosity. ROSAT X-ray data list HD 179949 as having at least double the X-ray flux (a measurement independent of i) as compared to other single

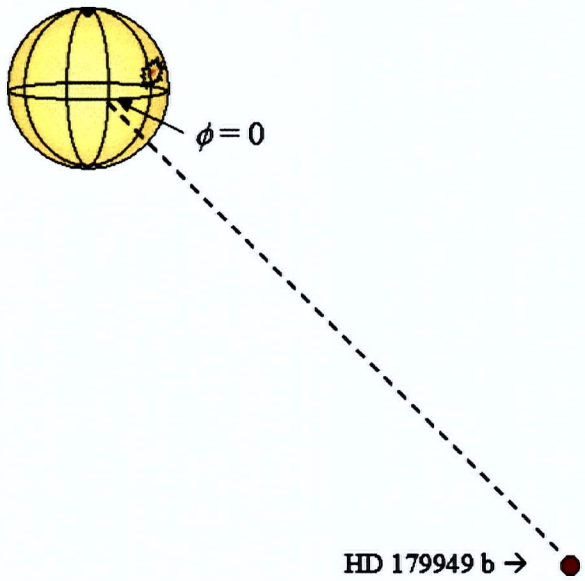

Figure 4.4 A schematic of the HD 179949 system drawn to scale with the hotspot leading by $\Delta\phi = 0.17$ at a latitude of 30°.

F8 – 9 dwarfs in Hünsch et al.'s (1998) catalog, and $\sim$ 10 times that of the sun's. As there is only suggestive evidence that HD 179949 is *not* synchronized with its planet, it is necessary to obtain photometric data to measure conclusively the rotation period of the star.

4.2.2 Ca II Emission from HD 179949 b?

The giant planet around HD 179949 orbits on average at the rate of 158 km s^{-1} (eccentricity e=0.05). Any Ca II K emission originating from the planet would be Doppler shifted by the planet's projected radial velocity. At maximum orbital velocity (ϕ = 0.25 and 0.75) emission from the planet would appear in the residuals of the K core at $\pm$ 2.07 Å from the K-line centre. Figure 4.5 displays the K residuals of HD 179949 offset by 0.01 in intensity. The arrow above each one indicates the expected location of any Doppler-shifted planetary emission. No clear signal is detectable. The mean residual flux at the expected location is 0.001. This sets an upper limit to the normalised intensity for planetary Ca II K emission.

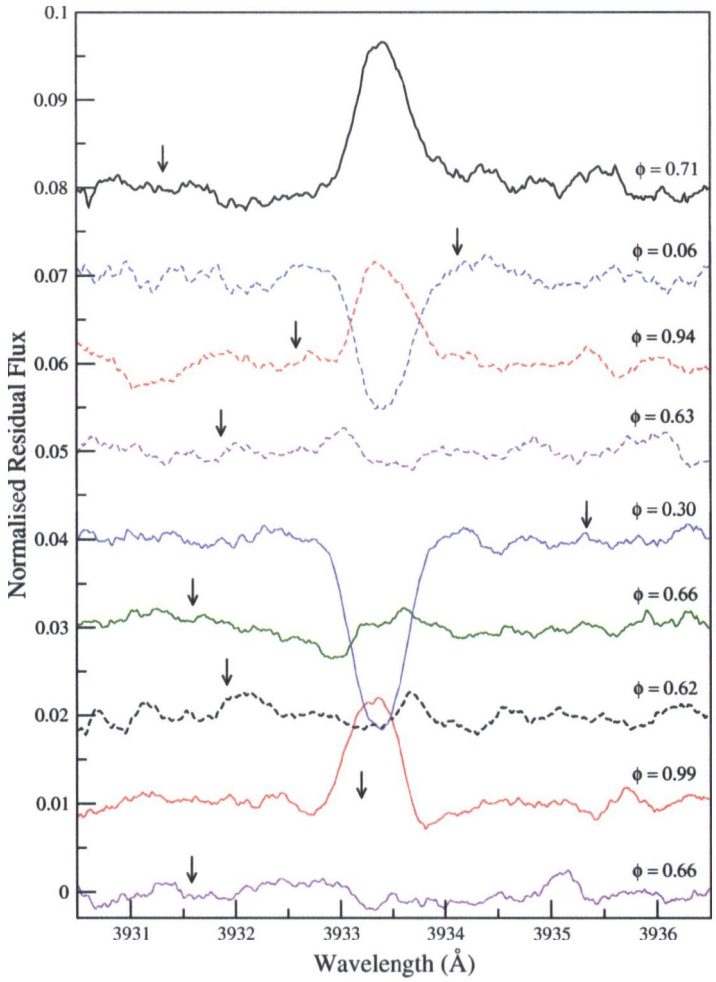

Figure 4.5 Ca II K residuals (smoothed by 21 pixels) from the normalised mean of HD 179949 with each subsequent line displaced by 0.01 in flux. The arrows indicate the expected location of any planetary K emission. Each residual is labeled with its corresponding orbital phase.

Chapter 5

ER Vul: An Exaggerated Case of Phase-dependent Activity

5.1 Introduction

RS Canum Venaticorum systems (RS CVn) are binary stars with orbital periods ranging from about 2 to 20 days. They are composed of two active late-type stars whose spectra are usually dominated by the giant or sub-giant primary. Both components have strong chromospheric, transition region and coronal emission. This is generally an effect of the rapid rotation and deep convection zones that together fuel the powerful dynamo mechanism that creates strong magnetic activity several orders of magnitude greater than the sun's (Vogt et al. 1997).

A bright, well-studied RS CVn system is ER Vulpeculae. This tidally-synchronized binary is unusual in that it consists of two solar-type stars orbiting each other with a relatively short period of 0.698 days. The stars are nearly identical (G0 V and G5 V) with equal radii (1.07 $R_{\odot}$) and a mass ratio of 0.947. They are only 3.97 $R_{\odot}$ apart in a circular orbit with an inclination of 67°. This configuration leads to partial eclipses of approximately 12% most recently observed photometrically by Harmanec et al. (2004). The projected rotational velocities of the primary and secondary components are $(v\sin i)_P = 97.4 \pm 1.3$ km s^{-1} and $(v\sin i)_S = 96.7 \pm 2.2$ km s^{-1} (Duemmler et al. 2003). This rapid rotation causes very broad and blended features in the double-lined spectrum with strong chromospheric emission.

The extreme stellar activity of both components makes ER Vul a perfect candidate for which to study phase-dependent activity.[1] It is also bright enough and located in the right part of the sky to be easily observed at the CFHT. Piskunov (1996) used Doppler imaging to map the surfaces of the two interacting but not contact stars of ER Vul. He acquired 12 high-resolution

[1]Section 1.5 contains examples of evidence for phase-dependent activity in other RS CVn systems.

spectra centered on 6440 Å at the Nordic telescope. He identified hot spots on both components at sub-stellar longitudes, which he presumed to be due to reflection effects.

Duemmler et al. (2003) also report phase-dependent activity on ER Vul observed as an asymmetry in the Ca II IRT line at 8662 Å. They measured deviations of $\sim$10 km s^{-1} from the radial velocity (RV) curve at the phases when either star is receding from the observer. They suggest that this is due to localized excess emission near the sub-stellar point on the star. Alternatively, a weakening of the emission at opposite orbital phases could induce distortions that appear as RV deviations. They measure a greater level of activity on the cooler secondary component which has been shown to be globally more active than the primary (Gunn & Doyle 1997; Çakirli et al. 2003). In addition, Montes et al. (1996) and Fernandez-Figueroa et al. (1994) have observed ER Vul in Ca II H & K as part of a large survey of chromospherically active binaries. However, the data were too few and sporatic to make any claims of phase-dependent activity.

In addition to the interest in the dynamics and geometry of RS CVn systems, we chose to study ER Vul as a test-bed for the proposition that '51 Peg'-type planets can induce chromospheric activity on their parent stars through tidal and/or magnetic interactions and that we could detect it with our observational approach. ER Vul is an ideal target for observing phase-dependent magnetic interaction at a magnified level.

5.2 The ER Vul Spectra

Ca II H & K observations were taken with Gecko, the high-resolution spectrograph at the CFHT, with the identical instrumental setup and data processing steps used for the other program stars. The details are described in Section 2.2. The B magnitude of ER Vul is 7.93 allowing a S/N of $\sim$ 180 to be achieved in an exposure time of 1200 s.

Of the three nights awarded, two were clear (2002 August 26, 27), giving us almost complete phase coverage, $\phi = 0.09 - 0.96$. Table 5.1 lists the time and orbital phase of each exposure. Russ Robb and Karun Thanjavur supplied an updated ephemeris from photometric monitoring done at the Climenhaga Observatory, the automatic 0.5-m telescope at the University of Victoria. The time of primary eclipse ($\phi = 0$), occured at HJD =

2452500.8453(3) [2] with a period of 0.69810(2) d. Specimen ER Vul spectra are shown in Figure 5.1 at three phases, $\phi = 0.25$, 0.50 and 0.62.

[2]Values in brackets are 1σ errors (Russ Robb, personal communication).

Table 5.1. ER Vul: 2002 August Observations

HJD − 2452000	Orbital Phase	RV (P) km s^{-1}	RV (S) km s^{-1}	Residual (P) K flux (Å)	Residual (S) K flux (Å)	Total Residual K flux (Å)
512.773	0.086	−86.0	65.4	29.67	36.47	66.14
512.789	0.109	−99.3	82.9	33.53	42.69	76.22
512.806	0.133	−113.5	92.1	33.61	44.13	77.74
512.822	0.156	−124.5	101.5	29.69	44.41	74.10
512.839	0.180	−132.7	115.5	29.51	44.68	74.19
512.855	0.203	−138.3	121.7	28.21	44.81	73.02
512.871	0.226	−141.2	126.0	30.07	46.46	76.53
512.887	0.249	−143.6	125.4	30.95	47.27	78.21
512.903	0.272	−145.1	126.9	33.06	45.36	78.42
512.919	0.295	−137.1	119.9	32.63	47.72	80.36
512.935	0.318	−130.2	116.3	33.26	48.23	81.48
512.950	0.340	−121.7	106.6	31.51	49.54	81.05
512.967	0.363	−112.8	93.1	35.31	46.99	82.30
512.983	0.386	−102.1	82.5	32.16	41.80	73.96
512.999	0.410	−71.8	73.9	33.63	37.44	71.07
513.015	0.433	−21.3	60.6	31.86	33.47	65.33
513.031	0.456	−14.1	−14.1	26.70	29.21	55.91
513.047	0.478	−14.8	−14.6	23.89	25.39	49.28
513.063	0.501	−13.7	−13.7	26.67	23.10	49.78
513.734	0.463	−16.8	−16.4	30.53	26.07	56.60
513.750	0.486	−15.0	−15.4	26.34	25.47	51.81
513.766	0.508	−13.3	−14.4	25.91	26.12	52.02
513.782	0.531	−7.6	−8.1	24.40	30.81	55.22
513.798	0.554	0.4	0.7	23.97	35.34	59.31
513.814	0.577	39.7	−79.1	27.45	34.22	61.68
513.829	0.599	71.3	−100.3	31.59	37.72	69.30
513.845	0.622	81.9	−116.3	34.59	34.93	69.52
513.861	0.644	92.3	−128.3	34.33	35.18	69.51
513.877	0.667	103.3	−137.9	36.79	34.84	71.63
513.893	0.690	109.1	−146.3	39.21	33.66	72.87
513.909	0.713	117.1	−149.5	37.31	34.21	71.51
513.924	0.735	112.5	−148.5	41.11	35.52	76.63
513.940	0.757	114.2	−154.6	40.61	32.81	73.42
513.955	0.780	112.7	−147.4	38.25	34.13	72.38
513.971	0.802	104.9	−142.6	38.62	34.52	73.14
513.987	0.825	101.6	−134.2	39.30	35.86	75.16
514.003	0.848	88.3	−122.2	40.06	38.01	78.07

Table 5.1 (cont'd)

HJD − 2452000	Orbital Phase	RV (P) km s^{-1}	RV (S) km s^{-1}	Residual (P) K flux (Å)	Residual (S) K flux (Å)	Total Residual K flux (Å)
514.019	0.871	77.6	−108.4	34.85	36.90	71.75
514.035	0.894	68.4	−94.6	31.66	40.05	71.72
514.051	0.916	43.4	−68.1	27.08	34.38	61.46
514.066	0.938	1.9	2.0	23.37	37.97	61.34
514.082	0.961	−8.5	−8.8	26.88	33.72	60.60

5.3 The Broadening Functions

In a rapidly rotating binary system such as ER Vul, disentangling the stellar activity of each component star is a difficult task that needs careful attention. Many researchers have used the stellar subtraction technique to isolate the chromospheric emission from each component as well as correct for any core-filling of the lines (e.g. Montes et al. 1994, Gunn & Doyle 1997). This method uses a spectrum of a chromospherically inactive star as a template. The template could either be a synthetic spectrum or a real spectrum of a sharp-lined (slowly rotating) star that is artificially Doppler broadened to match the velocities of the binary components. Subtracting a template spectrum from that of an active binary leaves only the emission from stellar active regions such as plages or prominences.

Slavek Rucinski, a co-investigator of this study of ER Vul, employs the Broadening Function (BF) formalism as a means of studying tight binary systems. The BF technique has permitted the measurement of radial velocities of complex multi-component stellar systems with a wide range of stellar rotational velocities. A series of papers has been published detailing the method and its benefits (e.g. Lu & Rucinski 1999; Rucinski & Lu 1999).

The BF is defined by Rucinski (2002) as "a function that transforms a sharp-line spectrum of a standard star into a broadened spectrum of a binary or, for that matter, of any other star showing geometrical, Doppler-effect line broadening." It is the convolution function that maps the standard-spectrum (template) T into a broad-lined spectrum of the programme star(s), P_*, be it a rapidly rotating single star or a multi-component system with varying degrees of broadening. The template spectrum must be of a slowly rotating

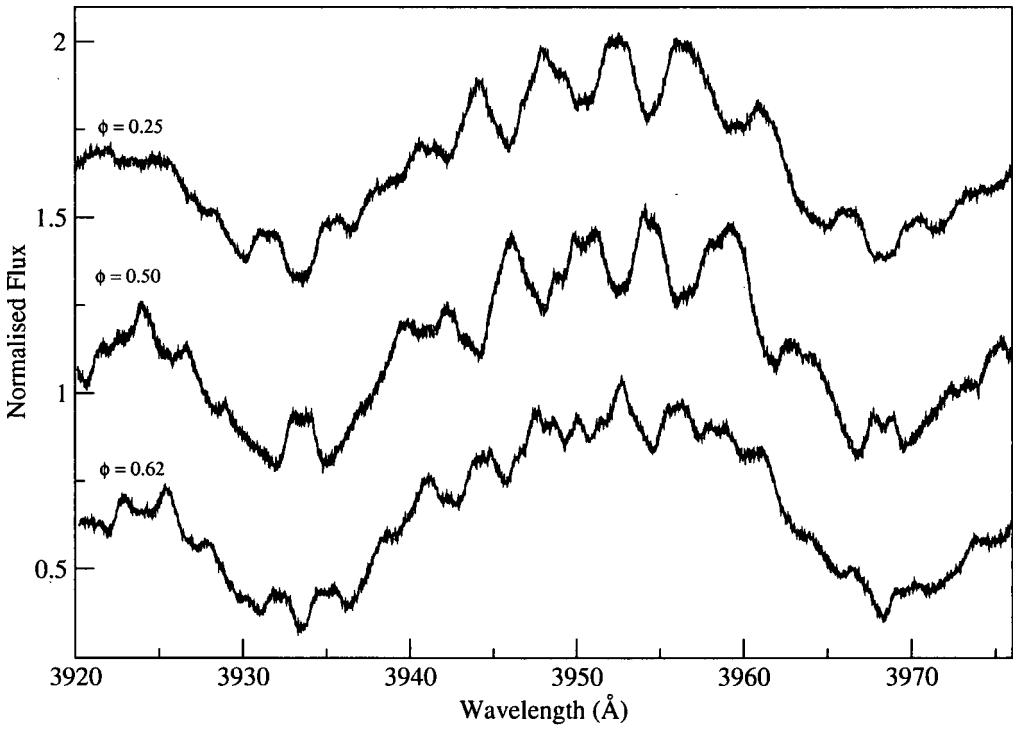

Figure 5.1 ER Vul spectra normalised to the peak intensity at three orbital phases. The differences in the spectra are mainly because of the large Doppler shifts caused by the large orbital motions of the two stars.

star of similar spectral type to the programme star(s). Mapping wavelength (λ) or velocity (v), the operation is

$$P_*(\lambda') = \int B(\lambda' - \lambda)T(\lambda)d\lambda \tag{5.1}$$

(Equation 1 of Rucinski 2002). This convolution can be written as an over-determined system of linear equations through which the parameters of the BFs are solved. The final BF for each orbital phase is that which creates the least-squares fit to the programme spectra once convolved with the template.

A mean spectrum of HD 209458, taken from a night during our 2002 August observing run, was used as the standard star with which to calculate the BFs for the ER Vul spectra. HD 209458 is a G0 V star making it a good match to both of ER Vul's stars. The resolution was reduced from 0.013 to 0.025 Å per pixel, equivalent to a velocity step of 1.9 km s^{-1}, in order to save on computation time. Considering that the spectral features of ER Vul are very broad, there is no significant loss of information from this step. Only the upper 2/3 of each ER Vul spectrum was used in the calculations to exclude the Ca II reversals such that any deviations due to chromospheric activity did not contribute. The BFs that Rucinski calculated are plotted in Figure 5.2. Figure 5.3 provides a closer look at the BFs at ϕ = 0.25, 0.50 and 0.62.

5.3.1 Radial Velocities from the BFs

I measured radial velocities (RVs) for each component of ER Vul by fitting gaussian curves to the BFs of each star. The velocity at the peak of the Gaussians was measured with an uncertainty of $\approx$ 0.5 km s^{-1}. The RV curve as a function of phase is plotted in Figure 5.4. The RVs at the phases near conjunction ($0.9 \leq \phi \leq 0.1$ and $0.4 \leq \phi \leq 0.6$) are inaccurate since only one Gaussian could be fit to the blended BFs. The solid curves are sine functions using the system parameters measured by Duemmler et al. (2003). The velocity amplitudes of the primary and secondary components are K_P = 135.20 $\pm$ 0.63 km s^{-1} and K_S = 142.82 $\pm$ 0.76 km s^{-1}, the eccentricity e = 0 and the systemic velocity γ = 25.49 $\pm$ 0.39 km s^{-1}. The dashed curves are the best-fit sine functions to the data using only the RVs outside of the conjunction region. For these, K_P = 130.55 km s^{-1}, K_S = 140.25 km s^{-1}, e = 0 and γ = 26.68 km s^{-1}. The RMS scatter of the data relative to the solid curves are 6.15 km s^{-1} for the primary and 4.30 km s^{-1} for the secondary.

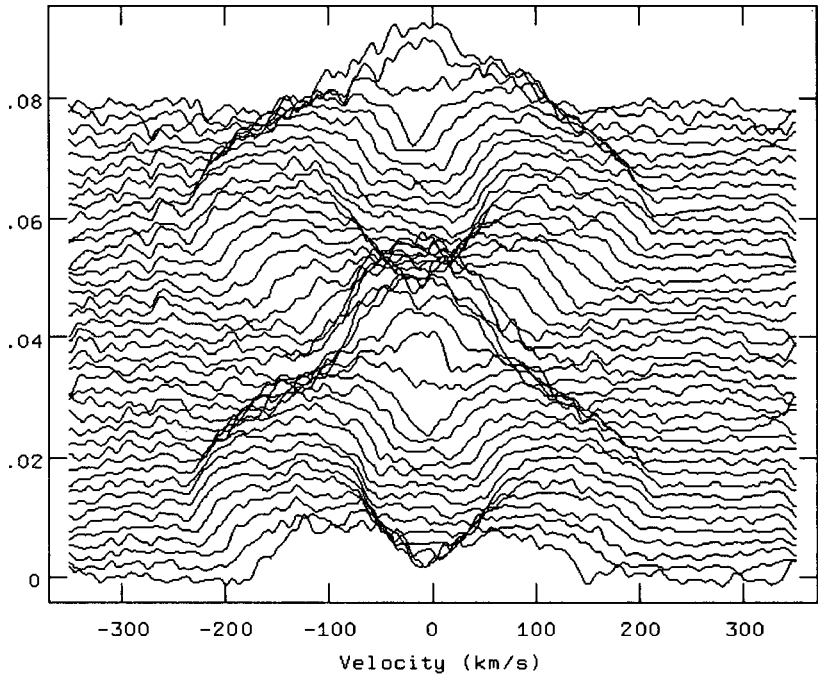

Figure 5.2 The broadening functions of ER Vul for all data starting with $\phi = 0.09$ (bottom curve) to 0.96 (top curve) as a function of BF intensity (calculated by Slavek Rucinski). The intensities are normalised to 0 but are displaced vertically.

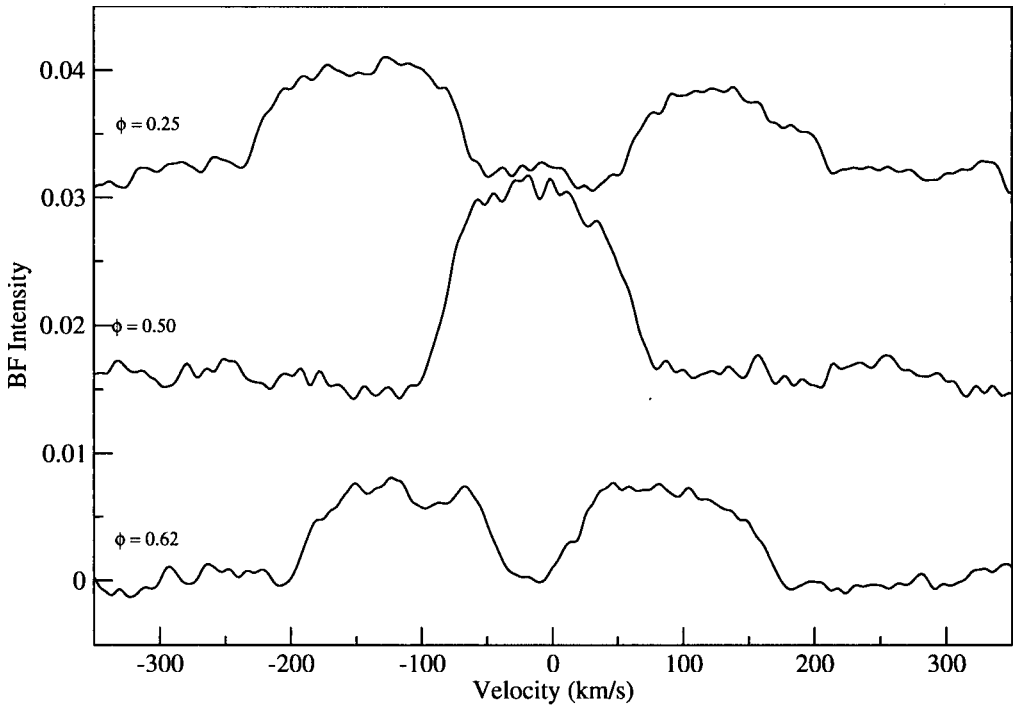

Figure 5.3 Example broadening functions at three orbital phases.

The deviation of the primary by ≈ -10 km s^{-1} at $\phi \approx 0.75$ may be due to spectral line distortions caused by less stellar activity relative to the rest of the star and could be an indication of relatively *inactive* longitudes. The RV of the secondary also deviates at its maximum, but by only ≈ -5 km s^{-1}.

5.4 H & K Activity in ER Vul

5.4.1 Separating the Star from its Activity

The rapid rotation and orbital velocities of the two components of ER Vul cause severe Doppler broadening and line blending, such that distinguishing the contributions from the two stars is a difficult task. The BF technique allows the chromospheric emission from the two stars to be isolated from the rest of the stellar flux by subtracting a template spectrum convolved with the appropriate BF. I performed the convolution of the HD 209458 template spectrum with the BF at each observed phase using IRAF's *convolve* routine. Figure 5.5 shows the sharp-lined spectrum of HD 209458, the BF at $\phi = 0.25$, the convolution of the two, and the corresponding ER Vul spectrum. Both the broadened template and the ER Vul spectrum were normalised to their highest intensity value before subtraction.

The residual spectrum is shown in Figure 5.6 where the H & K emission from both components remains. The fluctuations between them are most likely due to two processing issues:
1) the spectral type of HD 209458 matches ER Vul's primary star very well, but is off by 5 sub-classes for the secondary; and
2) when comparing broad-lined spectra with highly-blended features, the normalisation becomes a tricky task. This challenge arises during the calculation of the BFs and then again when setting the pseudo-continuum level of the standard and stellar spectra before subtraction. For this latter reason, we followed a similar procedure to the one described in Section 3.2.1 used to consistently extract the H and K reversals of the '51 Peg'-type stars.

5.4.2 Extracting the H & K Emission

Before subtracting the convolved templates, the ER Vul spectra had to be rebinned to the same 1.9 km s^{-1} per pixel as the BFs and templates. A cross-correlation was then performed with IRAF's *fxcor* routine of each ER

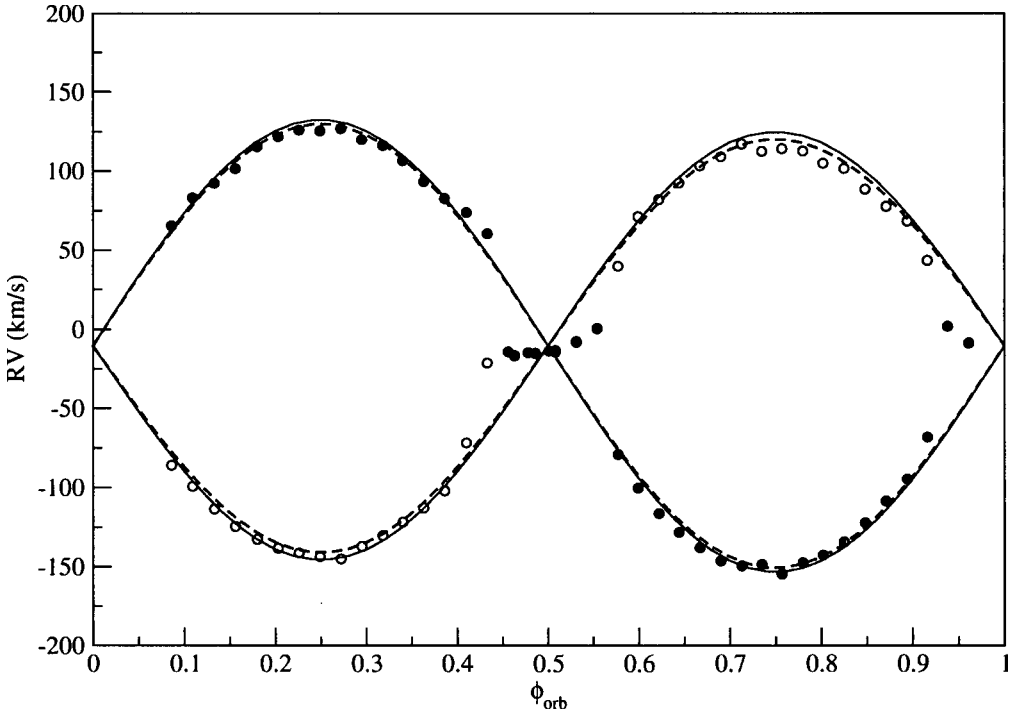

Figure 5.4 The ER Vul RV curve as a function of orbital phase determined from the BFs. The RVs of the primary are represented by the open circles, and the secondary by the filled circles. The data are listed in Table 5.1. The solid curves are orbital fits using values from Duemmler et al. (2003) and the dashed curves are the least-squares best fits to the data. See text for more details. The uncertainties in the RVs is ≈ 0.5 km s^{-1} for the values outside of the eclipses. During the eclipses, the BFs of the components are blended making the RVs difficult to measure. The error in ϕ is < 0.0001 since the ephemeris is very well known.

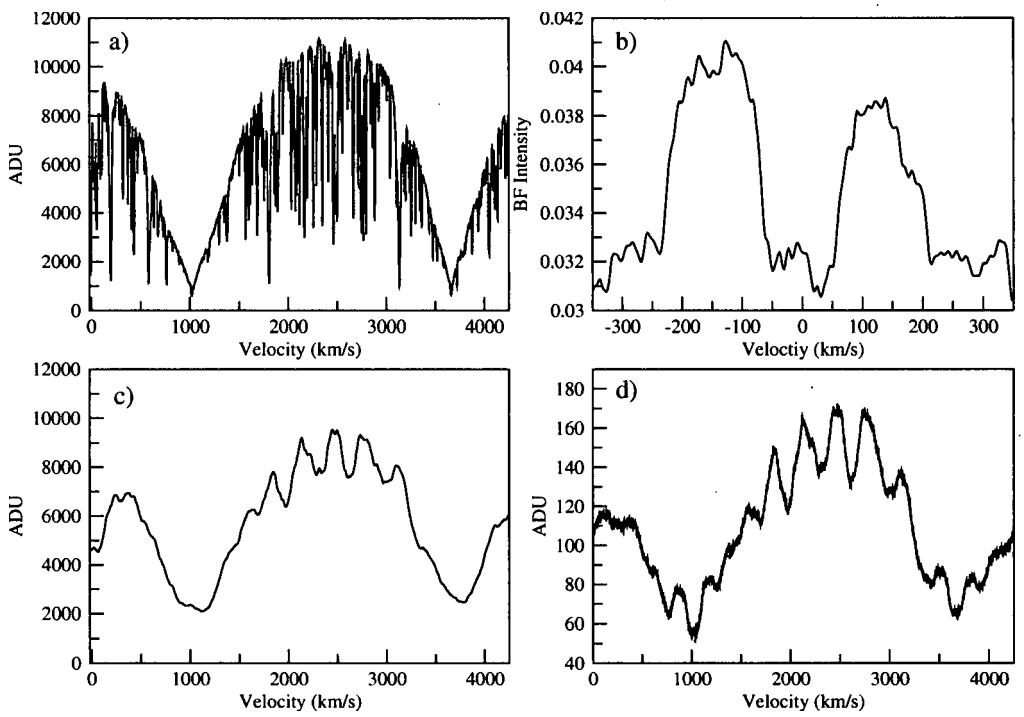

Figure 5.5 a) The template spectrum of HD 209458. b) The BF calculated for $\phi = 0.25$. c) The convolution of the template spectrum with the BF. d) The ER Vul spectrum at $\phi = 0.25$.

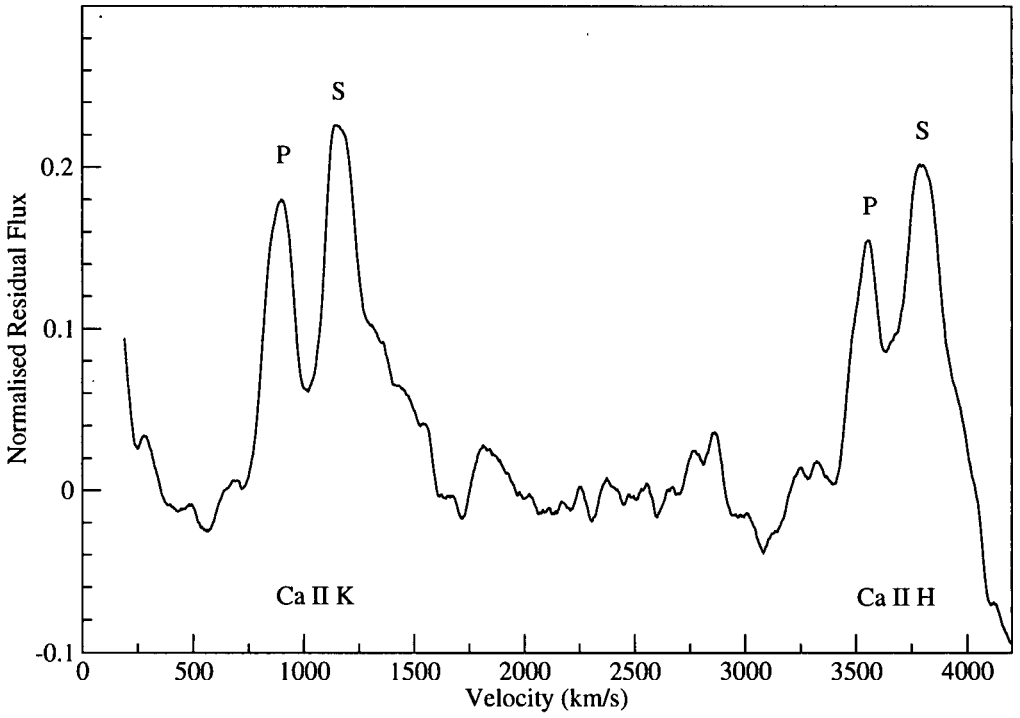

Figure 5.6 The full Ca II H & K residual spectrum of the broadened template subtracted from the corresponding ER Vul spectrum at $\phi = 0.25$. The emission from the primary and secondary are labeled with 'P' and 'S'.

Vul spectrum with its corresponding template, using only the photospheric flux between the H and K absorption lines in order to best line up the spectra before subtraction.

As for the other programme stars, two cuts, centered on the H and K lines and each 1000 km s^{-1} wide, were extracted from every template and ER Vul spectrum. These sub-spectra were normalised with a straight line fit to the end points. The H and K cores of the broadened templates were subtracted from the corresponding ER Vul spectra to isolate the chromospheric contribution. The residuals for all K cores are plotted in Figure 5.7 starting with $\phi = 0.09$ from the bottom with a closer look at three phases in Figure 5.8. The H residuals follow this plot as expected (see Figure 3.14).

The integrated K emission is plotted against orbital phase in Figure 5.9 for the primary star and in Figure 5.10 for the secondary. The two symbols on each plot distinguish between the two nights of observations. The total of the chromospheric K emission from both components is plotted in Figure 5.11. The drops in flux due to the two eclipses are apparent in all three plots at $\phi = 0$ and 0.5.

Both stellar components exhibit increased chromospheric emission at phases when their respective sub-binary points rotate into view. The primary star reaches a maximum enhancement after $\phi \simeq 0.75$ of 19% relative to the mean emission flux outside of the two eclipses. The secondary shows a 24% increase at $\phi \simeq 0.35$, just before it is eclipsed. The active region on each star is most likely not confined to a narrow longitudinal range but may cover as much as 30−40% of the hemisphere. However, it appears as if the centres of the large hotspots, on both stars, may lead the sub-binary points by $\sim 20-30°$. In this case, the reflection effect as the cause of the heating as suggested by Piskunov (1996) is not supported. A schematic of the system at $\phi = 0.35$ and 0.50 is displayed in Figure 5.12.

The increasing K emission of the secondary from $\phi = 0.1$ to 0.35 is consistent with a hotspot on the surface near the sub-stellar point. The active region gradually comes into view with the star's rotation and reaches a maximum just before entering secondary eclispe. The hotspot, however, is not detected as a travelling feature in the K residuals nor as a distortion in the RVs measured from the BFs. The greater variation in the activity of the secondary star as compared to the primary is consistent with previous observations by Gunn & Doyle (1997) and Çakirli et al. (2003).

The total residual flux from both components shows a significant depression of 6% relative to the peak at $\phi = 0.20$ and 0.77. These phases are

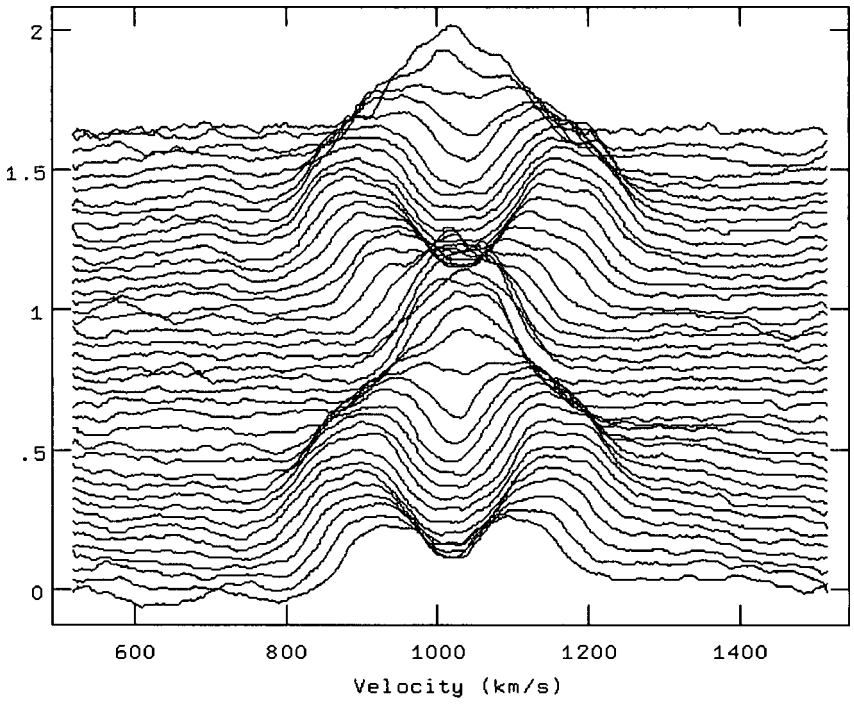

Figure 5.7 The Ca II K emission of ER Vul (smoothed by 9 pixels) at all observed phases starting at $\phi = 0.09$ (bottom curve) to 0.96 (top curve). The vertical axis is normalised residual flux with arbitrary vertical shift.

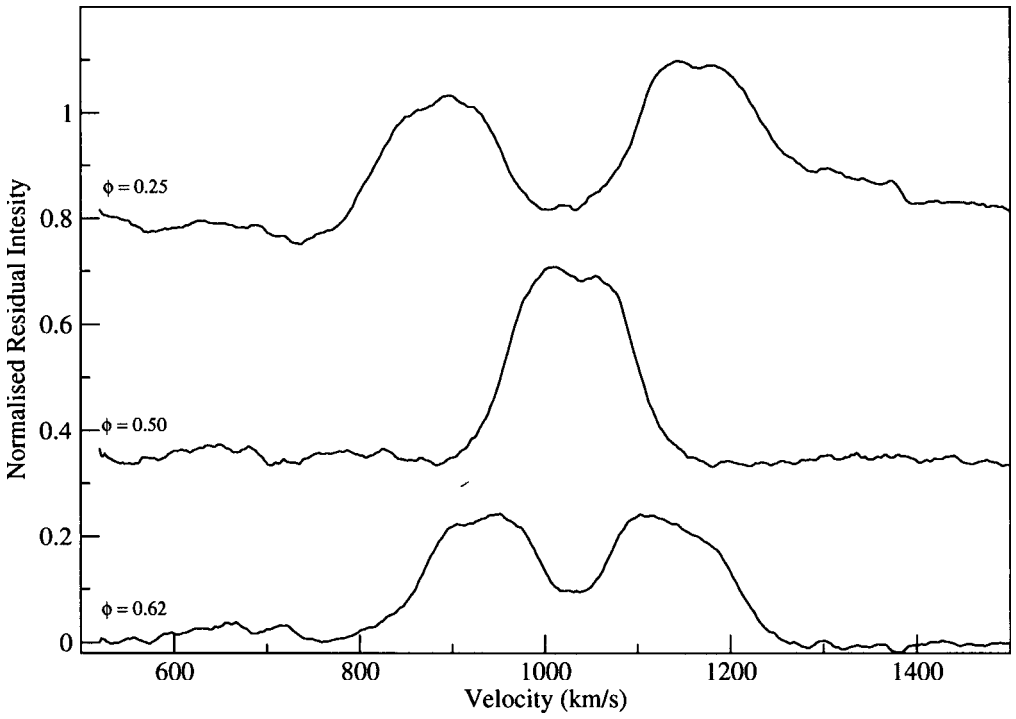

Figure 5.8 The Ca II K emission at three example phases (smoothed by 9 pixels). The vertical axis is normalised residual flux.

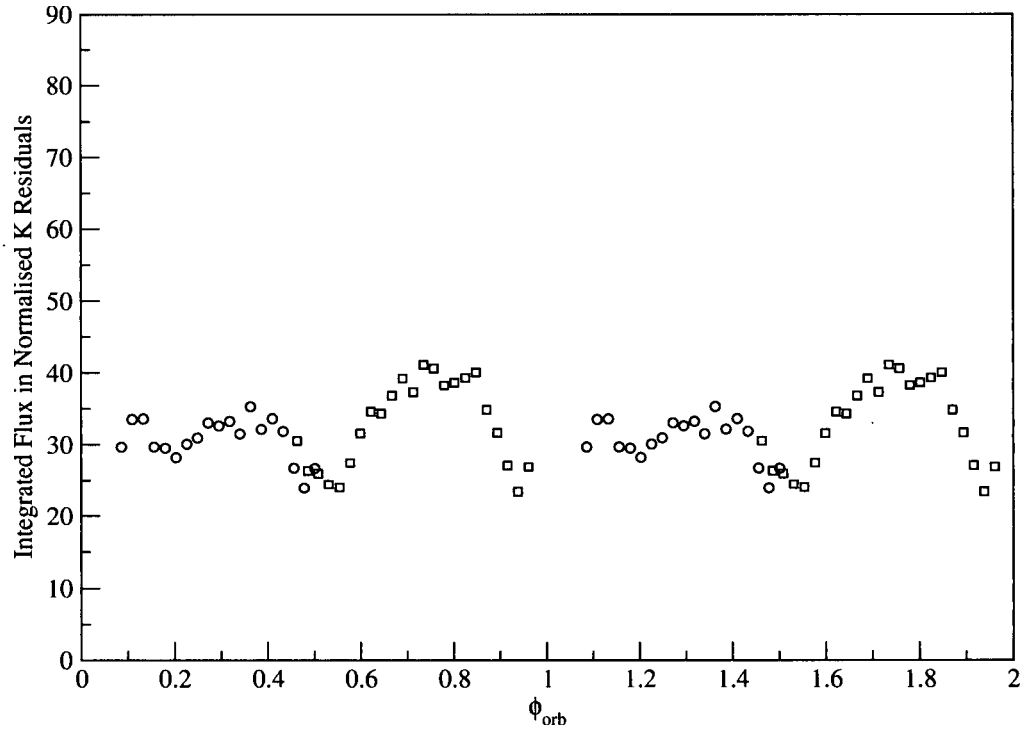

Figure 5.9 The integrated residual K flux as a function of orbital phase plotted for the primary star on Night 1 (circles) and on Night 2 (squares). Units of the integrated flux are in equivalent Angstroms relative to the normalisation level which is approximately 1/3 of the stellar continuum. The measurement error is represented by the size of the points for the observations made outside of the eclipses. During the eclipses ($0.9 \leq \phi \leq 0.1$ and $0.4 \leq \phi \leq 0.6$), the K emissions of the two components are blended making them difficult to measure as precisely as outside of eclipse. The error in ϕ is < 0.0001.

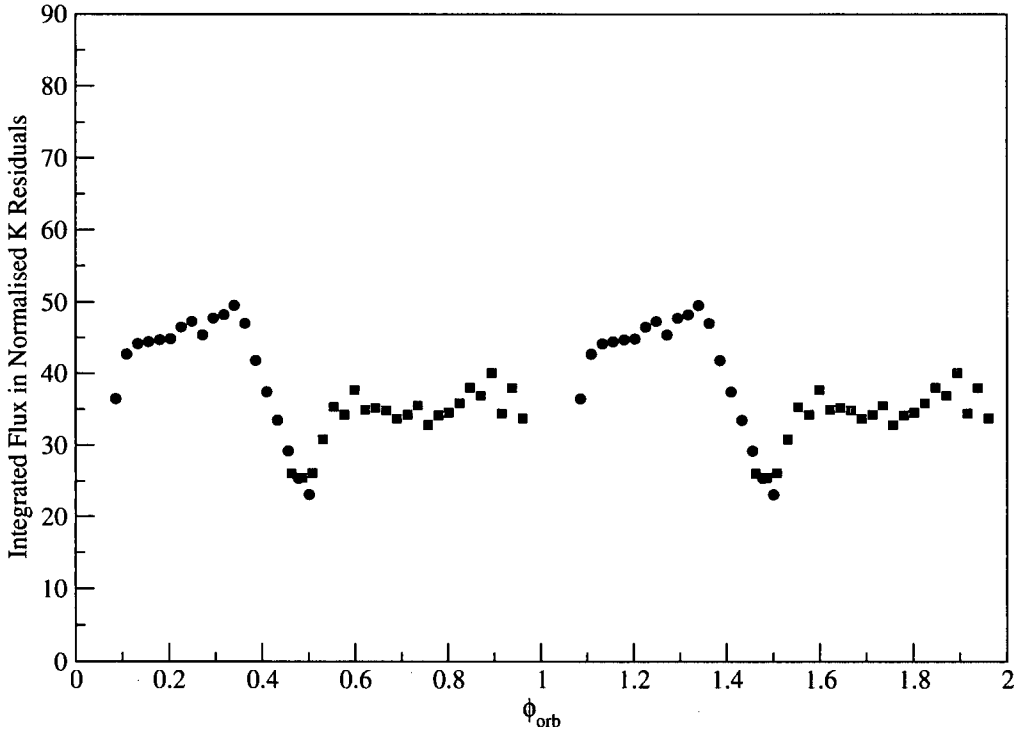

Figure 5.10 The integrated residual K flux as a function of orbital phase plotted for the secondary star.

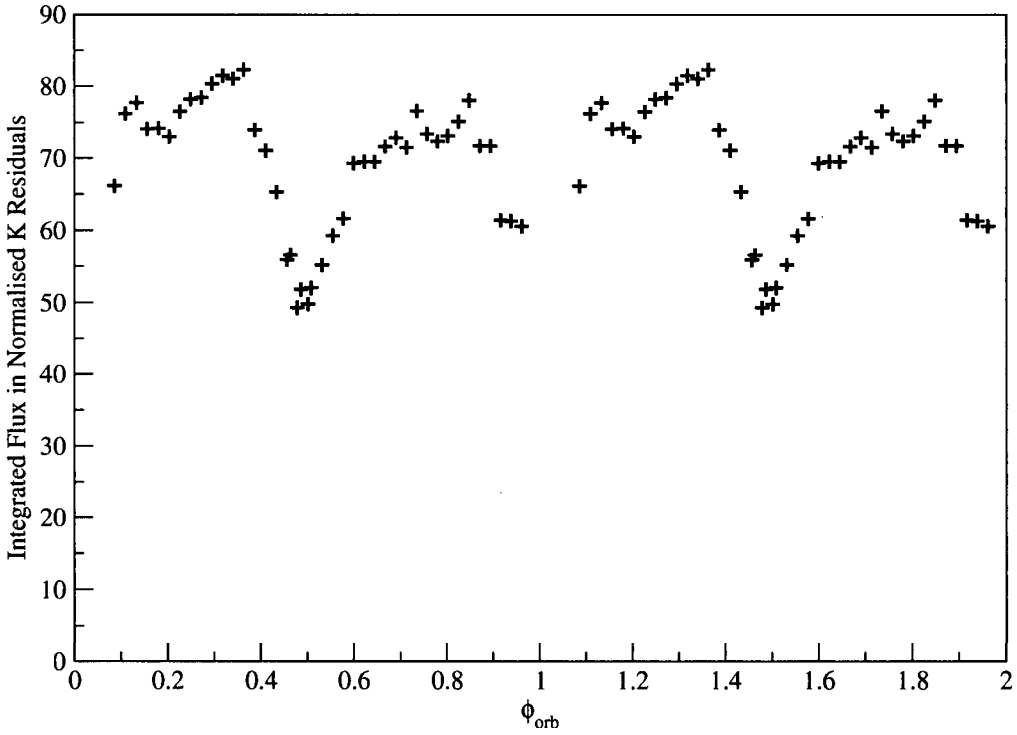

Figure 5.11 The total integrated residul K flux as a function of orbital phase for both components.

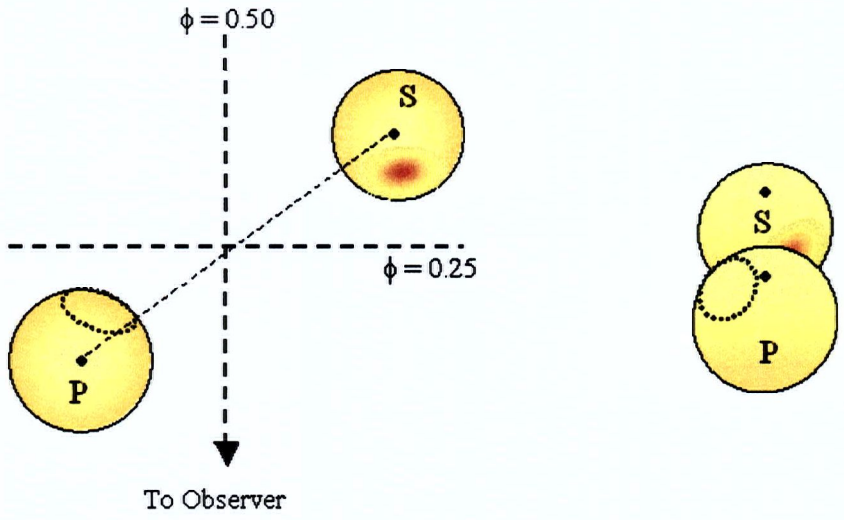

Figure 5.12 A schematic diagram of ER Vul at $\phi = 0.35$ (left; as seen from above) and $\phi = 0.50$ (right; as seen along the line of sight). The bright regions on the secondary represent the inferred hotspots while the dotted regions on the primary indicate hotspots on the unseen hemisphere of the star.

close to the times of maximum separation when the sub-stellar points are perpendicular to the line-of-sight. In the sub-stellar hotspot scenario, these would be the times of minimal activity, outside of the two eclipses, and may therefore indicate *inactive* longitudes on the stars.

In Figure 5.11, the depth of the secondary eclipse is 35% of the mean value outside of eclipse, 3 times the photometric drop during eclipse. This implies that 2/3 of the system's total Ca II K emission must come from somewhere other than the atmospheres of the two stars. From the geometry of the system, the beginning of secondary eclipse should occur at $\Delta\phi \approx 0.07$ before its centre, i.e. at $\phi \simeq 0.43$. But the drop in flux begins at $\phi = 0.35$. This early start indicates that there must be emission from between the two stars such that the emitting material is eclipsed earlier and more completely than the secondary. An estimate of how much of the emission is coming from the inter-binary gas is measured from the flux between the two K emission peaks, when the stars are furthest apart at $\phi = 0.25$ and 0.75. Approximately 10% of the mean stellar emission comes from between two stars, accounting for 1/3 of the flux drop eclipse. This is consistent with photometric peculiarities interpreted by Arévalo et al. (1988) to be due to hot circumstellar matter. Zeinali et al. (1995) see evidence for a gaseous stream flowing from the secondary to the primary in their photometric data of ER Vul.

5.5 Magnetic Heating of ER Vul

The results presented above are strong evidence of stellar activity modulated by the presence of a nearby companion. Both components of ER Vul clearly exhibit active longitudes near the sub-binary point. Ca II H & K emission increases at phases when these active regions are facing the line-of-sight. Since the enhancement appears only once per orbit for each star, the interaction between the two components is most-likely magnetic in nature. Aside from the strong Ca II emission from the two stars of ER Vul, there appears to be a significant contribution from between the two stars. This streaming gas emits approximately 10% of the K emission as measured by intergrating the flux between the two K reversals when they are maximally Doppler shifted. This inter-binary gas may play an important role in facilitating the magnetic interaction between the two stars.

The increased emission seen on each of the two component stars is anal-

ogous to the chromospheric enhancement of 2.5% seen on HD 179949. If the stars are magnetically interacting with their companions, ER Vul acts as an amplified example of HD 179949. Another interesting parallel between the two systems is the location of their hotspots. The hotspots on both components of ER Vul and on HD 179949 lead their respective sub-binary points. This will be an important constraint on the physical processes at work. Our observations of ER Vul offer supportive evidence to encourage further study of activity on and near HD 179949 and its planet. In any case, it does not contradict the interpretation of magnetic heating induced by the close-in giant planet and shows the method works when an easily detectable effect is predicted.

Chapter 6

Periodic Activity on κ^1 Ceti

6.1 Observations and Results

κ^1 Ceti is a magnetically active G5V single star with a relatively low $v\sin i$ of 3.8 km s^{-1} (Messina et al. 2001) and an age of $\approx$ 750 Myr (Guedel et al. 1997). This star has been part of the Mt. Wilson S_{HK} survey for many years. Those observations indicate a long-term magnetic cycle of 5.6 $\pm$ 0.1 yr (Baliunas 1995) while the long-term photometric variability has a comparable period of 5.9 $\pm$ 0.2 yr (Guedel et al. 1997). More relevant to the work of this thesis are the short-term variations. Both photometric and Ca II H & K variability suggest a rotation period of between 9.4 d (Baliunas et al. 1983) and 9.0 d (Messina 1998). The most recent photometric observations of κ^1 Ceti were taken by the MOST photometry satellite over the month of November in 2003. Those observations show a rotation period of 9.5 $\pm$ 0.2 d (Kuschnig, private communication), consistent with the Ca II variations.

Rubenstein and Schaeffer (2000) observed excess flare activity on nine single dwarf stars which they suggest may be due to stellar interactions with yet unseen close-in giant planets. κ^1 Ceti is a candidate for such a scenario. Its strong periodic activity could be easily monitored as part of our programme to search for planet-induced chromospheric activity. We therefore added κ^1 Ceti to our target list for the 2002 July and August observing runs.

The data reduction and processing was identical to that for the other programme stars and is described in Section 2.1. We took 1200-s exposures for which the average S/N was $\approx$ 100. The data taken on the same night was not averaged so that any brief flaring activity could be observed. A flat-fielded specimen spectrum is shown in Figure 6.1. The mean integrated emission of the K core for κ^1 Ceti is 0.977Å and with its $v\sin i$ = 3.8 km s^{-1}, sets it far above the other target stars in Figure 3.5. Table 6.1 lists the observations, the Heliocentric Julian Date, relative rotational phase (using P_{rot}=9.4 d) and the integrated residual Ca II K flux as done for all previous targets (see Section 3.2.1.).

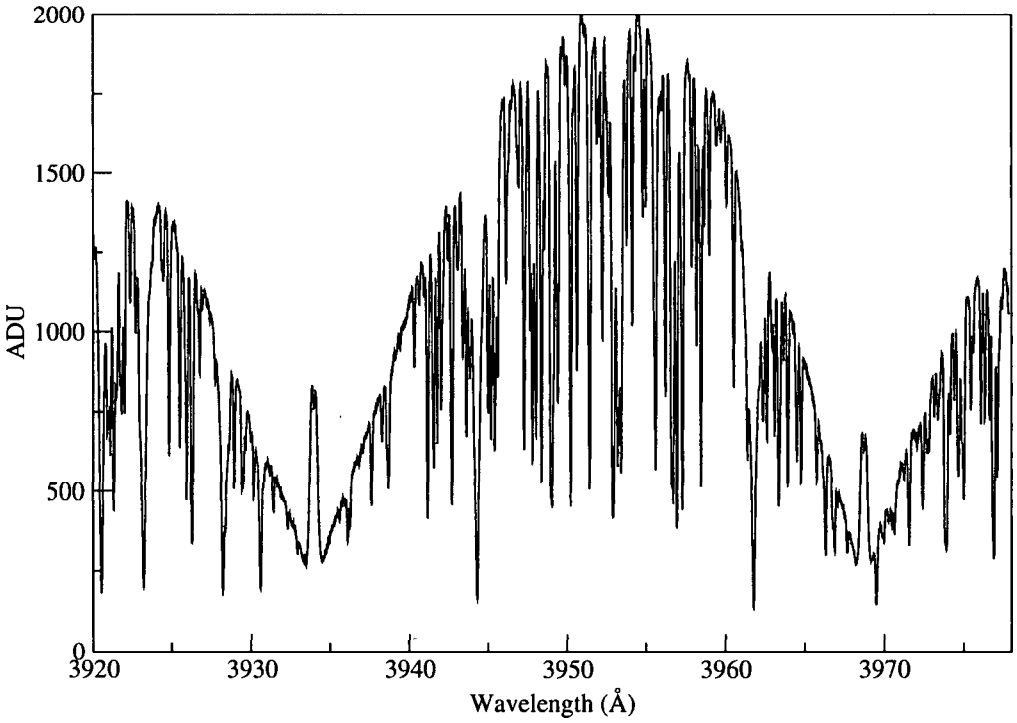

Figure 6.1 A single 1200 s flat-fielded spectrum of κ^1 Ceti.

Table 6.1. κ^1 Ceti Observations

UT Date	JD[a]	ϕ_{rot}[b]	Residual K[c] Flux (± 0.0017 Å)
7/28/2002	2452484.092	0.000	-0.01596
7/28/2002	2452484.107	0.002	-0.01634
7/30/2002	2452486.141	0.218	-0.01032
8/20/2002	2452507.145	0.452	0.04099
8/21/2002	2452508.122	0.556	0.02028
8/21/2002	2452508.136	0.558	0.02259
8/23/2002	2452510.122	0.769	0.00459
8/23/2002	2452510.137	0.771	0.00535
8/23/2002	2452510.151	0.772	-0.00161
8/26/2002	2452513.116	0.088	-0.02102
8/27/2002	2452514.131	0.196	-0.02851

[a]Julian Date at mid-exposure time. Exposure times are 1200 s.

[b]Rotational phases calculated using P_{rot} = 9.4 d.

[c]Integrated residual K flux from normalised mean of all spectra

The residuals of the Ca II K core relative to the normalised mean are shown in Figure 6.2 while their integrated flux is plotted against relative rotational phase in Figure 6.3 and shows an enhancement of $\approx 7\%$. The integrated residuals of the Al line at 3944Å average to 0.0012 implying that the activity is confined to the star's upper atmosphere. The coherence between the Ca II H and K activity is evident in Figure 6.4 for which the slope of the trend-line is 0.64, as expected for the ratio of H:K emission.

The *pdm* routine in IRAF shows the most significant value at 9.22 d for the integrated residual K emissions. This is consistent with published rotation periods. However, using this routine for only 11 data points is not very reliable. As a first attempt, a best-fit sine curve (with $P = 9.4$ d) fits the data reasonably well. As we would expect from such an active star, irregular flaring likely caused the excess scatter in the K emission.

6.2 Speculation

The stellar activity on κ^1 is well correlated with the its rotation. This 9.4-day modulation of the Ca II H & K emission has clearly persisted for over 20 years since Baliunas et al. (1983) first reported it in the S_{HK} index. To date, no physical interpretation for this persistent activity exists.

If κ^1 Ceti has a large active region carried around by rotation, the K emission should stay at a constant value for half of the rotation (as discussed for the model in Figure 4.1). The greatest emission falls off in intensity as expected with a $\cos(\phi)$ dependence. However, on the other hemisphere of the star, there seems to be a less active region that may also follow a $\cos(\phi)$ rise and drop but with a much smaller amplitude.

We speculate on two possibile sources for this activity:

(1) Using $P_{rot} = 9.4$ d, R_*=$R_\odot$, and $v\sin i = 3.8$ km s^{-1}, $v = 5.4$ km s^{-1} and hence the inclination of the star is 45°. An oblique magnetic dipole (one whose axis is inclined relative to the rotation axis of the star) can produce a search-light-type effect during observations. An extremely active region at each of the poles of the dipoles would be simultaneously darker in photospheric light and brighter in chromospheric emission, thus emitting strong Ca II radiation periodically with rotation. (Walker, personal communication).

(2) As Rubenstein & Schaefer (2000) first suggested, κ^1 Ceti could be magnetically interacting with a close-in companion that has not yet been detected. If this were the case, we can set some limits on the orbital parameters

using the scatter already observed in the radial velocities of κ^1 Ceti. Walker et al. (1995) observed a scatter of 50 m s^{-1} while looking for long-term periodicity over several years of data. The differential radial velocities (ΔRV) that I measured for the this star also appear to have a scatter of approximatedly 50 m s^{-1} as seen in Figure 6.5. (See Section 2.2 for details on the measurment of ΔRVs.) Due to the lower S/N of the spectra and the high levels of intrinsic stellar activity, a planetary orbit whose K_{max} is not larger than 50 m s^{-1} would be difficult to detect. At this stage, the Lick Survey (Cummings et al. 1999) has observed κ^1 Ceti for short-term radial velocity variations in search of close-in planets but none have been reported. However, we can set a limit on the orbital parameters using the information we have and assuming the planet is synchronized to the star's rotation. Using Kepler's laws, a nearby planet having an orbital period of 9.4 d must have a mass of 0.74 M_J and orbital semi-major axis of 0.084 AU in order to cause the reflex motion of the star to reach 50 m s^{-1}. This set an upper limit on the mass of any potential planet around κ^1 Ceti.

κ^1 Ceti is the third star/system of this thesis to exhibit persistent phase-dependent activity. As with HD 179949 and ER Vul, this star is an exciting one to continue monitoring in order to expand our knowledge of chromospheric heating, activity mechanisms on active late-type dwarfs, and potential planet-star interactions.

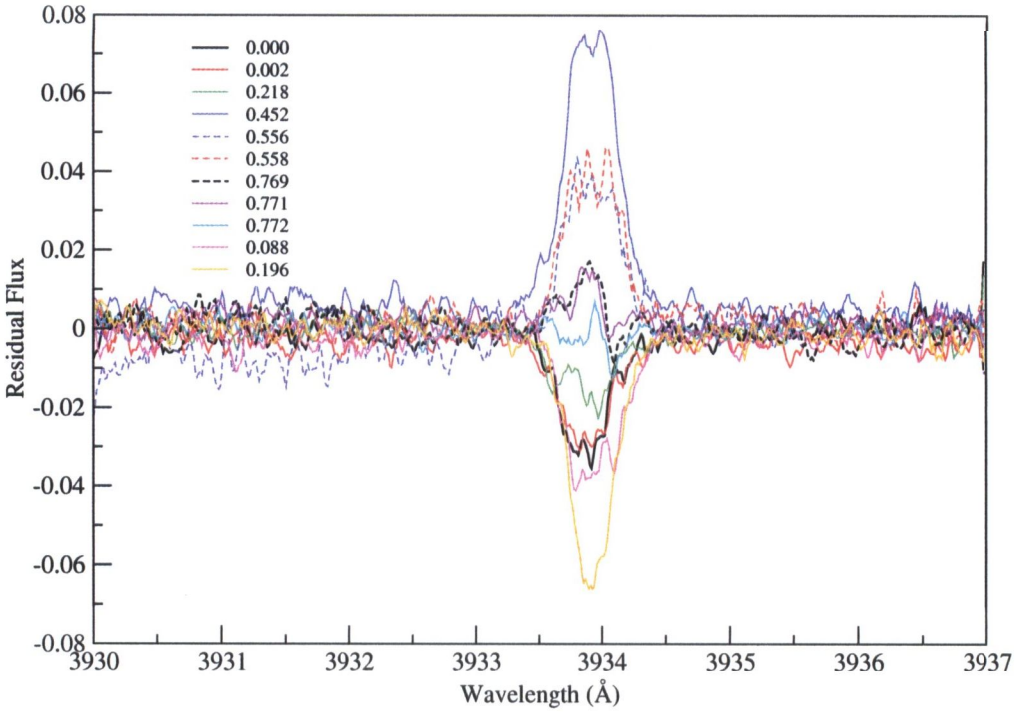

Figure 6.2 Residuals from the normalised mean spectrum of the Ca II K core of κ^1 Ceti. The relative rotational phases are labeled.

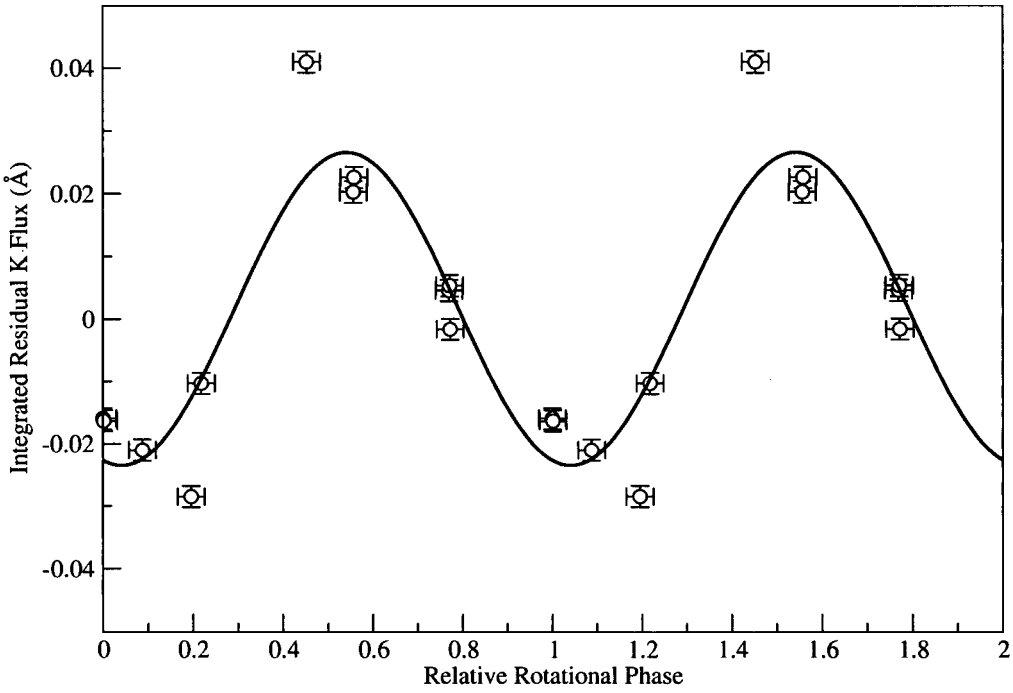

Figure 6.3 Integrated residual K flux of κ^1 Ceti plotted against relative rotational phase ($P_{rot} = 9.4$ d). The error bars in the flux residuals are $\pm$ 1 σ. The solid line is the least-squares best-fit sine curve.

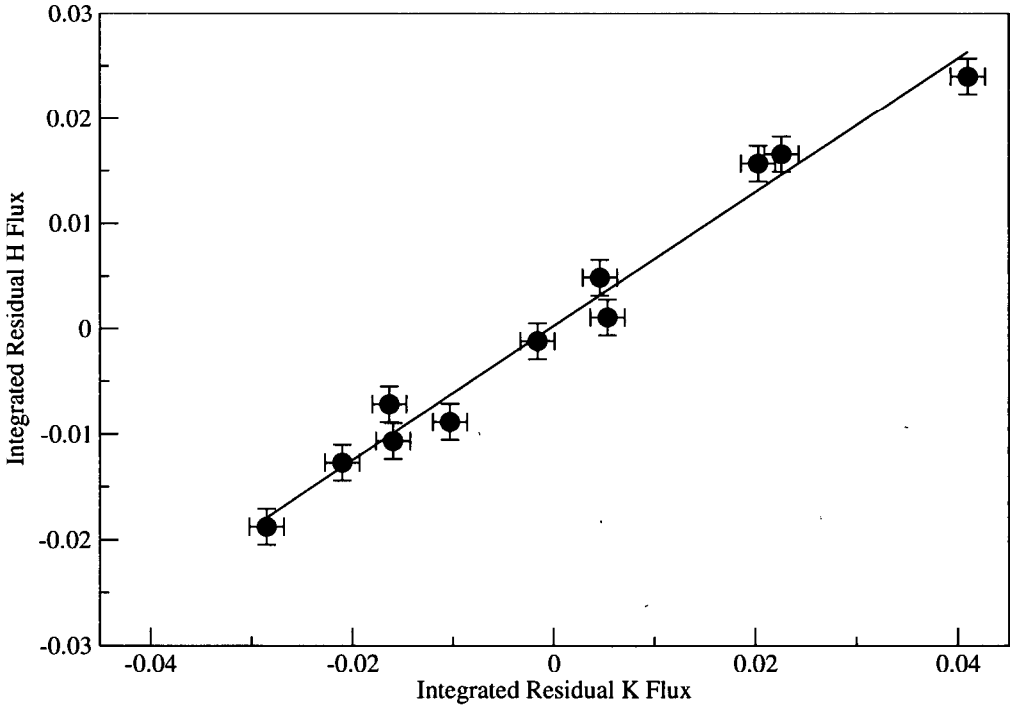

Figure 6.4 Integrated residuals for κ^1 Ceti's H and K cores. The error bars are $\pm$ 1σ. The slope of the best-fit line is 0.64.

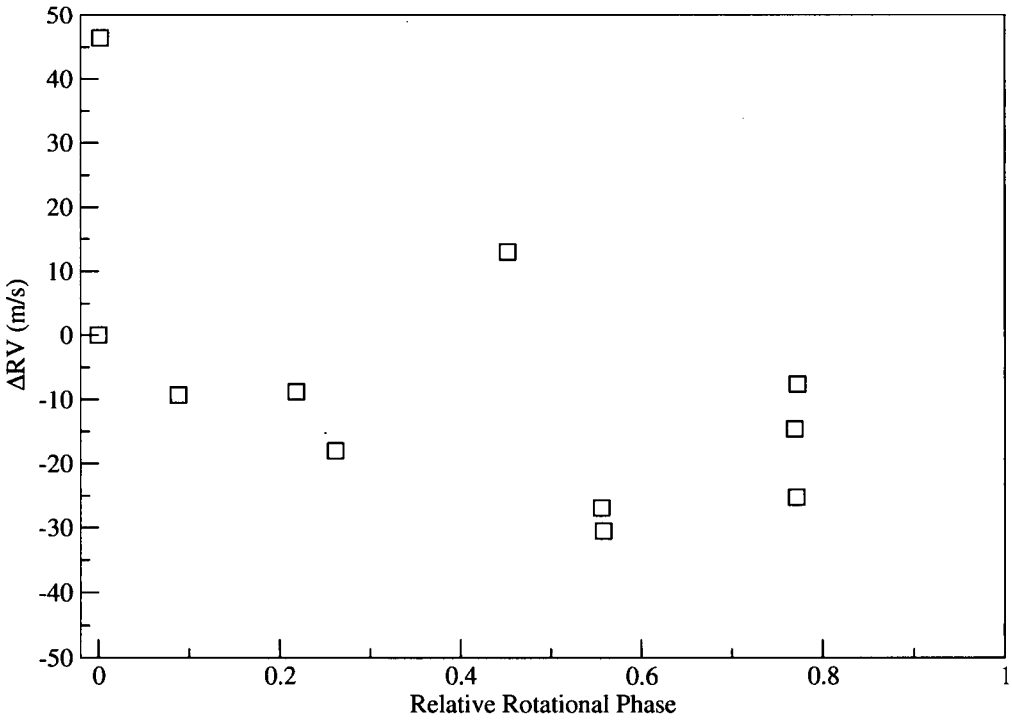

Figure 6.5 Differential radial velocities for κ^1 Ceti.

Chapter 7

Summary and Future

7.1 Observations and Results

More than 100 extrasolar planets have been discovered to date, of which $\approx$ 20% have close-in Jupiter-mass planets. Based on theoretical suggestions of planet-star interactions, we set out to search for variable stellar activity that would probe any magnetic and/or tidal interaction. Characterisation of such planet-star interactions will contribute constraints to chromospheric heating models and short-term stellar activity. An observed magnetic interaction would also provide the first glimpse of an extrasolar planetary magnetosphere. Finally, this method may provide the groundwork required for future use of periodic chromospheric activity as a planet-searching method in chromospherically active stars for which the Doppler method does not work (Saar & Donahue 1997).

We designed an observing programme to search for modulated chromospheric activity with the planet's orbital period. The observations were centered on the Ca II H and K resonance lines, which are classic diagnostics of chromospheric activity. Three observing runs at the CFHT yielded 10 nights of high-resolution, high S/N data. We observed five late-type dwarf stars with short-period giant planets ($P_{orb} < 5$ days) plus two standards, τ Ceti and the sun. The superb quality of the data yielded differential radial velocities with the precision of better than 20 m s^{-1}, from which updated ephemerides and accurate orbital phases were derived.

Of the five stars with planets, four exhibited significant ($> 3\sigma$) night-to-night modulation in the Ca II H & K emission while the two standards did not. There was a strong correlation between the $v\sin i$ of the stars with both the mean Ca II K emission and with the level of its night-to-night variability. Three of the stars, υ And, τ Boo and HD 209458, show variations that are not clearly coherent with orbital phase. This may be in part due to changes in the intrinsic level of stellar activity from year to year. In τ Boo's case, where the star and planet are tidally synchronized, it is possible that the activity

observed was due to surface features modulated by stellar rotation. The other two stars have much longer rotation periods, meaning that nightly variation due solely to rotation is unlikely. They are certainly worth following up on because with more observations across a longer baseline, a clearer picture of the nature of this activity will emerge.

The fourth of the 'active' stars, HD 179949, shows not only the greatest level of variability from night to night, but also a clear dependence on orbital phase. Data spanning over one year (108 orbits or 37 stellar rotations), repeatedly showed an increase of $\sim 2.5\%$ in chromospheric emission at phases near the sub-planetary point and a decrease at phases when the planet was behind the star. A model fit to the data consists of a hotspot travelling on the stellar surface at a latitude of 30° with the same period as the planet's orbit. The best-fit stellar inclination angle is $87° \pm 0.5°$ According to this geometric model, the peak enhancement leads the sub-planetary point by 0.174 ± 0.004 in phase. These parameters will aid the use of future chromospheric heating models to set constraints on the source of the activity. The enhancement occurring only once per orbit at nearly the expected phase is consistent with the magnetic heating scenario.

We also searched for Ca II K emission from the planetary atmosphere, as it would have been greatly displaced by its large orbital velocity (158 km s^{-1} or 2 Å from the centre of the K line). No such emission was detected.

The evidence for planet-induced heating that we collected for HD 179949 is the first of its kind. However, in short-period binary systems, such as RS CVn stars, stellar activity modulated with orbital phase had been previously observed. We, therefore, proposed another program, with the identical instrument setup and wavelength range, to observe ER Vul, a system consisting of two solar-type stars orbiting eachother within 4 $R_\odot$. The Ca II H & K emission of these stars were extracted from the spectra using the Broadening Function Technique. Both components were seen to exhibit increased chromospheric emission near their sub-binary points. Since the hotspots most likely lead the sub-binary point by approximately $20 - 30°$, the reflection effect offered as the cause of the heating is not strongly supported. Also, since the enhancements on both components appeared only once per orbit, magnetic heating is the likely cause. These observations of orbital phase dependent activity further support the scenario suggested for planet-induced activity on HD 179949.

A third source of Ca II emission is inferred from the excess depth of ER Vul's secondary eclipse. The data suggest the presence of a hot gas emitting

Ca II K as it streams between the two stars. The interplay between the three sources of Ca II emission makes ER Vul a dynamically exciting system for further study.

We also observed κ^1 Ceti, an unusually active single late-type dwarf. Its Ca II H & K emission varied sinusoidally with its rotation period of 9.4 d. This activity has persisted since the late 1970's when Baliunas et al. (1983) first reported such modulation in the S_{HK} index. This star is the third example in this thesis of persistent, periodic, phase-dependent activity. A possible explanation for the source of the activity could be an oblique magnetic dipole whose observed field varies due to the 45° stellar inclination. A second, quite speculative suggestion, is that there is a yet-unseen companion to κ^1 Ceti tidally locked to the star, that is stimulating the activiy via magnetic interactions.

7.2 Follow-up

From the 10 nights of CFHT data, night-to-night variations in Ca II emission were observed in four stars with planets. In at least one case, excess activity appears to be induced by its giant planet. Even though the effect observed on HD 179949 has persisted for > 100 orbits, this is not evidence that the travelling active region is permanent. The hotspot may drift or the effect fade away with time. Further monitoring of the system is surely necessary, especially to build a stronger case for magnetic heating, to sample the shape of the variation in more detail and to look at other spectral activity indicators. A fourth CFHT observing run of 5 nights was scheduled for 2003 September and immediately afterwards, a run of 7 nights at the 2.7-m telescope at the McDonald Observatory. There are also four short-period planetary systems in the southern sky that would be valuable additions to the current sample. We have proposed to observe these in Ca II H & K using the Very Large Telescope and its coudé echelle spectrograph in the next observing semester (Spring 2004).

As follow-up to the Ca II results of HD 179949, we started an observing program in 2003 May using Pheonix, a high-resolution infrared spectrograph mounted on the 8.1-m Gemini-South Telescope. For this program, the spectra are centered on the chromospheric He I line at 10830 Å. This line is thought to be back-heated by the corona, so if magnetic activity is externally induced, then the corona should show more than the 2.5% chromospheric en-

hancement. Preliminary results show strong variability in the line, however the project is not yet complete. We were awarded further observations in the next observing season.

The phenomenon of excess heating by a nearby planet needs to continue to be explored through space-based observations of transition region and coronal emission lines. Combined with the chromospheric activity measurements already obtained as part of this thesis, emission lines from these higher and hotter layers of the stellar atmosphere will allow a mapping of activity to stellar height. Potential space telescopes available for such observations are the HST and FUSE.

With FUSE one can observe the transition region emission lines of O VI (1032, 1038 Å) and C III (977 Å) to search for differential intensity variations at three critical orbital phases of HD 179949. Due the relatively low UV flux of inactive late-type dwarfs, a minimum of 60 ksec of exposing is necessary.With the HST, the best emission line to observe upper atomospheric heating is the upper transition region line Fe XXI 1354Å line. Again the sensitivity of the spectrograph requires long exposures. However, with enough time and future, more sensivie UV and X-Ray space observatories, we can identify the forms in which the heating takes place (e.g. microflaring, continuous magnetic reconnection, etc.) and a more robust model will begin to emerge.

Bibliography

Arévalo, M.J., Lazaro, C., Fuensalida, J.J., 1988, AJ, 96, 1061.

Baliunas, S.L., Hartmann, L., Noyes, R.W., Vaughan, H., Preston, G.W., Frazer, J., Lanning, H., Middelkoop, F., Mihalas, S., 1983, ApJ, 275, 752.

Baliunas, S.L., Horne, J.H., Porter, A., Duncan, D.K., Frazer, J., Lanning, H., Misch, A., Mueller, J., Noyes, R. W., Soyumer, D., Vaughan, A.H., Woodard, L., 1985, ApJ, 294, 310.

Baliunas, S.L., Donahue, R.A., Soon, W.H., Horne, J.H., Frazer, J., Woodard-Eklund, L., Bradford, M., Rao, L.M., Wilson, O.C., Zhang, Q., Bennett, W., Briggs, J., Carroll, S.M., Duncan, D.K., Figueroa, D., Lanning, H.H., Misch, T., Mueller, J., Noyes, R.W., Poppe, D., Porter, A.C., Robinson, C.R., Russell, J., Shelton, J.C., Soyumer, T., Vaughan, A.H., Whitney, J.H., 1995, ApJ, 438, 269.

Bastian, T. S., Dulk, G.A., Leblanc, Y., 2000, ApJ, 545, 1058.

Baudrand, J. & Vitry, R., 2000, Proceedings of the SPIE, 4008, 182.

Benedict, G.F., McArthur, B.E., Forveille, T., Delfosse, X., Nelan, E., Butler, R. P., Spiesman, W., Marcy, G., Goldman, B., Perrier, C., Jefferys, W. H., Mayor, M., 2002, ApJ, 581, 115.

Böhm-Vitense, E., 1989, *Introduction to Stellar Astrophysics*, Cambridge University Press.

Brown, T., Libbrecht, K., Charbonneau, D., 2002, PASP, 114, 826.

Butler, P., Marcy G., Williams, E., Hauser, H., Shirts, P., 1997, ApJL, 474, 115.

Çakirli, O., Ibanoglu, C., Frasca, A., Catalano, S., 2003, A&A, 400, 257.

Campbell, B., & Walker, G.A.H., 1979, PASP, 91, 540.

Campbell, B., Walker, G.A.H., Yang, S., 1988, ApJ, 331, 902.

Carroll, B.W., Ostlie, D.A., 1996, *An Introduction to Modern Astrophysics*, Addison-Wesley Publishing Company, Inc.

Catalano, S., Rodanò, M., Frasca, A., Cutispoto, P., 1996, *Stellar Surface Structure*, IAU Symp. 176, 403.

Cayrel de Strobel, G., 1996, A&ARv, 7, 243.

Charbonneau, D., Brown, T., Latham, D., Mayor, M., Mazeh, T.,1999, ApJ, 529, 45.

Charbonneau, D., Brown, T.M., Noyes, R.W., Gilliland, R.L., 2002, ApJ, 568, 377.

Collier-Cameron, A., Horne, K., Penny, A., James, D., 1999, Nature, 402, 751.

Cowling, T.G., 1957, *Interscience Tracts on Physics and Astronomy: Magnetohydrodynamics*, edited by R.E. Marshak, Interscience Publishers, Inc.

Cumming, A., Marcy, G.W., Butler, R.P., 1999, ApJ, 526, 890.

Cuntz, M., Rammacher, W., Ulmschneider, P., Musielak, Z.E., Saar, S.H., 1999, ApJ, 522, 1053.

Cuntz, M., Saar, S.H., Musielak, Z.E., 2000, ApJL, 533, 151.

Darling, D.J., , 2003, *The Encyclopedia of Astrobiology, Astronomy, and Spaceflight*, http://www.daviddarling.info/encyclopedia/ETEmain.html.

Donati, J.-F., Henry, G.W., Hall, D.S., 1995, A&A, 293, 107.

Dorminey, B., 2002, *Distant Wanderers: The Search for Planets Beyong the Solar System* Springer-Verlag New York, Inc.

Drake, S.A., Pravdo, S.H., Angelini, L., Stern, R.A, 1998, AJ, 115, 2122.

Duemmler, R., Doucet, C., Formanek, F., Ilyin, I., Tuominen, I., 2003, A&A, 402, 745.

Engvold, O., 1966, ApNr, 10, 101.

Fawzy, D., Rammacher, W., Ulmschneider, P., Musielak, Z.E., Stecedilpien, K., 2002, A&A, 386, 971.

Fekel, F.C., 1997, PASP, 109, 514.

Fernandez-Figueroa, M.J., Montes, D., De Castro, E., Cornide, M., 1994, ApJS, 90, 433.

François, P., Spite, M., Gillet, D., Gonzalez, J.-F., Spite, F., 1996, A&A, 310, 13.

Glebocki, R., Bielicz, E., Pastuszka, Z., Sikorski, J., 1986, AcA, 36, 369.

Giménez, A., 2000, A&A, 356, 213.

Gray, D.F., 1982, ApJ, 255, 200.

Gray, D.F., Toner, C.G., 1985, PASP, 97, 543.

Gray, D.F., 1986, PASP, 98, 319.

Gray, D.F., Baliunas, S.L., Lockwood, G.W., Skiff, B.A., 1996, ApJ, 465, 945.

Groot, P.J., Piters, A.J.M., van Paradijs, J., 1996, A&AS, 118, 545.

Guedel, M., Guinan, E.F., Skinner, S.L., 1997, ApJ, 483, 947.

Gunn, A.G., Doyle, J.G., 1997, A&A, 318, 60.

Hatzes, A.P., Cochran, W.D., Endl, M., McArthur, B., Paulson, D.B., Walker, G.A.H., Campbell, B., Yang, S., 2003, ApJ, accepted, astroph/0305110.

Harmanec, P., Božić, H., Robb, R.M., Ruždjak, D., Sudar, D., Thanjavur, K., 2004, A&A, 415, 289.

Henry, G.,W., Baliunas, S.L., Donahue, R.A., Fekel, F.C., Soon, W., 2000, ApJ, 531, 415.

Henry, G.W., Donahue, R.A., Baliunas, S.L., 2002, ApJ, 577, 111.

Hünsch, M., Schmitt, J.H.M.M., Voges, W., 1998, A&AS, 132, 155.

van de Kamp, P., 1963, AJ, 68, 515.

Lanza, A.F., Rodonò, M., Mazzola, L., Messina, S., 2001, A&A, 376, 1011.

Linsky, J.L., 1980, ARA&A, 18, 439.

Marcy, G., Butler, P., Williams, E., Bildsten, L., Graham, J., 1996, ApJ, 481, 926.

Mariska, J.T., 1992, *The Solar Transition Region*, Cambridge University Press.

Mazeh, T., Naef, D., Torres, G., Latham, D.W., Mayor, M., Beuzit, J.-L., Brown, T.M., Buchhave, L., Burnet, M., Carney, B.W., Charbonneau, D., Drukier, G., Laird, J.B., Pepe, F., Perrier, C., Queloz, D., Santos, N.C., Sivan, J.-P., Udry, S., Zucker, S., 2000, ApJL, 532, 55.

Messina, S., Rodonò, M., Guinan, E.F., 2001, A&A, 366, 215.

Messina, S., Guinan, E.F., 2002, A&A, 393. 225.

Montes, D., Fernandez-Figueroa, M.J., de Castro, E., Cornide, M., 1994, A&A, 285, 609.

Montes, D., Fernandez-Figueroa, M.J., Cornide, M., de Castro, E., 1996, A&A, 312, 221.

Musielak, Z.E., Rosner, R., Stein, R.F., Ulmschneider, P., 1994, ApJ, 423, 474.

Narain, U., Ulmschneider, P., 1996, SSRv, 75, 453.

Noyes, R.W., Hartmann, L.W., Baliunas, S.L., Duncan, D.K., Vaughan, A.H., 1984, ApJ, 279, 763.

Pasquini, L., de Medeiros, J.R., Girardi, L., 2000, A&A, 361, 1011.

Piskunov, N.E., 1996, *Stellar Surface Structure*, IAU Symp. 176, 45.

Rubenstein, E.P., Schaeffer, B.E., 2000, ApJ, 529, 1031.

Rucinski, S.M., 2002, AJ, 124, 1746.

Saar, S.H., Donahue, R.A., 1997, ApJ, 485, 319.

Saar, S.H., Cuntz, M., 2001, MNRAS, 325, 55.

Saar, S.H., Shkolnik, E., Cuntz, M., 2003, IAUS, 219, 119.

Sanford, R.F., Wilson, O.C., 1939, ApJ, 90, 235.

Santos, N.C., Mayor, M., Naef, D., Pepe, F., Queloz, D., Udry, S., Burnet, M., Revaz, Y., 2000, A&A, 356, 599.

Santos, N.C., Udry, S., Mayor, M., Naef, D., Pepe, F., Queloz, D., Burki, G., Cramer, N., Nicolet, B., 2003, A&A, 406, 373.

Schneider, J., *Extrasolar Planets Catalog*, http://www.obspm.fr/encycl/catalog.html.

Seager, S., Sasselov, D., 2000, ApJ, 537, 916.

Shkolnik, E., Walker, G.A.H., Bohlender, D.A., 2002, AAS 201.4616.

Stellingwerf, R.F., 1978, ApJ, 224, 953.

Strand, K.A., 1943, PASP, 55, 29.

Tinney, C., Butler, P., Marcy, G., Jones, H., Penny, A., Vogt, S., Apps, K., Henry, C., 2001, ApJL, 551, 507.

Toner, C.G., Gray, D.F., 1988, ApJ, 334, 1008.

Ulmschneider, P., Priest, E.R., Rosner, R., 1991, Proceedings of the International Conference, Heidelberg, Springer-Verlag Berlin Heidelberg New York.

Ulmschneider, P., Musielak, Z.E., 1998, A&A, 338, 311.

Vidal-Madjar, A., Lecavelier des Étangs, A., Désert, J.-M., Ballester, G., Ferlet, R., Hébrard, G., Mayor, M., 2003, Nature, 422, 143.

Vogt, S.S., 1981, ApJ, 250, 327.

Vogt, S.S., Hatzes, A.P., Misch, A.A., Kürster, M., 1999, ApJS, 121, 547.

Walker, E.C., 1944, JRASC, 38, 249.

Walker, Gordon A. H., Bohlender, D.A., Walker, A.R., Irwin, A.W., Yang, S.L.S., Larson, A., 1992, ApJ, 396, 91.

Walker, G.A.H., Walker, A.R., Irwin, A.W., Larson, A.M., Yang, S.L.S., Richardson, D.C., 1995, Icar, 116, 359.

Walker, G.A.H., Shkolnik, E., Bohlender, D.A., Yang, S., 2003, PASP, 115, 700.

Wiedemann,G., Deming, D., Bjoraker, G., 2001, ApJ, 546, 1068.

Wolszczan, A., 1994, Science, 264, 538.

Yeşilyurt, S., Del Popolo, A., Ercan, N., 2003, IJMP, accepted, astro-ph/0308021.

Zeinali, F., Edalati, M.T., Mirtorabi, M.T., 1995, IBVS, 4190, 1.